

University of Kentucky

UKnowledge

Theses and Dissertations--Molecular and Cellular Biochemistry

Molecular and Cellular Biochemistry

2022

DEFINING PATIENT COHORTS FOR GUIDING CLINICAL TRIALS AND TREATMENT IN LAFORA DISEASE: A MODEL FOR THE RARE DISEASE COMMUNITY

Katherine Janae Donohue

University of Kentucky, kjanaed89@gmail.com

Digital Object Identifier: <https://doi.org/10.13023/etd.2022.463>

[Right click to open a feedback form in a new tab to let us know how this document benefits you.](#)

Recommended Citation

Donohue, Katherine Janae, "DEFINING PATIENT COHORTS FOR GUIDING CLINICAL TRIALS AND TREATMENT IN LAFORA DISEASE: A MODEL FOR THE RARE DISEASE COMMUNITY" (2022). *Theses and Dissertations--Molecular and Cellular Biochemistry*. 61.

https://uknowledge.uky.edu/biochem_etds/61

This Doctoral Dissertation is brought to you for free and open access by the Molecular and Cellular Biochemistry at UKnowledge. It has been accepted for inclusion in Theses and Dissertations--Molecular and Cellular Biochemistry by an authorized administrator of UKnowledge. For more information, please contact UKnowledge@lsv.uky.edu.

STUDENT AGREEMENT:

I represent that my thesis or dissertation and abstract are my original work. Proper attribution has been given to all outside sources. I understand that I am solely responsible for obtaining any needed copyright permissions. I have obtained needed written permission statement(s) from the owner(s) of each third-party copyrighted matter to be included in my work, allowing electronic distribution (if such use is not permitted by the fair use doctrine) which will be submitted to UKnowledge as Additional File.

I hereby grant to The University of Kentucky and its agents the irrevocable, non-exclusive, and royalty-free license to archive and make accessible my work in whole or in part in all forms of media, now or hereafter known. I agree that the document mentioned above may be made available immediately for worldwide access unless an embargo applies.

I retain all other ownership rights to the copyright of my work. I also retain the right to use in future works (such as articles or books) all or part of my work. I understand that I am free to register the copyright to my work.

REVIEW, APPROVAL AND ACCEPTANCE

The document mentioned above has been reviewed and accepted by the student's advisor, on behalf of the advisory committee, and by the Director of Graduate Studies (DGS), on behalf of the program; we verify that this is the final, approved version of the student's thesis including all changes required by the advisory committee. The undersigned agree to abide by the statements above.

Katherine Janae Donohue, Student

Dr. Matthew S. Gentry, Major Professor

Dr. Trevor Creamer, Director of Graduate Studies

DEFINING PATIENT COHORTS FOR GUIDING CLINICAL TRIALS AND
TREATMENT IN LAFORA DISEASE: A MODEL FOR THE RARE DISEASE
COMMUNITY

DISSERTATION

A dissertation submitted in partial fulfillment of the
requirements for the degree of Doctor of Philosophy in the
College of Medicine
at the University of Kentucky

By
Katherine Janae Donohue
Lexington, Kentucky
Director: Dr. Matthew S. Gentry, Professor of Molecular and Cellular Biochemistry
Lexington, Kentucky
2022

Copyright © Katherine Janae Donohue 2022

ABSTRACT OF DISSERTATION

DEFINING PATIENT COHORTS FOR GUIDING CLINICAL TRIALS AND TREATMENT IN LAFORA DISEASE: A MODEL FOR THE RARE DISEASE COMMUNITY

In the US, approximately 8000 rare diseases have been identified. Combined, rare diseases impact more than 30 million people in the U.S. alone, with 75% of those being children. However, research, funding, and therapeutic development for the rare disease community remains challenging because of the incredible diversity – not only between diseases, but often even within a single disease.

LD is an ultra-rare childhood dementia and epilepsy caused by mutations in one of two driver genes: *EPM2A*, which encodes for the glycogen phosphatase laforin, and *EPM2B/NHLRC1*, which encodes the E3 ubiquitin ligase malin. Children with LD develop seemingly normal until their pre-teen years when they experience increasingly severe seizures coupled with neurodegeneration. While all patients follow the same trajectory, there is substantial variation in the rate of their decline. This variability presents a challenge for therapeutic development and structuring clinical trials.

To that end, this work presents a method for rapid characterization of novel *EPM2A* mutations. Additionally, this work devises a strategy for interrogating differences and similarities between the two driver genes of LD. This information is then used to assess the impact and viability of an antisense oligonucleotide (ASO) therapy to halt disease progression in LD. Finally, these lessons are extrapolated to build a genotype-phenotype correlation for Glut1 Deficiency Syndrome, another rare metabolic disease, showing the adaptability of these methods for the broader rare disease community.

KEYWORDS: Lafora Disease, Personalized Medicine, Glut1 Deficiency Syndrome,
Glycogen, Glycogen Storage Disease, Antisense Oligonucleotide

Katherine Janae Donohue

10/17/2022

Date

DEFINING PATIENT COHORTS FOR GUIDING CLINICAL TRIALS AND
TREATMENT IN LAFORA DISEASE: A MODEL FOR THE RARE DISEASE
COMMUNITY

By

Katherine Janae Donohue

Dr. Matthew S. Gentry

Director of Dissertation

Dr. Trevor Creamer

Director of Graduate Studies

10/17/2022

Date

DEDICATION

To the Lafora Disease Community, in the hopes that a therapy will soon be available.

ACKNOWLEDGMENTS

First and foremost, I would like to thank all my teachers and mentors who inspired and guided me along the journey of writing my dissertation. I am incredibly grateful to all the members of my dissertation committee for challenging me to dig deeper and critically evaluate my data. A special thanks to Dr. Matthew Gentry and Dr. Craig Vander Kooi for their mentorship and advice when planning experiments and making career decisions. I am also deeply thankful for the support of my other committee members, Dr. David Rodgers and Dr. Bret Smith, who proved to be invaluable sounding boards for guiding my dissertation research and career search. I would also like to thank my mentors who helped me decide to return to academia for my PhD. To my high school chemistry teacher, Zach Matson, thanks for getting me interested in chemistry and for continuing to support and encourage me over the years. To my undergraduate mentor, Dr. Robert Rabel, thank you for encouraging me to pursue a career in academia. And to my Patterson School Graduate Advisor, Dr. Karen Mingst, thank you for challenging me to think critically about public policy and encouraging me to pursue my full potential.

Thank you to all my friends and family members for your prayers and support over the years. Your encouragement and regular check-ins were much appreciated. I am also grateful for the new friends and colleagues who worked with me in the Gentry-Sun Labs. A special thanks to Dr. Ramon Sun, Dr. Ron Bruntz, Dr. Robert Murphy, Dr. Katy Brewer, Dr. Zoe Simmons, and Dr. Corey Brizzee for guiding me through new laboratory techniques. I would also like to thank Dr. Lyndsay Young for her assistance with collecting and managing data in the lab. This dissertation would not have been possible without the support and teamwork from my colleagues in the lab, particularly Dr. Anna Juras, Dr. Andrea Kuchtova, Dr. Jessica Macedo, Annette Mestas, Kia Markussen, Alex Cantrell, Tara Hawkinson, and Harrison Clarke. I am also grateful for the opportunity to work with so many talented undergraduate students, especially Maya Abul-Khoudoud, Laiken Griffith, Trey Coburn, Kayli Bolton, and Meredith Williams, who assisted with data collection and analyses for various projects within this dissertation. I learned so much from all of you. Thank you for your support and contributions to this dissertation.

Finally, thank you to all the collaborators who made this dissertation possible. Thank you to Dr. Sheng Li for performing HDX analysis of laforin patient mutations and to Dr. Pascual Sanz and Rosa Viana for their assistance with running the yeast two-hybrid experiments for laforin patient mutations. A special thank you to Dr. Anna DePaoli-Roach for supplying mouse models and tissues for analysis. I would also like to thank all the researchers, clinicians, and Lafora Disease family members whose collaborations through Chelsea's Hope Lafora Children Research Fund inspired this project.

TABLE OF CONTENTS

ABSTRACT OF DISSERTATION.....	ii
ACKNOWLEDGMENTS	iii
TABLE OF CONTENTS	iv
List of Tables	vi
List of Figures.....	vii
CHAPTER 1. THE ROLE OF BASIC SCIENCE IN DEVELOPING PERSONALIZED MEDICINE FOR RARE DISEASES	1
1.1 The Evolution of Personalized Medicine.....	1
1.2 Defining the Scope of Personalized Medicine.....	1
1.3 The Current Landscape of Personalized Medicine	2
1.3.1 Precision Oncology.....	2
1.3.2 Cancer Immunotherapy	3
1.3.3 The Opportunities for Expanding Personalized Medicine for Rare Disease	4
1.3.4 Cystic Fibrosis: A Case Study in Applying Personalized Medicine for Rare Disease.....	5
1.3.5 The Barriers to Expanding Personalized Medicine for Rare Disease.....	6
1.4 Lafora Disease: A model for expanding PM in the Rare Disease Community.....	8
1.5 Overview of the Dissertation.....	9
CHAPTER 2. MATERIALS AND METHODS.....	15
2.1 Methods for Bioinformatics and Biochemical Analyses of Laforin and Glut1 Mutations	15
2.1.1 Protein Expression and Purification	15
2.1.2 SDS-PAGE & Native Gels	15
2.1.3 Differential Scanning Fluorimetry (DSF).....	16
2.1.4 Para-nitrophenylphosphate (pNPP) Assay	16
2.1.5 Yeast Two-Hybrid Assay (Y2H).....	16
2.1.6 Hydrogen-Deuterium eXchange (HDX) Mass Spectrometry.....	17
2.1.7 Bioinformatics	17
2.1.8 Statistics.....	18
2.2 Methods for Mouse Model Analyses to Determine Driver-Gene Variations and ASO Therapy Efficacy	18
2.2.1 Mice and ASO Delivery	18
2.2.2 Gys1 mRNA Expression Analysis.....	19
2.2.3 Gys1 Protein Expression Analysis.....	19
2.2.4 Histological Analysis.....	20
2.2.5 Gas Chromatography Mass Spectrometry (GCMS) Analysis	20
2.2.6 Glycogen and Glycan Quantification via MALDI Analysis	20
2.2.7 Measurement of Neuronal Excitability.....	21
2.2.8 Statistical Analyses of Mouse Tissue Samples.....	21
CHAPTER 3. RAPID PATHOGENICITY ASSESSMENT DEFINES PATIENT COHORTS FOR LAFORA DISEASE	22

3.1	<i>Introduction</i>	22
3.2	<i>Results</i>	23
3.2.1	<i>In silico</i> analysis provides a baseline for <i>in vitro</i> screening of patient mutations	23
3.2.2	<i>In vitro</i> pipeline clarifies uncertain <i>in silico</i> predictions for patient mutations	24
3.2.3	Bioinformatics screen identifies novel SNPs for pipeline analysis	25
3.2.4	Pipeline analysis supports confident <i>in silico</i> predictions	26
3.2.5	Pipeline analysis defines pathogenicity predictions from <i>in silico</i> analysis.....	27
3.2.6	Multivariate analysis clusters novel SNPs with known pathogenic mutations	28
3.3	<i>Discussion</i>	28
CHAPTER 4. DEFINING DRIVER-GENE CHARACTERISTICS FOR LAFORA DISEASE IN MOUSE MODELS		43
4.1	<i>Introduction</i>	43
4.2	<i>Results</i>	44
4.2.1	LKO mouse model shows rapid glycogen accumulation compared to LCS and MKO mouse models	44
4.2.2	Metabolomics profiles are driver-gene dependent in LD mouse models	45
4.2.3	Glycosylation defects differ between LKO and MKO mouse models	46
4.3	<i>Discussion</i>	46
CHAPTER 5. GYS1 ANTISENSE THERAPY PREVENTS DISEASE-DRIVING AGGREGATES AND EPILEPTIFORM DISCHARGES IN A LAFORA DISEASE MOUSE MODEL.....		55
5.1	<i>Introduction</i>	55
5.2	<i>Results</i>	56
5.2.1	Gys1-ASO Decreases <i>Gys1</i> mRNA and Gys1 Protein Expression	56
5.2.2	Gys1-ASO Treatment Reduces Glycogen Accumulation	56
5.2.3	Gys1-ASO Treatment Decreases Neuronal Excitability in MKO Mice.....	57
5.3	<i>Discussion</i>	58
CHAPTER 6. ADAPTING THE PERSONALIZED MEDICINE PIPELINE FOR GLUT1 DEFICIENCY SYNDROME		67
6.1	<i>Introduction</i>	67
6.2	<i>Results</i>	68
6.2.1	Identifying mutations groups for Glut1	68
6.2.2	Mapping phenotypes to elucidate a genotype-phenotype correlation for Glut1DS.....	69
6.2.3	Elucidating genotype-phenotype correlations from patient data	70
6.3	<i>Discussion</i>	71
CHAPTER 7. CONCLUDING REMARKS.....		85
7.1	<i>Overall Summary</i>	85
7.2	<i>Limitations and Future Directions</i>	86
REFERENCES		89
VITA.....		101

LIST OF TABLES

Table 3.1 Bioinformatics Analysis of Recently Identified Patient Mutations	32
Table 3.2 Preliminary screening of laforin SNPs in the NCBI dbSNP Database.....	33
Table 3.3 Bioinformatics Analysis of Eight Novel Laforin SNPs in the NCBI dbSNP Database.	34
Table 6.1 Bioinformatics Analysis and Mutation Group Classification Based on Structural Analysis from Literature.....	74
Table 6.2 List of Amino Acids in Glut1 Critical for Transporter Function Based on Structural Analysis from Literature.....	77

LIST OF FIGURES

Figure 1.1 Publications on Personalized Medicine.....	11
Figure 1.2 Timeline of Progress in Personalized Medicine.....	12
Figure 1.3 Overview of Lafora Disease Pathology	13
Figure 1.4 Summary of Collaborations in the Lafora Disease Community	14
Figure 3.1 Laforin Function and Pipeline Overview	35
Figure 3.2 Methods Utilized in Pipeline Analysis.....	36
Figure 3.3 Pipeline Analysis of Laforin Patient Mutations	37
Figure 3.4 Pipeline Analysis of Laforin SNPs with Clear Pathogenicity Predictions via Bioinformatics	38
Figure 3.5 HDX Analysis of R108H Laforin Compared to WT Laforin	39
Figure 3.6 Pipeline Analysis of Laforin Mutations with Uncertain Pathogenicity Predictions via Bioinformatics	40
Figure 3.7 HDX Analysis of G101S Laforin Compared to WT Laforin.....	41
Figure 3.8 Multivariate Analysis of SNP Pipeline Results and Pathogenicity Assignments	42
Figure 4.1 IHC and MALDI Analysis of Glycogen Content in LKO and Laforin C266S (LCS) Mice Compared to WT	49
Figure 4.2 MALDI Analysis of Glycogen Content in WT, LKO, and MKO Mice	50
Figure 4.3 Quantification of MALDI Analysis of Glycogen Content in WT, LKO, and MKO Mice at 3 Months of Age.....	51
Figure 4.4 Quantification of MALDI Analysis of Glycogen Content in WT, LKO, and MKO Mice at 9 Months of Age.....	52
Figure 4.5 Metabolomics analysis of WT, LCS, LKO, and MKO mouse models.....	53
Figure 4.6 MALDI Analysis of Glycosylation in WT, LKO, and MKO Mice.	54
Figure 5.1 Using Antisense Oligonucleotide (ASO) Administration to Halt Lafora Body Aggregation.	62
Figure 5.2 Confirming Knock-Down of Glycogen Synthase (GYS1).	63
Figure 5.3 Quantifying Lafora Body Aggregation in the Hippocamps.....	64
Figure 5.4 Representative Images of MALDI Analysis Showing Glycogen Accumulation in Female Mouse Cohorts	65
Figure 5.5 Electrophysiology Analysis of Hippocampus Using Multi-Electrode Array	66
Figure 6.1 Schematic of Glut1 localization and function.....	78
Figure 6.2 Key Structural Features Reported in Glut1 Literature	79
Figure 6.3 Glut1 Proposed Mutation Groups	80
Figure 6.4 Glut1 Genotype-Phenotype Clustering from Literature-Reported Cases	81
Figure 6.5 Glut1 Proposed Phenotype Classifications	82
Figure 6.6 Glut1 Genotype-Phenotype Analysis from Uniformly-Reported Patient Data.....	83
Figure 6.7 Glut1 Genotype-Phenotype Analysis from Patients who Started KDT After 2 Years of Age.....	84
Figure 7.1 Roadmap for Building Genotype-Phenotype Correlations in Rare Disease Communities.....	88

CHAPTER 1. THE ROLE OF BASIC SCIENCE IN DEVELOPING PERSONALIZED MEDICINE FOR RARE DISEASES

1.1 The Evolution of Personalized Medicine

Hippocrates, the traditional Father of Medicine, observed in his writings that proper diagnoses of patients required an “examination of the patient’s constitution, age, physique, the season of the year, and the fashion of the disease”[1]. He elaborated on this concept, noting that patients with different predispositions would respond differently to the same disease. He similarly noted that patients with the same illness would respond differently when treated with the same therapy, and attributed this to the nature of their idiosyncratic differences [1, 2]. Over the next several millennia, physicians would work to explain this intuitive observation by Hippocrates. It was not until the 1950s that the understanding of biological molecules advanced to the point where they could be systematically manipulated, laying the foundation for predicting a patient’s response to a given drug [3, 4].

A giant leap forward came in 2003, with the completion of the Human Genome Project. The sequencing of the human genome presented an opportunity to link disease progression and severity to genetic drivers. Many cite this project as the birth of our modern concept of personalized medicine (also referred to as precision medicine) [3-5]. The term itself began to appear with growing frequency in medical publications starting in the early 2000s (Figure 1.1). Tracing the evolution of personalized medicine remains difficult, however, because the term has been widely applied to cover a variety of ideas in medicine and healthcare – from the differentiation of phenotypes within a patient cohort, to the variability in drug response, to the use of biobanks in biomarker discovery, to the development of designer drugs, and more. This expanding field claims the potential to revolutionize our healthcare system, but what exactly is meant by “personalized medicine?”

1.2 Defining the Scope of Personalized Medicine

In 2015, The National Institute of Health launched their Precision Medicine Initiative. In their executive summary, they defined precision, or personalized, medicine as: an approach to disease treatment and prevention which seeks to maximize effectiveness by taking into account individual variability in genes, environment and lifestyle [6]. In order to harness the power of big data to accelerate personalized medicine development, the initiative proposed a building cohort of one million volunteers willing to submit biospecimen and health data for research purposes [6].

The European Union similarly prioritized personalized medicine in the 2010s and committed nearly 1 billion dollars over the past decade to advance multi-omics

technologies for personalized diagnoses [7]. Additionally, in 2016, the European Commission launched the International Consortium of Personalized Medicine (ICPerMed) to coordinate international healthcare and research policies to facilitate the implementation of personalized medicine [8].

The transformative potential of personalized medicine is enormous. Francis Collins, Former Director of NIH, summed up the scope of transformation with the following observation:

*“Personalized medicine is a fantastic opportunity to take a **“one size fits all”** approach to diagnostics and drug therapy and prevention and turn it into an individualized approach. We all are similar, of course, but we are also different. And **the idea that medicine would be applied in a fashion that ignores those differences can’t be any more correct than going to the shoe store and buying any old pair of shoes without checking the size”** [9].*

As personalized medicine elucidates novel disease mechanisms, physicians and pharma companies can take a patient’s “shoe size” into account, tailoring medications to ensure the maximum benefit for each patient [7]. For conditions with multiple therapies, that means patients can be assigned the therapy or combination of therapies most likely to improve their condition. Even within each approved therapy, patients can be prescribed dosage based on their individual prognosis. In short, the goal of personalized medicine is to “target the right treatments to the right patients at the right time” [10].

1.3 The Current Landscape of Personalized Medicine

Personalized medicine accounts for more than a quarter of all new drugs approved by the FDA in the past seven years [11]. There are three primary fields of medicine pioneering new technologies for implementing personalized medicine: precision oncology, cancer immunotherapy, and rare diseases [12]. Of the 48 new molecular therapeutic drugs approved in 2021, 17 were designated as personalized medicine therapies, including nine for precision oncology, two for cancer immunotherapy, and seven for rare diseases [11]. The role of personalized medicine in each of these fields has been broadly reviewed [4, 7, 13-16]. However, a brief overview of the history and current strategies in each field is helpful to establish the existing barriers to expanding use of personalized medicine (Figure 1.2).

1.3.1 Precision Oncology

Precision oncology has evolved over the past 25 years, beginning in 1990s, with the discovery and targeting of proteins specific to a particular tumor. One of the earliest examples was the overexpression of HER2 in about a quarter of breast cancer patients [17]. These patients were often associated with poorer prognosis compared with those who did

not display HER2 overexpression in the tumor tissue [17]. The drug trastuzumab was approved by the FDA in 1998 to target HER2 overexpression in these tumors. While not a cure for the cancer, it did improve the prognosis for HER2 positive patients [18, 19]. In the following decades, additional molecular profiles in tumors were identified, leading to targeted drug development for these patient subgroups. In the early 2000s, histology was used to discover potential biomarkers and resulted in the identification of targets like BCR-ABL tyrosine kinase overexpression in chronic myeloid leukemia and mutations in the epidermal growth factor receptor (EGFR) in non-small cell lung cancer (NSCLC) [19]. Biomarker identification accelerated in the 2010s with the emergence of new DNA and RNA sequencing technologies, allowing for rapid epigenetic and proteomic analyses [19].

As more tumor profiles were collected, low frequency mutations that drive tumor growth were detected, raising a new challenge – how to decide what is targetable? And if a patient has multiple drivers, which one should they receive treatment for? These questions led to the development of master protocols, where researchers worked to automate the identification of therapeutic targets and therapy recommendations for individual patients [13]. Two types of master protocols emerged: basket studies, which identified drivers of tumorigenesis regardless of tumor tissue-type, and umbrella studies, which use genetic profiling to assign the best therapy option to patients who share the same tumor tissue-type [16]. In 2016, a comparison of cancer patients in genotype-matched treatments versus non-matched treatments revealed a higher response rate in patients that received a genotype-matched treatment [20]. Clinical studies are currently underway to define tumor profiles for metastatic cancers [21]. Challenges remain, including patients displaying acquired immunity to targeted treatments and keeping drug development on pace with the rate of target discovery, however, the progress made in cancer prognosis over the past several decades illustrates the promise of applying personalized medicine on a broad scale [22].

1.3.2 Cancer Immunotherapy

Cancer immunotherapy takes a slightly different approach from precision oncology. Rather than looking for patterns in genotype-phenotype correlation between groups of individuals, it seeks to use the unique properties of an individual's immune system to target tumor cells. The strategy of activating the body's immune system to fight cancer traces back to the 1890s, when William Bradley Coley noted that his cancer patients experienced tumor regression after erysipelas infection [23]. He isolated the bacterial strain responsible for the infection and began injecting those bacteria into the tumors of his cancer patients to attempt to induce tumor regression [14, 23].

In the 1980s, the discovery of immune checkpoints sparked new interest in cancer immunotherapy. Immune checkpoints regulate the body's immune system to prevent a cytotoxic immune response that kills cells. In cancerous cells, however, these immune checkpoints help the cells to survive immune attack. Inhibiting these checkpoints in tumor cells would allow the body's own immune system to target and destroy the cancer cells

[14]. Cytotoxic T-lymphocyte associated protein 4 (CTLA-4) was the first immune checkpoint to be discovered in 1987 [23]. In 2011, the first immune checkpoint inhibitor, ipilimumab was approved by the FDA [24]. Immune checkpoint inhibitors revolutionized cancer treatment, and researchers began to consider whether the immune system could be trained to recognize and target cancer cells through vaccination.

While the idea of cancer vaccination was more than a century old, the advancements in technology allowed for a personalized targeting of cancer cells in patients. To develop the vaccine, a patient's immune cells would be extracted and then processed to train them to recognize the cancerous cells. These processed cells are then re-injected into the patient's circulation to trigger their immune response against the cancerous cells. The FDA approved the first autologous cancer vaccine, sipuleucel-T, to treat a specific form of prostate cancer in 2011 [23]. While it did not appear to halt disease progression, it did extend the overall survival of diagnosed patients. The next evolution in cancer immunotherapy was the emergence of Adoptive Cell Therapy (ACT). With ACT, a patient's tumor-targeting T-cells are removed, modified and multiplied in a laboratory, and then re-introduced into the patient's circulatory system. Perhaps the best-known form of this therapy came from Chimeric antigen T-Cells (CAR-T therapy). The first CAR-T cells therapy was approved by the FDA in 2017 to treat relapsed B-cell acute lymphoblastic leukemia in children [25]. As with precision oncology, the threat of acquired resistance remains a challenge that needs to be addressed [23]. However, this technology demonstrates the power of harnessing our immune system to fight cancer and achieve long-lasting remission.

1.3.3 The Opportunities for Expanding Personalized Medicine for Rare Disease

The Orphan Drug Act of 1983 defined rare disease as a disease with less than 200,000 people affected in the United States [26]. While individual prevalence is low, collectively, the more than 7,000 recognized rare diseases in the United States affect an estimated 30 million people [27]. To put that in perspective, the National Cancer Institute estimates 16.9 million Americans are cancer survivors, with an estimated 1.8 million new cases annually. For cancer, the evolution of personalized medicine was driven by the discovery of genetic drivers for aggressive variants of specific cancers. In the rare disease community, more than 80% of the 7,000 diseases have a known genetic driver [28]. In spite of that, less than 5% of rare diseases have effective treatment [27]. A significant challenge lies in finding a patient cohort large enough to study using the methods of traditional medicine. This is where the approach of precision medicine offers several advantages. First, biomarker discovery, as demonstrated by precision oncology, can aid with diagnosis and set the path for early diagnosis and treatment. Second, genotype-phenotype correlations can be employed not only for diagnosis, but also for patient prognosis, opening the door for new therapeutic targets based on the disease mechanism for an individual [29]. With the development of mechanism-based therapies comes the ability to restructure drug approval on a personalized basis. Non-profit companies like N-Lorem are working to

develop N-of-1 models as a pathway to approve therapies for ultra-rare genetic diseases, which may have as little as a single case in a given country [30].

The advent of big data also presents exciting possibilities for applying precision medicine to rare disease. Biobanks provide material for multi-omics analysis. RNAseq, proteomics, and metabolomics are data-rich sets allowing for untargeted analysis and unbiased discovery of novel biomarkers. Additionally, the development of high-throughput cell screening and organ-on-a-chip technology creates an opportunity for more precise drug targeting and mutation analysis [31, 32]. As these tools become more integrated and broadly accessible, the ability to quickly assess the impact of specific mutations on disease makes personalized medicine feasible, even for rare diseases [29, 33]. To support greater integration of basic and translational sciences, a set of master protocols will need to be developed, much as they were for precision oncology, to allow for broad adaptation between rare diseases to expand capacity for personalized medicine.

1.3.4 Cystic Fibrosis: A Case Study in Applying Personalized Medicine for Rare Disease

In the field of rare diseases, an early pioneer in personalized medicine was Cystic Fibrosis (CF). Patients with Cystic Fibrosis have a mutation in their cystic fibrosis transmembrane conductance regulator (CFTR), which is a cAMP-modulated chloride and bicarbonate channel on the apical plasma membrane of epithelial cells [34-36]. The disruption of CFTR function leads to mucosal build up in the airways and chronic inflammation [36]. While this impacts multiple organs, it is the deterioration of the lungs and respiratory system that prove fatal [37]. Patients slowly suffocate, requiring incubators to assist with their breathing as they progress through the disease [37]. Around 70,000 people worldwide are currently diagnosed with CF [38]. There are more than 2000 known mutations in the *CFTR* gene, contributing to a high variability in observed patient phenotype and severity of disease progression [39]. Noting the spectrum of disease progression, researchers began work in the 1990s to identify a genotype-phenotype link that would distinguish late-onset CF from classic CF and identify new therapeutic options for patients with mild disease progression [40].

Basic science analysis of the CFTR mutations allowed the 2000+ reported mutations to be grouped into classes based on their effect on CFTR protein function. Six distinct classes emerged: mutations that impacted *CFTR* mRNA transcription (I), mutations that impacted CFTR trafficking to the plasma membrane (II), mutations that fully obstructed the CFTR ion channel (III), mutations that partially obstructed the channel (IV), splicing or missense mutations that reduced expression levels of CFTR (V), and mutations that destabilized the CFTR protein leading to a reduced half-life of the protein (VI) [41, 42]. Mutation classes I-III correlated with classic CF disease progression, while IV – VI were frequently associated with late-onset CF. This definition

of mutation classes allowed for targeted therapeutic development based on the functional defect introduced by the mutation [43].

Within the Class I mutations, the most severe cases were linked to complete loss of *CFTR* gene expression, which, in the absence of gene editing, had no potential solution [43]. The second cohort of patients in Class I had a premature stop codon. The use of read-through compounds was proposed to serve this cohort [43]. The Class II mutations produce a highly destabilized protein that gets targeted for degradation in the endoplasmic reticulum. For these patients, a high-throughput screen of pharmacological small molecules was performed to identify correctors that could rescue protein trafficking to the membrane [43-45]. For Class III and IV mutations with full or partial blockage of chloride ion transport, small molecule potentiators were developed to open the mutated channel and restore ion transport [43, 44]. Class V and VI mutations had no damage to the channel, but in Class V the splicing mutation reduced the amount of protein synthesized, and Class VI missense mutations led to a destabilization of the transporter, increasing the rate of ubiquitination and protein turn-over. Antisense Oligonucleotide (ASO) therapies were proposed to address the splicing errors, and stabilizer molecules were screened to treat patients with Class VI mutations [43]. Based on this roadmap, therapy options were pursued in parallel, and currently the correctors for protein trafficking (Class III) and potentiator therapies for channel gating mutations (Class IV) have received FDA approval [41]. The basic science research proceeded in parallel to studies of CF patients, identifying and improving diagnosis of biomarkers for *CFTR* impairment [39]. The Cystic Fibrosis success narrative demonstrates the critical role of basic science in providing a roadmap to guide pharmaceutical development and translational sciences. The question becomes, why are more rare diseases not pursuing this route?

1.3.5 The Barriers to Expanding Personalized Medicine for Rare Disease

As with any significant change to the status quo, systemic challenges have slowed the development and implementation of personalized medicine. In 2015, the European Commission Coordination and Support Action (CSA) PerMed released their Strategic Research and Innovation Agenda (SRIA). In the SRIA, five primary challenges to implementing personalized medicine are outlined: (1) developing awareness and empowerment, (2) bringing innovation to the healthcare market, (3) integrating big data and information and communication technology (ICT) solutions, (4) making PM healthcare sustainable, and (5) translating basic science to clinical research [8].

Of the five identified barriers, the first four are largely tied to the healthcare system itself. Consider the first barrier of raising awareness: as new information becomes available, how does one educate physicians so they can utilize these new diagnostic technologies and prescribe personalized treatment strategies? This question leads to the second barrier: bringing innovation to the healthcare market. How do you ensure the

patients who most need the treatment will be able to access it? New infrastructure will be required to support personalized analyses, such as expanded use of biobanks and shared access to patient records. As more patient information is collected, the problem becomes: how does that data get processed, stored, and shared? There is great potential to integrate big data to identify targets for personalized medicine, but this collection of data will be of little use without ICT solutions and strategies for interpreting and analyzing the data. Addressing these barriers will go a long way toward making personalized medicine more accessible.

Another aspect of accessibility is affordability, which leads to the challenge of making personalized medicine sustainable. The healthcare market would need to be adjusted to account for more expensive medications and have the flexibility to allow patients to take the therapy best suited for their needs. With the increased expense, payment strategies would need to be revisited and restructured to make healthcare sustainable without disincentivizing pharma companies from pursuing therapies for personalized medicine. As it stands currently, some of the most expensive medications in the world are personalized medications for rare diseases – pharma companies argue that the high price is needed to cover the cost of therapy development. In this area at least, several strategies are being developed to mitigate the cost and risks associated with rare disease therapy development. The Orphan Drug Designation, first piloted in the EU in the early 2000s, provides a suite of incentives for pharma companies working on rare disease therapies: including tax breaks, fee exemptions, and market exclusivity for a set period of time [33, 46].

All of these challenges identified in the SRIA present barriers to the implementation of personalized medicine, but the fifth barrier determines what is possible: translating basic science to clinical research. Without a stronger integration of basic science and clinical research, the personalized medicine solutions will not exist. Standards should be implemented to facilitate better integration between reported clinical data and basic science investigations. An additional challenge to translational science is funding. Even with the push in recent years to provide grant money for collaborative projects, the number of funded labs will never match the number of rare diseases. In order to secure funding, patient advocacy groups need a scientist or research-clinician advocate to coordinate collaborative grant applications. Even when funding is available, the small patient sample size presents a challenge to rare disease research. Patterns driven by specific gene mutations become harder to detect when the patients are scattered all over the globe with greatly different environmental factors. And with patients being geographically diverse, there is rarely consensus on what phenotype data should be recorded for the patient [29]. Without sufficient phenotype data, the goal of genotype-phenotype correlation breaks down, limiting the ability to develop personalized therapies.

To address genotype-phenotype knowledge gap, we have utilized the rare disease Lafora Disease to construct a framework that other rare diseases may apply.

1.4 Lafora Disease: A model for expanding PM in the Rare Disease Community

Lafora disease (LD) is an ultra-rare fatal childhood dementia and epilepsy. LD was first identified in 1911 by Spanish neurologist Gonzalo Lafora [47]. During *post mortem* investigations, he observed glycogen-like aggregates in their brain, and these aggregates were later termed Lafora Bodies (LBs). For the next several decades, patients were diagnosed by skin biopsy and identification of LB aggregates. In the late 1990s and early 2000s, two genetic drivers for LD were determined: a mutation in *epilepsy, progressive myoclonus 2A (EPM2A)* or a mutation in *epilepsy, progressive myoclonus 2B (EPM2B)* [48-51]. *EPM2A* encodes a phosphatase, laforin, which has the ability to remove phosphate groups from glycogen. *EPM2B* encodes an E3 ubiquitin ligase, malin, which has been shown to ubiquitinate multiple enzymes involved in glycogen synthesis and degradation (Figure 1.3A-D) [52-56].

While the precise mechanism for LD remains to be elucidated, the impact of functional impairment in either laforin or malin has been well-characterized. Together, laforin and malin regulate glycogen metabolism, the macromolecule storage unit for glucose. Glycogen is a soluble polyglucosan synthesized by Glycogen Synthase (GYS1), which creates linear chains of α -1,4-linked glucose moieties, and Glycogen Branching Enzyme (GBE), which synthesizes α -1,6-linked branch points every 10-12 glucose moieties. The result is a soluble macromolecule that can store up to 22,000 glucose moieties. When glucose is needed, glycogen is degraded by Glycogen Phosphorylase (GP), which releases the linear α -1,4-linked moieties, and Glycogen Debranching Enzyme (GDE), which removes the α -1,6-linked branch points. When laforin or malin are functionally impaired, the architecture of glycogen changes: linear chain lengths are extended, branch points are less frequent, and the glycogen becomes hyper-phosphorylated (Figure 1.3A) [57-59]. Collectively, these changes decrease glycogen solubility, and the aberrant glycogen begins to aggregate into insoluble LBs in the cytoplasm of nearly all tissues in the body (Figure 1.3B) [59, 60]. LBs are particularly damaging in the brain, where they have been linked to neurodegeneration [61, 62]. Importantly, multiple studies from different laboratories have demonstrated that LBs drive the progression of LD, therefore, the LBs and glycogen synthesis have been the primary targets of therapeutic development [63-67].

Regardless of the driver gene, LD patients exhibit LB aggregation and a similar phenotypic progression [49, 68-71]. In Classic LD, children develop seemingly normal until adolescence, when they begin to experience absence and generalized tonic-clonic seizures with increasing frequency and severity [70, 72]. As the seizures progress, movement disorders emerge, including ataxia, dysphasia, and dysarthria [72, 73]. Cognitive decline is observed as the LB-driven neurodegeneration worsens, resulting in childhood dementia [73, 74]. Within the span of 10 years, patients experience almost continuous myoclonus in a vegetative state, and most die from respiratory failure during this stage [68, 73, 74]. In the 2010s, reports of a Late-onset LD emerged [75-77]. While these patients experienced the same phenotypic progression, the seizures did not present until their late teens or early twenties [75-77]. One patient was reported to survive into their forties [78]. It was hypothesized that these patients had milder mutations and research to construct a genotype-phenotype spectrum for LD began. If the rate of disease progression

could be predicted from the patient mutation, then clinical trials could select the patients most likely to benefit from the therapy, and as therapies were approved for treatment, patients could be matched with the therapy and dosage best suited for their rate of disease progression.

Defining a spectrum for personalized medicine in LD faced the same challenges many other rare diseases experience. As an ultra-rare disorder, only several hundred patients exist worldwide and many of them exhibit novel, *de novo*, mutations [71, 73]. While genetic mutations play a critical role in defining the rate of disease progression, environmental and lifestyle factors are not insignificant, and with such a small sample size, teasing apart the genetic contribution from the environment and lifestyle contributions becomes extremely challenging. Therefore, researchers turned to structure-function characterization of each patient mutation to construct a genotype-phenotype spectrum, which is often a time- and resource-intensive process.

At the same time, the LD community has overcome barriers that other rare diseases encounter when seeking to create a personalized medicine platform. First, the genetic drivers have been identified [48, 51]. Second, there were clinical and basic science champions for LD research. [79]. Third, an organized patient community played an instrumental role in bringing together LD research laboratories around the world to apply for joint funding through the NIH. Upon the receipt of that grant, the research laboratories were able to accelerate basic science analysis of patient mutations: determining the 3-dimensional structure of laforin, characterizing known patient mutations, and elucidating the physiological impact of loss of function in laforin or malin [79-81]. Impressively, this work identified multiple therapeutic targets and led to the development of three potential therapies for LD: an antibody-enzyme fusion that degrades LBs, a small molecule to inhibit glycogen synthesis, and an antisense oligonucleotide (ASO) to inhibit glycogen synthesis. Additionally, the LD community has benefited from collaboration between researchers and clinicians who determined the best parameters to track for patient phenotypes and potential biomarkers. Once again, an active and engaged patient community helped to secure grant funding for the start of a global patient registry with uniform reporting and record-keeping, allowing for better phenotype-genotype correlation. In this collaborative environment, LD is evolving as a model for other rare diseases seeking to define patient cohorts for personalized medicine (Figure 1.4).

1.5 Overview of the Dissertation

The goal of this dissertation is to present a model for the role of basic science in developing personalized medicine platforms for rare disease. This dissertation will (1) define a suite of tools for structure-function characterization in LD to define patient cohorts, (2) evaluate the efficacy of a potential therapeutic for LD given the defined patient cohorts, and (3) demonstrate the flexibility of the model by adapting it to study another rare disease, Glut1 Deficiency Syndrome (G1D).

In Chapter 2, we highlight the methods of biochemical and omics analyses utilized for genotype-phenotype correlation. In Chapter 3, we present a pipeline for rapid *in vitro* characterization of function loss of laforin, allowing for the definition of patient cohorts based on the genetic mutation. In Chapter 4, we demonstrate the role of mouse models and cell culture in elucidating genotype-phenotype correlations. In Chapter 5, we evaluate an ASO recently developed by Ionis Pharmaceuticals to treat LD and discuss the implications of this therapy for the defined patient cohorts. Finally, in Chapter 6, we extrapolate our model for another rare metabolic disease, G1D, to illustrate how this model can provide a framework for other rare diseases to create platforms for personalized medicine.

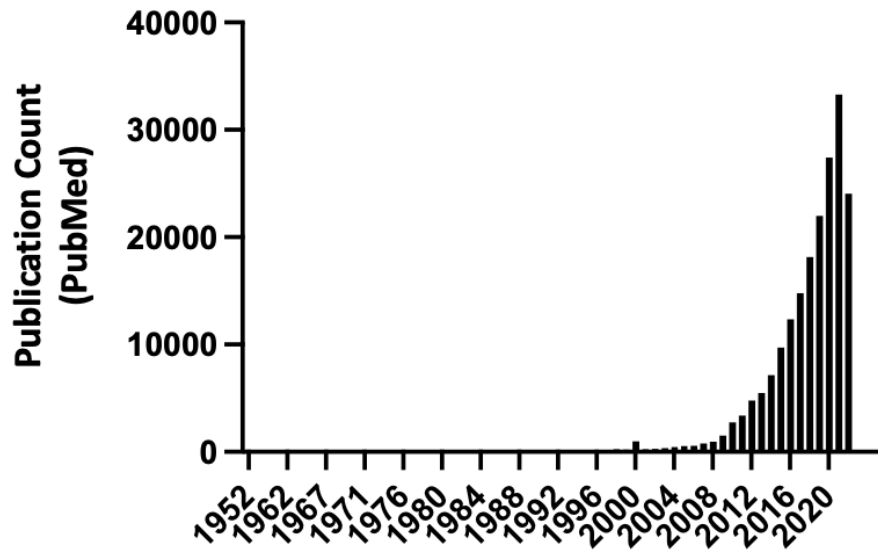


Figure 1.1 Publications on Personalized Medicine

Graph shows the results of a PubMed search on the number of publications referencing personalized or precision medicine since 1952.

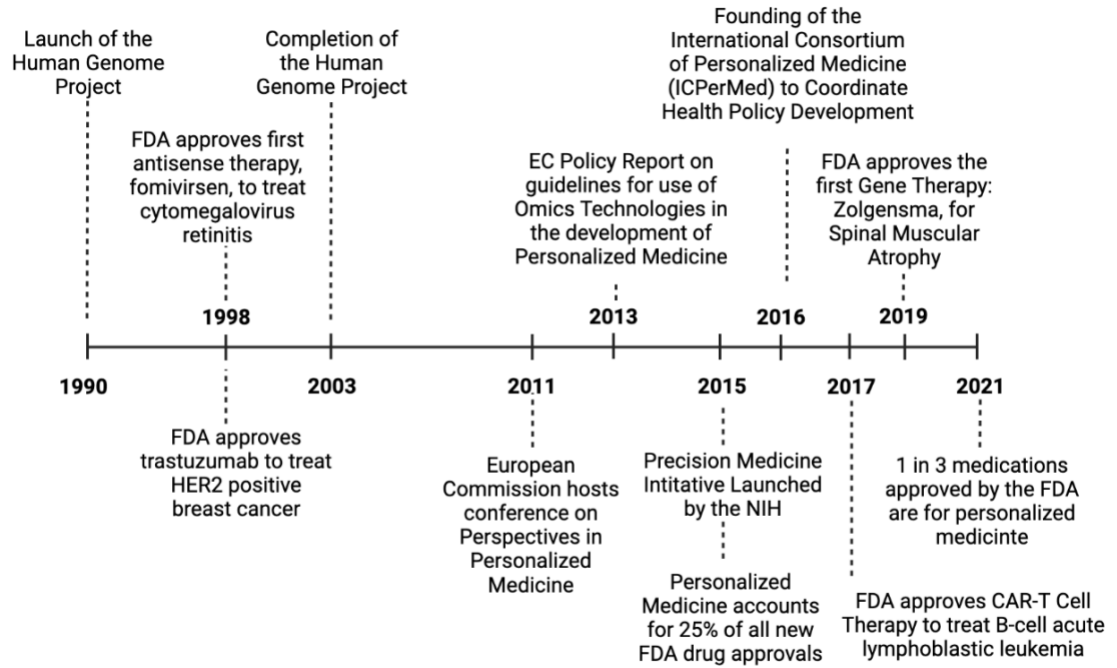


Figure 1.2 Timeline of Progress in Personalized Medicine

This timeline highlights some, but by no means all, of the key project and policy developments in the field of personalized medicine since the launch of the Human Genome Project.

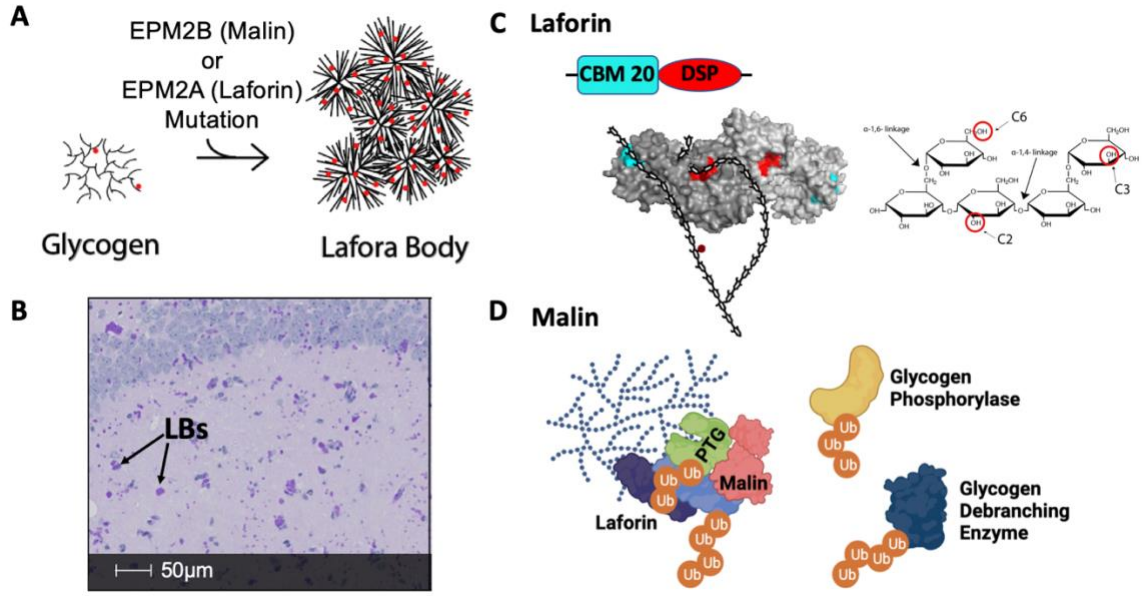


Figure 1.3 Overview of Lafora Disease Pathology

A) Schematic reflecting the changes in glycogen architecture when there is a loss-of-function mutation in *EPM2A* or *EPM2B*. Aberrant glycogen is characterized by extended chain-lengths, poor branching, and hyper-phosphorylation.

B) Periodic Acid-Schiff (PAS)-stained mouse brain tissue in the hippocampus. Arrows indicate the resulting Lafora Body (LB) deposits in the tissue.

C) Schematic of laforin protein, highlighting the two functional domains, the Carbohydrate Binding Module (CBM) and Dual Specificity Phosphatase (DSP) domains, paired with a hypothetical interaction with a glycogen chain (protein structure from PDB: 4rkk). To the right of the structure is a highlight of the glucose moiety connectivity, showing the C2, C3, and C6 positions where phosphate can be attached. Laforin can remove phosphate from any of these sites.

D) Cartoon illustrating proposed activity of the E3 ligase malin. Malin is known to ubiquitinate laforin, as well as other glycogen-regulating enzymes – including protein targeting to glycogen (PTG), Glycogen Phosphorylase, and Glycogen Debranching Enzyme.

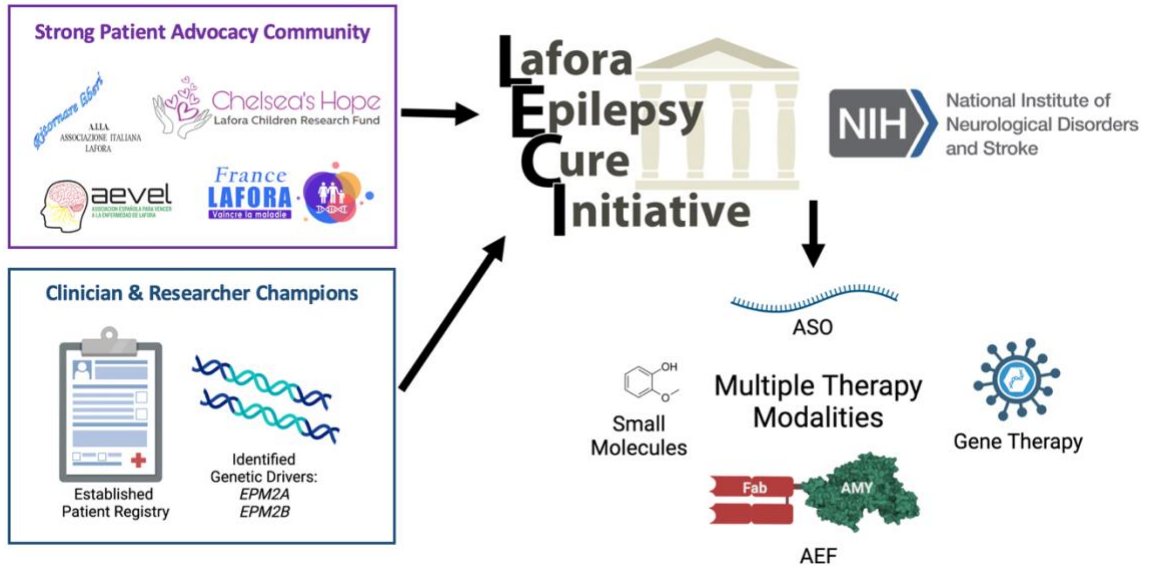


Figure 1.4 Summary of Collaborations in the Lafora Disease Community

This graphic highlights the various organizations and collaborations within the Lafora Disease (LD) Community. The LECI funded through the NIH led to the development of multiple therapy modalities to treat LD.

CHAPTER 2. MATERIALS AND METHODS

2.1 Methods for Bioinformatics and Biochemical Analyses of Laforin and Glut1 Mutations

2.1.1 Protein Expression and Purification

Residues 1-328 of *H. sapiens* (Hs) laforin were expressed from pET28b (Novagen) with an N-terminal His₆ tag fusion. Site-directed mutagenesis was performed by Genscript to generate mutant constructs in pET28b plasmids. Wildtype and mutant proteins were then transformed into BL21 DE3 Competent *E. coli* cells and grown in 2xYT media (16g Tryptone, 5g NaCl, 10g Yeast, 1L DI H₂O) while shaking at 37°C and allowed to reach OD₆₀₀ = 0.6. Protein expression was then induced with 0.4mM isopropyl β-D-thiogalactoside and allowed to incubate at 16°C for 16 hours and then spun down on the centrifuge at 3500xg. Cells were lysed in HEPES buffer (100mM NaCl, 1mM 2-Mercaptoethanol, 50mM HEPES at pH 8). Lysates were then sonicated and centrifuged at 13,500xg at 4 °C for 15 minutes. The supernatant was then decanted and incubated with 5 mL of His-Select Nickel Affinity Gel for 30 minutes and then subjected to multiple washes before eluting with 300mM imidazole. Soluble proteins were then loaded onto a fast protein liquid chromatography machine (FPLC) and run on the S75 column after equilibration with HEPES gel filtration buffer, pH 8. Fractions with the eluted proteins were then concentrated for use in assays, and samples from each fraction were run on SDS-PAGE to confirm mutant purification.

2.1.2 SDS-PAGE & Native Gels

Protein samples were subjected to SDS-polyacrylamide gel electrophoresis in order to assess purity using pre-made 12% stain free mini gels (BioRad). The samples ran at 240V for 27 minutes. Samples were loaded with 15 µg protein per well using 4x Lamaelli loading buffer (BioRad).

Protein samples were run using the Native-PAGE protocol as previously described [82]. Briefly, the gels were composed of acrylamide (9mL), riboflavin (10mg/mL solution), and TEMED (20µL). The gels were run in Tris-Borate 5X Running Buffer (15.15g Tris Base, 3.86g Boric Acid, 500mL ddH₂O, pH 8.7)) and samples prepared in Tris-Borate Loading Buffer (0.66g Tris Base, 0.15g Boric Acid, 20mg Bromophenol Blue, 1mL Glycerol, 10mL ddH₂O). The proteins were run at a concentration of 0.5mg/mL in 1X running buffer. 5µL of NativeMark protein ladder was used for each gel. The gels were run at 100V for 5 hours. Gels were stained for 30 min using Coomassie stain, then incubated

overnight in destain buffer (10% acetic acid, 50% methanol, and 40% ddH₂O). The gels were imaged on a BioRad ChemiDoc system.

2.1.3 Differential Scanning Fluorimetry (DSF)

Measurement of thermal stability of the laforin constructs was accomplished using a CFX96 Real Time PCR system. DSF buffer (50mM HEPES, 100mM NaCl, 2.5mM BME, pH 8.0) was mixed with 5X SYPRO Orange Protein Dye (ThermoFisher) and 0.5 μ M of protein. The final volume for each sample was 40 μ L. The samples were then heated using a thermal gradient from 20 – 90°C at a rate of 1°C/60s). The relative fluorescence units were measured and used to determine the melting temperature of each construct. For the thermal shift assays, a gradient of 0 – 125mM of maltoheptaose (DP7) (CarboExpert) was dissolved in DSF buffer and used as a substrate for each mutant to assess carbohydrate-protein interactions. All data were analyzed using GraphPad Prism.

2.1.4 Para-nitrophenylphosphate (pNPP) Assay

Laforin wildtype and mutant phosphatase activity was measured using the pNPP assay which has been previously described [83]. Briefly, using a flat-bottom 96-well plate (Corning), each well received 10 μ L of 5X pNPP buffer (0.5M Na-Acetate, 0.25M Bis-Tris, 0.25M Tris, pH 6), 1 μ L of 100mM DTT, 5 μ L of 0.5M pNPP, 200ng of purified laforin protein, and MiliQ for a total volume of 50 μ L H₂O. The pNPP substrate was added last. The plate was then incubated at 37 °C for either 10 or 30 minutes. After the appropriate incubation period, the reaction was quenched with 200 μ L of 0.25M NaOH, and absorbance levels were read at 410nm using a UV Spectrophotometer.

2.1.5 Yeast Two-Hybrid Assay (Y2H)

Saccharomyces cerevisiae strain THY-AP4 were transformed with combinations of the following plasmids: pACT2-GAD \emptyset , pACT2-GAD-Malin, pACT2-GAD-R5/PTG and pEG202 LexA-Laforin (for wildtype laforin, SNPs and patient mutations). pEG202 LexA-Laforin SNPs and patient mutations were prepared by GeneWiz. Transformants were grown in SC medium up to an OD = 0.5 and were permeabilized with chloroform/SDS. Extracts were prepared as previously described [84]. Samples were separated by SDS-PAGE and analyzed via Western blotting using the corresponding anti-LexA (Santa Cruz Biotechnology), anti-HA (haemagglutinin; Sigma) antibodies. Y2H assays were performed as previously described [85]. Transformants were screened for activity using a β -galactosidase qualitative filter lift assay. The β -galactosidase reaction was completed at

30°C in the presence of o-nitrophenyl-β-D-galactopyraniside (ONPG). Activity was quantified at 420nm and measured in Miller Units.

2.1.6 Hydrogen-Deuterium eXchange (HDX) Mass Spectrometry

Deuteration experiments on laforin wildtype (WT), G101S, and R108H were performed as previously described [86]. Deuterated laforin samples were prepared by incubation of 10μg protein with D₂O buffer (300mM NaCl, 50mM Tris-HCl, 3mM TCEP, pD 7.1) at 0°C for 10, 30, 100, 300, 1000, 3000, and 10000s, and then quenched (5.3% v/v formic acid, 15% v/v glycerol, 2.5M GuHCl, 39mM TCEP, pH 2.4). Quenched samples were digested with pepsin and peptides were separated by chromatography. Mass spectrometric analysis of peptides was performed using an LCQ Classic (Thermo Fisher) electrospray ion trap-type mass spectrometer and an electrospray Q-TOF mass spectrometer (Waters Corp, Milford, MA). Data from all sample sets were acquired from a single automated run of 8 hours. Deuteration experiments were also performed with 5mg/ml rabbit liver glycogen (Sigma). Maximum changes in deuteration for peptides were used to determine the difference between WT and mutant laforin and differences with each protein binding to glycogen.

2.1.7 Bioinformatics

Using the NCBI dbSNP database, more than 300 SNPs for EPM2A were identified. From that list, SNPs producing a missense mutation in an exonic region were selected. The list was further narrowed to 25 SNPs with “uncertain” clinical significance in ClinVar. From this list, 8 SNPs were selected for analysis via the pipeline.

Multiple bioinformatics tools were used to assess the impact of each patient and SNP missense mutation. *PolyPhen-2* was used to predict the effect an amino acid substitution will have on laforin function and structure [87]. Cologne University Protein Stability Analysis Tool (CUPSAT) and Site Directed Mutator (SDM) were used to predict the effect of each mutation on protein stability [88, 89]. For the novel SNPs, additional analyses were run on Meta-SNP and PhD-SNP toolkits that integrate multiple bioinformatics engines to predict pathogenicity, along with SNAP, a bioinformatics engine that predicts pathogenicity based on allelic frequency [90-94]. For bioinformatics analyses requiring a protein structure, the structure of C266S laforin was accessed from the PDB (4rkk) [86].

2.1.8 Statistics

DSF, pNPP, and Y2H assays were run in triplicate. The mean and standard deviation were calculated in Excel and imported into GraphPad prism for further analysis. Statistically significant differences from the WT laforin were determined using the two-tailed student t-test. Significance levels are indicated by asterisks: *, $p < 0.05$, **, $p < 0.01$, and ***, $p < 0.001$.

For multivariant analysis of laforin mutations, data points from DSF, pNPP, and Y2H assays were reported as a percent difference from the WT mean value. To account for variation in WT values, three individual WT profiles were entered with values reported as the percent difference from the WT mean value. All values were normalized using range scaling. Heatmap clustering was performed by importing the normalized data into MetaboAnalyst using Euclidean distance measuring and Ward clustering.

For phenotype clustering of Glut1 patients from literature, mutations were listed and labeled with the group number matching the predicted loss of function. Phenotype parameters were then marked as “1” (present), “0” (absent), or “NA” (not specified). The data were imported into MetaboAnalyst for Heatmap clustering using Euclidean distance measuring and Ward clustering. In the phenotype clustering from the German patient cohort treated by Dr. Jeorg Klepper, additional non-binary parameters were added. The retardation, epilepsy, and movement scores were calculated as an aggregate of the number of manifestations reported (for example, a patient with focal, absence, and tonic-clonic seizures received a score of “3”). Additionally, the age of onset and the glucose CSF levels were included in the dataset. All values were then normalized with range scaling to prevent bias toward the non-binary values. Finally, the heatmap clustering was performed as previously described using the MetaboAnalyst Heatmap function with Euclidean distance measuring and Ward clustering.

Statistical analyses were carried out using GraphPad Prism. All numerical data are presented as mean \pm SD. Grouped analysis was performed using two-way ANOVA. Column analysis was performed using one-way ANOVA and Tukey’s multiple comparisons test or student t-test as indicated in the figures. A P-value less than 0.05 was considered statistically significant.

2.2 Methods for Mouse Model Analyses to Determine Driver-Gene Variations and ASO Therapy Efficacy

2.2.1 Mice and ASO Delivery

The malin KO (MKO) mouse model breeding and injection protocols were carried out by Ionis Pharmaceuticals. All animal procedures were approved by Ionis Pharmaceuticals Institutional Animal Care and Use Committees [58, 65]. In brief, male and female mice were anesthetized with isoflurane, and 300 μ g ASO in 10 μ l PBS were

injected intracerebroventrically (ICV) at 4-, 7-, and 10-months, alternating ventricles at successive time points. Stereotactic injection coordinates were 0.3mm anterior/posterior (anterior to bregma), 1.0mm to right or left medial/lateral and -3.0mm dorsal/ventral. The *Gys1*-ASO sequence is 5'-CATGCTTCATTTCTTTATTG-3'. Littermate controls received injections of a non-target ASO, 5'-CCTATAGGACTATCCAGGAA-3' (Control ASO), or PBS. Mice were sacrificed at 13 months by cervical dislocation and decapitation. The hemisphere ipsilateral to the injection site was snap-frozen in liquid nitrogen for qRT-PCR and biochemical analyses, and the other immersed in 10% neutral buffered formalin for histo- and immunohisto-pathology as well as matrix-assisted laser desorption/ionization (MALDI) analysis.

2.2.2 *Gys1* mRNA Expression Analysis

Sample RNA was extracted utilizing the Qiagen RNeasy Mini Kit. Prior to usage, samples were homogenized with a QIAgen QIAshredder. Homogenized tissue was centrifuged at full speed for 3 minutes and the supernatant was added to RNeasy columns for subsequent steps. DNase digestion was performed with the RNase-Free PureLink DNase set (Invitrogen). mRNA expression was measured using qRT-PCR with Reliance One-Step Multiplex RT-qPCR Supermix (Bio-Rad) for cDNA synthesis and Bio-Rad PrimePCR probes for *Gys1* (assay id: qHsaCIP0032887) and GAPDH (assay id: qMmuCEP0039581).

2.2.3 *Gys1* Protein Expression Analysis

Frozen brain tissue was homogenized using a SPEX Sample Prep Freezer/mill 6775 and placed into RIPA buffer (50mM Tris-HCl, 2% SDS, pH 7.4) containing protease and phosphatase inhibitors (SigmaAldrich 5872S). Protein concentration was determined using a BCA Protein Assay Kit (Thermo Scientific 23225). Protein was standardized at 30µg and diluted with 6X SDS loading buffer. Samples were boiled (96°C, 5 minutes) and loaded onto a 4-15% Stain-Free TGX Gel (Bio-Rad #4568085) for Western blotting. A wet transfer was performed overnight at 10V to ensure the transfer of protein onto the PVDF membrane (Bio-Rad). Anti-GYS1 (Cell Signaling #3893) and anti-beta actin (Bio-Rad #12004163) were utilized as primary antibodies and Goat Anti-Rabbit HRP-conjugated secondary antibody (Bio-Rad #1706515) was utilized and developed with Clarity ECL-Substrate (Bio-Rad #1705060). After developing, blots were analyzed using a ChemiDoc Imaging System (Bio-Rad #27444). To quantify the blots, blots were analyzed using ImageJ software with the rectangle and integration tools to measure the intensity of each band. Data were exported and graphed in GraphPad Prism and analyzed using a one-way ANOVA.

2.2.4 Histological Analysis

Formalin-fixed brains were embedded in paraffin blocks. Samples were sectioned, placed on slides, and stained with periodic acid-Schiff (PAS) or IV58B6 anti-glycogen antibody (29). Slides were scanned using a Zeiss Axio Scan Z1, then loaded into HALO v3.3.2541.345 software designed by Indica Labs. HALO software was used to annotate brain regions including the hippocampus and the cerebellum, then Indica Labs Area Quantification v1.0 was used to quantify the percent positive stain. Results were graphed in GraphPad Prism and analyzed using both a one-way ANOVA and a student t-test as indicated in the figures.

2.2.5 Gas Chromatography Mass Spectrometry (GCMS) Analysis

Polar metabolites were extracted from 20mg of pulverized frozen tissue using 50% methanol. Samples were vortexed and placed on a cell disruptor for 3 minutes, then spun down at 15,000rpm. 250 μ L of the supernatant was transferred to a v-shaped amber chromatography vial and dried using a SpeedVac. Dried samples were derivatized by the addition of 20mg/mL methoxyamine hydrochloride in pyridine and incubation for 1.5 hr at 30°C. Sequential addition of N-methyl-trimethylsilyl-trifluoroacetamide (MSTFA) followed with an incubation time of 30 min at 37°C with thorough vortexing between addition of solvents completed the derivatization process. An Agilent 7800B gas-chromatography (GC) coupled to a 7010A triple quadrupole mass spectrometry detector equipped with a high-efficiency source was used for this study. GCMS protocols were similar to those described previously [95, 96]. Relative abundance was corrected for recovery using the L-norvaline standard and adjusted to protein input represented by pooling amino acids detected by GCMS [97]

2.2.6 Glycogen and Glycan Quantification via MALDI Analysis

Tissues were sectioned at 4 μ m and mounted on positively charged glass slides for MALDI imaging with 3 brains represented on each slide according to a previously described protocol [98]. Slides were prepared for MALDI analysis using a previously described method [99, 100]. In brief, the slides were heated at 60°C for 1hr, allowed to cool, then deparaffinized by washing twice in xylene (3min each). Tissue sections were rehydrated by submerging the slide twice in 100% ethanol (1min each), once in 95% ethanol (1min), once in 70% ethanol (1min), and twice in water (3min each). After the water wash, each slide was transferred to a coplin mailer containing the citraconic anhydride buffer for antigen retrieval and the mailer was placed in a vegetable steamer for 25min. Citraconic anhydride (ThermoFisher) buffer was prepared by adding 25mL citraconic anhydride in 50mL water and adjusted to pH 3 with HCl. After cooling, the buffer was exchanged with water five times. The slide was then desiccated prior to

enzymatic digestion. An HTX spray station (HTX) was used to coat the slide with a 0.2mL aqueous solution of isoamylase for glycogen analysis and/or PNGase for glycan analysis (4 Units/slide). The spray nozzle was heated to 45°C and the spray velocity was 900m/min. Slides were then incubated at 37°C for 2hr in a humidified chamber and dried in a desiccator prior to matrix application [a-cyano-4-hydroxycinnamic acid matrix (0.021g CHCA in 3mL 50% acetonitrile/50% water and 12mL TFA) applied with HTX sprayer]. For the detection of glycogen, a Waters SynaptG2-Xs high-definition mass spectrometer equipped with traveling wave ion mobility was used. The laser was operating at 1000Hz with an energy of 200AU and spot size of 50mm, mass range is set at 500 – 3000m/z. Images of glycogen were generated using the Waters HDI software [98].

2.2.7 Measurement of Neuronal Excitability

MKO mice and wildtype littermates at 4 months of age were selected and divided into treatment groups: ICV vehicle-injected wildtype mice, ICV vehicle-injected MKO mice, and ICV Gyl1-ASO injected MKO mice, with n=10 (5 males and 5 females). Mice were injected with vehicle or ASO as described previously [65]. 3-months post-injection, the MKO mice and wildtype littermates were assessed using multiple-electrode analysis (MEA) at NeuroService Alliance. Mice were sacrificed by fast decapitation and the brains soaked in ice-cold oxygenated buffer (2mM KCl, 7mM MgCl₂, 1.2mM NaH₂PO₄, 0.5mM CaCl₂, 25mM NaHCO₃, 11mM glucose, and 250mM sucrose). Slices from the hippocampus were cut in the horizontal plane with a Leica VT1200S vibratome. Slices recovered at 32°C for 60 minutes in artificial cerebrospinal fluid (aCSF). Throughout the experiment, slices were continuously perfused with oxygenated (95% O₂/5% CO₂) aCSF. Hippocampal slices were placed on MEA and spontaneous firing activity and possible occurrences of epileptiform discharge (ED) were monitored for 60 minutes after recovery. For the first 20 minutes, slices were treated with 3.5mM K⁺, during the next 20 minutes, potassium ion concentration was increased to 7mM, and during the final 20 minutes, 100nM Kainic acid was administered. For spontaneous firing analysis, raw data of neuron firing was filtered with a high pass filter at 200Hz and the firing rate detected at each electrode was averaged over 30 second time slots. For ED analysis, raw data was filtered with a Low Pass filter set at 20Hz. Events had to be higher than 15μV in order to be counted as an ED, with 200ms of dead time applied from each ED detected.

2.2.8 Statistical Analyses of Mouse Tissue Samples

All data points are represented with the mean ± SEM. GraphPad Prism 9.3.1 was used to perform all statistical analyses. A student t-test or one-way ANOVA with Tukey's multiple comparisons test was used to assess significance as indicated in each figure. Significance levels are indicated by asterisks: *, p<0.05, **, p<0.01, and ***, p<0.001.

CHAPTER 3. RAPID PATHOGENICITY ASSESSMENT DEFINES PATIENT COHORTS FOR LAFORA DISEASE

3.1 Introduction

Lafora Disease (LD) is a fatal, autosomal recessive disorder that presents as a childhood epilepsy and dementia. Patients develop seemingly normal until adolescence, at which point they begin to experience seizures with increasing frequency and severity coupled with neurodegeneration, leading to the patient's untimely death, usually in early adulthood [47, 68, 71, 101]. Patients with LD have a mutation in one of two genes, *EPM2A* or *EPM2B*, which encode for the glycogen phosphatase laforin and E3 ubiquitin ligase malin, respectively, and both proteins play a critical role in regulating glycogen metabolism [48, 51, 52, 54, 102, 103]. A loss or reduction of function mutation for either protein results in perturbed glycogen metabolism and aberrant glycogen-like aggregates in the cytoplasm of most tissues in the body, making LD part of the family of Glycogen Storage Diseases (GSD), which impact approximately 1:20,000 people [62, 104-106]. These glycogen-like aggregates, termed Lafora Bodies (LBs), drive LD progression [60, 61, 63, 107-109].

There is no cure for LD; however, multiple therapies are in development [65, 66, 110, 111]. Studies in LD murine models suggest that early detection is critical for improving the efficacy of these therapies [65, 109]. Therefore, physicians will need a reliable tool to diagnose patients as early as possible. Multiple bioinformatics engines can predict pathogenicity. Unfortunately, they are not always reliable predictors of pathogenicity for mutations that do not reduce protein stability, and can often produce conflicting results [112, 113]. Therefore, mutations disrupting critical protein functions could go undetected if physicians rely solely on bioinformatics engines. For this reason, we developed a rapid workflow to assess laforin function for novel patient *EPM2A* mutations that can be used to predict degree of pathogenicity and patient progression.

Importantly, work from multiple groups suggests that the rapidity of LD patient progression is linked to the specific patient mutations in *EPM2A* or *EPM2B* [68, 70, 76, 85, 114, 115]. We recently analyzed dozens of LD patient *EPM2A* missense mutations via biochemical and biophysical methods and classified the mutations based on the loss or reduction of function induced by the mutation [112]. These mutation groups were then linked with patient data to predict rapidity of disease progression based on the type of reduction in laforin function [112]. Laforin performs multiple functions in regulating glycogen metabolism. Laforin is comprised of an amino-terminal carbohydrate binding-module (CBM) and a carboxy-terminal Dual Specificity Phosphatase (DSP) domain, existing as a dimer in solution through DSP-DSP interaction (Figure 3.1A) [86, 116]. The CBM allows laforin to bind to glycogen while the laforin DSP removes phosphate from glycogen [53, 86, 117, 118]. Additionally, data suggests that laforin acts as a scaffold,

bringing together the E3 ligase malin and protein targeting to glycogen (PTG) to regulate glycogen metabolism (Figure 3.1B) [106, 119]. Previous work demonstrated that mutations resulting in a complete loss of binding to glycogen corresponded with the most rapid disease progression, while missense mutations that exhibit only partial decreases in protein function corresponded with a less rapid progression [112].

Herein, we build on the analyses of known LD patient mutations and develop a pipeline to rapidly characterize novel *EPM2A* mutations in laforin (Figure 3.1C). We identified three assays to streamline the characterization of each novel mutation, allowing for rapid classification of patient mutations and single nucleotide polymorphisms (SNPs). To demonstrate proof-of-concept we used the pipeline to characterize three recently identified patient mutations and eight laforin SNPs of unknown significance reported in the NCBI dbSNP database. This workflow gives researchers the ability to rapidly assess pathogenicity and predict disease progression for novel LD mutations, laying the foundation to identify ideal candidates for upcoming clinical trials. At the same time, this pipeline will allow for earlier patient diagnosis and the advancement of personalized treatment regimen based on specific patient mutations.

3.2 Results

3.2.1 *In silico* analysis provides a baseline for *in vitro* screening of patient mutations

While bioinformatics has limitations for determining mutant pathogenicity, it provides a good baseline for identifying mutations that require additional analysis. Therefore, six novel patient mutations recently identified by clinicians in newly diagnosed patients were screened using multiple *in silico* tools for assessing pathogenicity. Polyphen2, CUPSAT, and Site-Directed Mutator (SDM) were used to assess the impact of the patient mutation on laforin structural stability and functionality (Table 3.1). Polyphen2 uses amino acid sequence homology to predict pathogenicity, while CUPSAT and SDM use published protein structures to predict the impact on protein stability [88, 89, 120]. Five of the six patients are in their teens and were already symptomatic when they received their diagnosis, while the sixth was a mutation identified in an infant who presented with seizures. We decided to use these patient mutations to investigate the efficacy of our rapid classification workflow.

The workflow starts with bioinformatics analyses. While we knew all these mutations were pathogenic, the bioinformatics analyses yielded conflicting results for many of the mutations, highlighting the need for additional methods to determine pathogenicity. We can improve upon the predictive power of bioinformatics analyses by referring to previous structure-function analyses examining the functional significance of the amino acid that was mutated. Adding this to our suite of *in silico* diagnostic tools, we could confidently predict pathogenicity in four out of the six cases using bioinformatics. For the uncertain cases, we turned to the pipeline to assess laforin pathogenicity and the specific impact on laforin function.

3.2.2 *In vitro* pipeline clarifies uncertain *in silico* predictions for patient mutations

Based on previous mutant characterizations in our laboratory, pathogenic mutations exhibited a severe loss of stability, loss of binding to glycogen, decreased phosphatase activity, and/or a reduction or loss of protein-protein interactions [112]. We selected three simple assays that are easy to scale-up for screening multiple mutations: Differential Scanning Fluorimetry (DSF) thermal shift assay, para-nitrophenylphosphate (pNPP) assay, and yeast two-hybrid (Y2H) analysis.

The thermal shift assay using DSF allowed us to quantify changes in protein stability [121, 122]. Wildtype (WT) and mutant proteins were incubated with a SYPRO orange dye that fluoresces when exposed to hydrophobic amino acids. When subjected to a heat gradient, the protein melts and begins to unfold, exposing the hydrophobic core. The resulting fluorescent emissions are measured and graphed to determine the melting temperature of the protein compared to WT laforin (Figure 3.2A). The DSF thermal shift assay can also be used to assess protein-ligand interactions [121]. When laforin binds to glycogen, it stabilizes the protein, producing a shift in melting temperature (Figure 3.2B). To reduce the background fluorescence produced by heterogeneous glycogen molecules, we used the linear polysaccharide maltoheptaose (DP7), which mimics the linear chains of glycogen, to quantify carbohydrate-protein interactions.

The pNPP assay was utilized to measure phosphatase activity. Active phosphatases can remove the phosphate from pNPP. A strong base, like sodium hydroxide, can be used to produce the conjugate base, para-nitrophenol, which is yellow with an absorbance at 410nm (Figure 3.2C). The intensity of the absorbance can be measured on a spectrophotometer and reports laforin phosphatase activity [83].

Finally, a Y2H assay was selected to determine changes in protein-protein interaction. WT laforin or a laforin mutant was expressed in yeast fused to LexA, a DNA binding domain. The laforin interacting proteins malin or PTG were then co-expressed in the yeast fused to GAD, a transcription factor activating domain. When laforin interacts with malin or PTG, the LexA and GAD domains also interact, turning on the lacZ reporter gene that produces β -galactosidase (Figure 3.2D). The amount of β -galactosidase activity can be measured through a colorimetric assay, reporting the level of protein-protein interaction (Figure 3.2E-F) [112].

To test the functionality of this pipeline, we assessed the confidently predicted G24R pathogenic mutation from our bioinformatics analysis. Additionally, we tested the two mutations whose functional contribution to laforin were not available in literature: the V249L mutation and the novel A268T mutation recently identified as a homozygous EPM2A mutation in an infant. Using the three assays detailed above, we tested the three mutants for overall stability, interaction with carbohydrates, phosphatase activity, and protein-protein interaction.

G24R was predicted to be damaging by *in silico* tools using sequence homology and structural analysis [123]. G24R is at the edge of a beta-sheet structure in the core of

the laforin CBM domain (Figure 3.3A). G24R exhibited a melting temperature of 50.11°C, similar to that of wildtype laforin (Figure 3.3B). However, the raw fluorescence curve from the DSF assay revealed high background fluorescence, which can indicate protein aggregation or that a domain was partially unfolded before the thermal shift assay initiated. Our previous work demonstrated that mutations in the core of the CBM yielded a severe stability and functionality deficit [112]. In fact, mutations similar to G24R produced spontaneous proteolytic cleavage during protein purification. To further assess G24R, we analyzed the purified protein via native gel electrophoresis alongside WT laforin and other laforin mutations. While G24R runs at the expected value on SDS-PAGE stain-free gels, the native gel, using a more sensitive stain, reveals substantial proteolytic cleavage (Figure 3.3C).

Next, we assessed the stability of V249L and A268T. Both mutations are located in the DSP domain (Figure 3.3A). V249L is at the core of the DSP domain at the center of an alpha helix. A268T, by contrast, is within the glucan phosphatase signature active site motif CXAGXGR [86, 124]. While A268T displayed a melting temperature of 49.5°C, nearly identical to that of WT, V249L demonstrated a significant loss of stability with a melting temperature of 39.46°C (Figure 3.3B). The loss of stability in V249L correlates with similar pathogenic patient mutations in the core of the DSP [112].

Having determined the stability of each mutation, the specific functions of laforin were then assessed. In order to characterize carbohydrate binding, we performed a DSF thermal shift assay by incubating each protein with 5mM DP7 (Figure 3.3D) [86]. G24R exhibited no interaction with DP7. Conversely, V249L and A268T displayed an increase in stability with the addition of DP7, with increased melting temperatures of 4.72°C and 3.18°C, respectively (Figure 3.3D). The phosphatase activity for each mutant was then determined using the pNPP assay. Both G24R and V249L retained phosphatase activity, while A268T, with the mutation at the phosphatase active site, displayed no phosphatase activity (Figure 3.3E).

Finally, each mutation was assessed for its impact on protein-protein interactions with malin and PTG. When interaction with either protein is disrupted, patients develop LD [106, 125]. Mutant constructs were co-expressed with either malin or PTG in a Y2H assay. The A268T mutation retained the ability to interact with both proteins at levels similar to WT (Figure 3.3F-G). However, G24R interactions with both PTG and malin are significantly reduced, and V249L showed a greatly reduced interaction with malin and would not co-transform with PTG in yeast (Figure 3.3F-G). It is possible that the loss of stability observed in V249L and G24R negatively impacts their ability to interact with other proteins.

3.2.3 Bioinformatics screen identifies novel SNPs for pipeline analysis

The ultimate goal of developing the pipeline to pair with bioinformatics is to characterize novel patient mutations before symptoms emerge when pathogenicity is unclear – as with the case of the infant with a homozygous A268T mutation. To test the potential of the pipeline for characterizing novel mutations, 309 laforin single nucleotide

polymorphisms (SNPs) resulting in missense mutations were identified from the NCBI dbSNP database. From the list of SNPs, those occurring in exons with unknown clinical significance were selected, resulting in 25 SNPs of interest (Table 3.2). These SNPs were then subjected to preliminary screening with PolyPhen-2. From this analysis, 8 laforin SNPs were selected for characterization through the biochemical pipeline as a proof-of-concept demonstration (Figure 3.4A). R108H and K87R were selected as examples of confident pathogenic mutation predictions, while C109S and A227V were selected as mutations that bioinformatics confidently predicted to be benign. The other four mutations, E100V, G101S, N102D, and N102S were selected as examples of uncertain pathogenicity where bioinformatics predictions conflicted and no previous structure-function analysis for the mutated amino acid was available, making pipeline analysis necessary to determine pathogenicity (Table 3.3).

3.2.4 Pipeline analysis supports confident *in silico* predictions

To test the efficacy of screening novel patient mutations with our suite of *in silico* tools, R108H, K87R, C109S and A227V were analyzed via the biochemical pipeline. Recombinant protein for each mutant was purified from *E. coli* to near homogeneity. The stability of each mutant was defined via DSF. As predicted, R108H exhibited a loss of stability and was observed to possess two-state melting (Figure 3.4B). One domain melted at 38.44°C while the other melted at 51.5°C. We hypothesized that the CBM domain was destabilized by the mutation, causing the CBM and DSP domains to decouple and melt separately. Both C109S and A227V displayed stabilities similar to that of WT laforin, while K87R displayed a significant increase in stability, with a melting temperature of 53.6°C (Figure 3.4C).

Each SNP was then further analyzed to characterize functionality of the protein. A thermal shift assay was performed with DSF using a concentration of 5mM DP7. K87R displayed a loss of interaction with DP7 compared to WT, while C109S and A227V both showed increased stability with the addition of 5mM DP7 (Figure 3.4D). When DP7 was added to R108H, the two-state melting observed in the stability assay disappeared. Further analysis was required to determine if the increased stability of the CBM occurred through binding to glycogen. Phosphatase activity of each mutant was assessed using the pNPP assay, and all four SNPs exhibited phosphatase activity comparable to WT (Figure 3.4E). Using the Y2H assay, all four SNPs also retained some protein-protein interaction with malin and PTG. K87R exhibited a significant increase in malin interaction compared to WT and a significant decrease in PTG interaction (Figure 3.4F-G). R108H showed a significant decrease in interaction with both malin and PTG compared to WT (Figure 3.4F-G).

In order to better investigate the two-state melting exhibited by R108H, the protein was subjected to additional analysis using Hydrogen-Deuterium eXchange Mass Spectrometry (HDX). HDX reports the solvent accessibility of each amino acid within the protein. By comparing the solvent accessibility of the amino acids in WT laforin to R108H

laforin, we could determine if the mutation led to a disruption in the CBM-DSP interface. Additionally, we incubated R108H laforin with glycogen and performed HDX analysis, allowing us to determine if the CBM retained the ability to bind to glycogen. The data revealed increased solvent accessibility for the amino acids at the CBM-DSP interface, supporting our hypothesis that the mutation disrupts the CBM-DSP domain interaction (Figure 3.5A-B). Furthermore, incubation with glycogen resulted in decreased amino acid solvent accessibility at the glycogen binding site on the CBM, supporting our hypothesis that the CBM retains its ability to bind to glycogen, leading to the increase in protein stability observed in the thermal shift assay (Figure 3.5C-D).

3.2.5 Pipeline analysis defines pathogenicity predictions from *in silico* analysis

Having confirmed that the pipeline appropriately characterized the SNPs with confident pathogenic predictions, we sought to use the pipeline to clarify the SNPs with uncertain pathogenicity: E100V, G101S, N102S, and N102D. These amino acids are all located near the surface of the CBM domain, close to the DSP (Figure 3.4A). We expressed and purified all four of these SNPs for testing *in vitro*. We then employed the DSF thermal stability assay. N102S and N102D both showed melting temperatures similar to that of WT while E100V showed increased stability compared to WT (Figure 3.6A). G101S, however, was found to have two-state melting similar to that seen in R108H with one domain melting at 40.28°C, while the other domain melted at 52.44°C (Figure 3.6B).

To test the glycogen binding function of laforin, the thermal shift assay was run using 5mM DP7. N102S and N102D showed increased stability with the addition of 5mM DP7, similar to that of WT (Figure 3.6C). E100V, however, exhibited no increase in stability with the addition of DP7 (Figure 3.6C). G101S shifted from two-state to single-state melting upon the addition of DP7, as was observed with the R108H mutant. The impact of each mutation on phosphatase activity was then determined. For overall phosphatase activity, N102S and N102D displayed similar levels of activity compared to WT while G101S showed significantly reduced activity, and E100V showed no phosphatase activity (Figure 3.6D). Finally, each SNP was assessed for protein-protein interactions with the Y2H assay. Once again, N102S and N102D displayed similar interaction levels compared to WT. G101S exhibited almost complete loss of PTG interaction, but retained WT levels of interaction with malin (Figure 3.6E-F). E100V showed near complete loss of both PTG and malin interaction (Figure 3.6-F).

Given the similarities observed by DSF analysis of G101S and R108H, the G101S mutant was also analyzed with HDX to determine if it exhibited a similar loss of CBM-DSP interaction and retention of binding to glycogen. As with R108H, G101S laforin showed increased solvent accessibility at the CBM-DSP interface compared to WT, and the addition of glycogen led to decreased solvent accessibility at the CBM glycogen-binding site (Figure 3.7A-D). The similarities of these analyses allow us to confidently interpret the two-state melting observed in the thermal shift assay as a functional loss of CBM-DSP domain interaction.

3.2.6 Multivariate analysis clusters novel SNPs with known pathogenic mutations

While the assessment of specific function loss is useful for predicting pathogenicity, most mutations show partial loss of multiple functions, complicating the ability to use this information to predict disease progression. Previous work analyzed pairwise-correlations between laforin functions and detected no significant correlations [112]. However, a multi-variate analysis, like Principle Component Analysis (PCA) combined with Heatmap clustering can be utilized to group laforin mutants with similar function-loss profiles. Six parameters defined in this study were used for multi-variate analysis: protein stability (melting temperature, T_m), DP7 interaction (ΔT_m), phosphatase activity (percent of WT activity levels), PTG interaction (percent of WT interaction levels), malin interaction (percent of WT interaction levels), and a sixth binary parameter to account for mutants that exhibit two-state melting, which indicates disruption of the CBM-DSP interface. We used previously published laforin mutant data to create a baseline of pathogenic laforin mutant profiles along with data from three independently run analyses of WT laforin through the pipeline [112]. To allow for uniform comparison, all values were reported as a delta change from the wildtype control in their respective experiments. Mutant data was then run through a PCA to identify mutation clusters. These clusters were then labeled according to their strongest shared function loss: Glycogen binding loss, domain interface disruption, protein-protein interaction loss, or stability loss.

Once an initial set of mutant profiles had been established, we added the newly characterized patient mutations and SNPs as mutants of “unknown” profile. Heatmap analysis was used to assess the resulting mutant profiles (Figure 3.8A). As predicted by the pipeline, C109S, N102S, N102D, and A227V were closely related to the WT laforin profile. E100V and G24R were closely related to the mutants in the glycogen binding loss profile. Surprisingly, A268T also clustered with this group, perhaps because the mutants that lost glycogen binding usually also show significant or complete loss of phosphatase activity. K87R was most closely related to the loss of protein-protein interaction group, however the K87R mutation possessed a unique gain-of-function for malin interaction that made it difficult to align with a defined mutation profile. V249L closely aligned with the stability loss group. As expected, G101S and R108H clustered with the domain interface disruption group. The data was then mapped onto 2D and 3D PCA plots (Figure 3.8B&C). The resulting clusters closely aligned with the Heatmap clustering profiles. In the PCA, there is imperfect separation between the WT and protein-protein interaction loss cluster, which may reflect the wide variability within that profile group. Indeed, the Heatmap analysis clusters the mutants with complete loss of protein interaction separately from the partial loss mutations. As more data becomes available, these groups may be further refined for greater specificity and predictive power.

3.3 Discussion

Bioinformatics engines for pathogenicity prediction provide an easily accessible resource for researchers and physicians to assess the impact of a missense mutation. These

in silico tools, such as PolyPhen-2, CUPSAT, SDM, and SNAP provide results within minutes. However, when compared, bioinformatics engines can produce conflicting results. Even *in silico* tools that draw upon multiple bioinformatics engines to make their predictions, like PhD-SNP and Meta-SNP, are subject to limitations baked into the system. Bioinformatics engines for pathogenic predictions rely primarily upon amino acid sequence homology and conservation, predicted changes in protein stability based on structural data, or allelic frequency of a mutation. An engine relying on sequence homology or stability might miss substitutions that result in a loss of enzymatic function [126]. Allelic frequency can be useful for identifying benign mutations, however, for rare diseases it is a less reliable predictor, as almost any mutation would be considered rare or ultra-rare, leading to an over-assumption of pathogenicity [127]. These inaccurate or inconclusive assessments hinder the ability of physicians to diagnose patients prior to the emergence of symptoms. Given that the symptoms of LD are accompanied by neurodegeneration, early diagnosis will be critical to improve patient outcomes once treatment is available.

Even when pathogenicity is predicted with accuracy, bioinformatics engines return a binary outcome: benign or pathogenic. Therefore, bioinformatics analyses are insufficient to provide predictions for the rate of disease progression. Biochemical characterization of patient mutations, however, elucidates the type and degree of function loss and allows physicians to predict prognoses for individual patients based on their specific mutation. As multiple treatments for LD approach clinical trials, understanding patient prognosis will be critical for forming appropriate patient cohorts, as there is likely a threshold level of LB accumulation that leads to the observed disease phenotype. Patients with accelerated rates of progression would likely have accumulated sizeable LBs prior to clinical trials, and would benefit most from therapies that target and remove LB aggregations. Meanwhile, patients with slower rates of progression may benefit from therapies that slow or halt LB aggregation through knock-down of glycogen synthesis in the brain [65, 66].

In rare autosomal recessive diseases such as LD, patients frequently exhibit *de novo* mutations, making it unlikely that the exact mutation has already been characterized [73, 128]. While certain regions with high rates of consanguinity, like the Mediterranean, find patients with well-characterized homozygous mutations due to a founder effect, the majority of LD patients have compound heterozygous mutations, which can further complicate the use of bioinformatics analyses to determine patient outcomes. Bioinformatics analyses coupled with biochemical characterization, however, lays the foundation for rapid classification of novel mutations based on their function loss profile. To demonstrate how such a pipeline could be useful for researchers and clinicians, three novel patient mutations and eight SNPs reported in NCBI dbSNP database were analyzed to produce a mutation profile that could then be matched against the disease progression of reported mutations to predict patient outcomes.

The novel patient mutations present a unique opportunity to test the pipeline, as the patient's progression and predicted profile can be compared to previously reported cases with similar function loss profiles. The patient with a homozygous G24R mutation began to experience loss of consciousness at the age of 11. By the time the patient was 16, they experienced more frequent loss of consciousness, convulsions and hallucinations. When mapped against previously characterized patient mutations, G24R displayed a similar profile to K87T. The patient with the K87T mutation started to experience seizures at the

age of 11 and cognitive decline by age 15 [68]. The majority of *in silico* tools predicted the G24R mutation to be pathogenic, however, using the pipeline we extracted a mutation profile that could be matched to documented patient mutations, facilitating the prediction of the patient's rate of progression through the disease.

The LD patient with the V249L mutation is compound heterozygous with the other allele having a deletion in exon2. Through initial bioinformatics assessment, the patient had one pathogenic mutation while the other was a variant of unknown significance. Further bioinformatics analyses returned conflicting results for V249L, therefore, the pipeline provided a path to not only determine the pathogenicity, but also to predict patient progression through the disease. As of 2019, the patient could act independently, but continued to suffer from seizures increasing in severity. Biochemical characterization produced a profile that clustered with other proteins where reduction in stability was the primary defect. Similar mutation profiles with reported patient data are V7A and G279S. The patient with a homozygous V7A mutation experienced myoclonus at age 17, with generalized seizures emerging at age 21, and cognitive decline detected by age 22 [68]. The patient with G279S was compound heterozygous with the other allele having a premature stop codon at R241X [77]. This patient experienced their first generalized tonic-clonic seizure at age 21, with the onset of ataxia and cognitive impairment at age 24 [77]. Therefore, the patient with V249L compound heterozygous would be predicted to have a moderate rate of disease progression, with onset of symptoms delayed compared to patients with classic LD progression.

The homozygous A268T mutation was recently identified in a newborn infant, screened for epilepsy-linked gene mutations due to the emergence of seizures around 6 months after birth. The screen returned multiple gene candidates, one being a heterozygous PRRT2 (proline-rich transmembrane protein 2) mutation, which is linked with infantile epilepsy, and the other being EPM2A. Therefore, we used the pipeline to provide insight into what contribution, if any, the A268T mutation played in the early seizure onset. We predicted a pathogenic outcome due to the mutation occurring in the phosphatase active site motif of laforin, CXAGXGR [124]. However, no patient mutations directly in the active site motif had been characterized previously. The profile that emerged did not match completely with any existing cohort, but the complete loss of phosphatase activity clustered this mutation near the loss-of-glycogen-binding functions, which are often accompanied by a severe or complete loss of phosphatase activity. Patients with a loss-of-glycogen-binding profile mutation do not tend to experience seizures until early adolescence, making it unlikely that A268T was driving seizures in the infant [112]. However, the placement of A268T between the loss-of-glycogen-binding cluster and the protein-protein-interaction cluster on the PCA suggests that A268T is indeed pathogenic, and the physicians should monitor the patient for development of LBs, perhaps opening the door for early treatment once a therapy becomes available.

The analysis of A268T was complicated by its unique profile. As more patient mutations are classified through the pipeline, it is possible that a new mutation profile will emerge, allowing for better predictive capacity for future patients. One way to expand the predictive power is to characterize SNPs in EPM2A that produce missense mutations. As a proof of concept, we characterized 8 SNPs of unknown significance reported in the NCBI dbSNP database using the pipeline. The results demonstrated that K87R, E100V, G101S,

and R108H clustered with known patient mutation profiles, suggesting they are pathogenic, while N102S, N102D, C109S, and A227V clustered with the WT laforin profile. Our characterizations of these SNPs demonstrate that our biochemical pipeline can be a powerful tool for matching novel mutations with known mutation profiles, making a personalized LD diagnosis feasible, quick, and accessible.

Table 3.1 Bioinformatics Analysis of Recently Identified Patient Mutations

Six newly identified mutations in patients were assessed for pathogenicity using three different bioinformatics engines: PolyPhen-2, CUPSAT, and SDM. A literature search was then performed to identify any previous structure-function analysis of mutations in that amino acid. The variability in pathogenicity and stability predictions highlights the need for a biochemical pipeline to assess uncertain predictions. Previous literature aids in the prediction of pathogenicity, however, the literature cannot always clarify conflicting results from bioinformatics analyses.

	PolyPhen-2		CUPSAT		SDM		Previous Structure-Function Analyses of the Amino Acid
	Prob. Score	Prediction	$\Delta\Delta G$ (kcal/mol)	Predicted stability	$\Delta\Delta G$ (kcal/mol)	Outcome	
G24R	1	Probably damaging	0.39	Stabilizing	-2.42	Reduced stability	G24, highly conserved near CBM binding site (Wang et al. 2002)
K87E	1	Probably damaging	-1.24	Destabilizing	-0.32	Reduced Stability	K87, directly interacts with glucose residues to bind glycogen (Raththagala et al. 2015)
V249L	0.924	Possibly damaging	0.93	Stabilizing	0.31	Increased stability	N/A
G279V	1	Probably damaging	-1.57	Destabilizing	-0.28	Reduced stability	G279, mutations impact stability and protein-protein interactions (Brewer et al. 2021)
A268T	1	Probably damaging	1.79	Stabilizing	0.2	Increased stability	N/A
D306V	0.998	Probably damaging	1.46	Stabilizing	1.73	Increased stability	D306, mutations impact stability, also borders DSP active site and impacts phosphatase activity (Brewer et al. 2021)

Table 3.2 Preliminary screening of laforin SNPs in the NCBI dbSNP Database

SNPs with known pathogenicity were excluded, along with any intronic SNPs. The remaining 25 SNPs were screened using Polyphen-2. From these results, 8 SNPs were selected for proof-of-concept pipeline analysis.

Mutation	Frequency	Clinical Significance	Polyphen 2
W32R	N/A	Uncertain	1.00 Probably Damaging
R108L	Ultra Rare	Uncertain	1.00 Probably Damaging
R108H	Ultra Rare	Uncertain	1.00 Probably Damaging
R91Q	Ultra Rare	Uncertain	0.989 Probably Damaging
R91W	N/A	Uncertain	1.00 Probably Damaging
N148H	N/A	Uncertain	0.003 Benign
K87R	N/A	Uncertain	1.00 Probably Damaging
L97V	Ultra Rare	Uncertain	0.042 Benign
G24E	Ultra Rare	Uncertain	1.00 Probably Damaging
N102D	Ultra Rare	Uncertain	0.920 Possibly Damaging
G101S	N/A	Uncertain	0.937 Possibly Damaging
C109S	N/A	Uncertain	0.023 Benign
E100V	N/A	Uncertain	0.820 Possibly Damaging
N102T	Ultra Rare	Uncertain	0.852 Possibly Damaging
N102S	Ultra Rare	Uncertain	0.021 Benign
T143A	Ultra Rare	Uncertain	0.429 Benign
I149T	N/A	Uncertain	0.842 Possibly Damaging
F145L	N/A	Uncertain	0.999 Probably Damaging
T142A	N/A	Uncertain	0.999 Probably Damaging
A150V	Ultra Rare	Uncertain	0.325 Benign
G151D	N/A	Uncertain	0.132 Benign
Y146H	N/A	Uncertain	0.999 Probably Damaging
H152Y	N/A	Uncertain	0.896 Possibly Damaging
P214T	N/A	Uncertain	1.00 Probably Damaging
V64G	Rare	Uncertain	1.00 Probably Damaging

Table 3.3 Bioinformatics Analysis of Eight Novel Laforin SNPs in the NCBI dbSNP Database

Eight laforin SNPs were assessed for pathogenicity using three different bioinformatics engines: PolyPhen-2, CUPSAT, and SDM. Additionally, the SNPs were run through three SNP analysis engines that use a combination of bioinformatics tools to predict pathogenicity. For some mutations, like R108H, the prediction of pathogenicity is clear. However, the variability in pathogenicity and stability predictions once again highlights the need for a biochemical pipeline to assess uncertain predictions.

	PolyPhen-2		CUPSAT		SDM		Meta-SNP	PhD-SNP	SNAP	Previous Structure-Function Analyses of the Amino Acid
	Prob. Score	Prediction	$\Delta\Delta G$ (kcal/mol)	Predicted stability	$\Delta\Delta G$ (kcal/mol)	Outcome	Outcome	Outcome	Outcome	
K87R	1	Probably Damaging	1.37	Stabilizing	-0.58	Reduced Stability	Disease	Disease	Disease	K87 (Raththagala et. Al 2015)
E100V	0.82	Possibly Damaging	7.07	Stabilizing	1.31	Increased Stability	Disease	Disease	Disease	N/A
N102S	0.021	Benign	-0.65	Destabilizing	-0.48	Reduced Stability	Neutral	Neutral	Disease	N/A
N102D	0.92	Possibly Damaging	0.47	Stabilizing	-0.22	Reduced Stability	Neutral	Neutral	Disease	N/A
R108H	1	Probably Damaging	-0.01	Destabilizing	-0.3	Reduced Stability	Disease	Disease	Disease	R108 (Brewer et al. 2021)
C109S	0.023	Benign	2.09	Stabilizing	-0.78	Reduced Stability	Neutral	Neutral	Disease	N/A
A227V	0.001	Benign	-6.15	Destabilizing	1.72	Increased Stability	Neutral	Neutral	Neutral	N/A
G101S	0.937	Possibly Damaging	1.52	Stabilizing	-2.93	Reduced Stability	Neutral	Disease	Disease	N/A

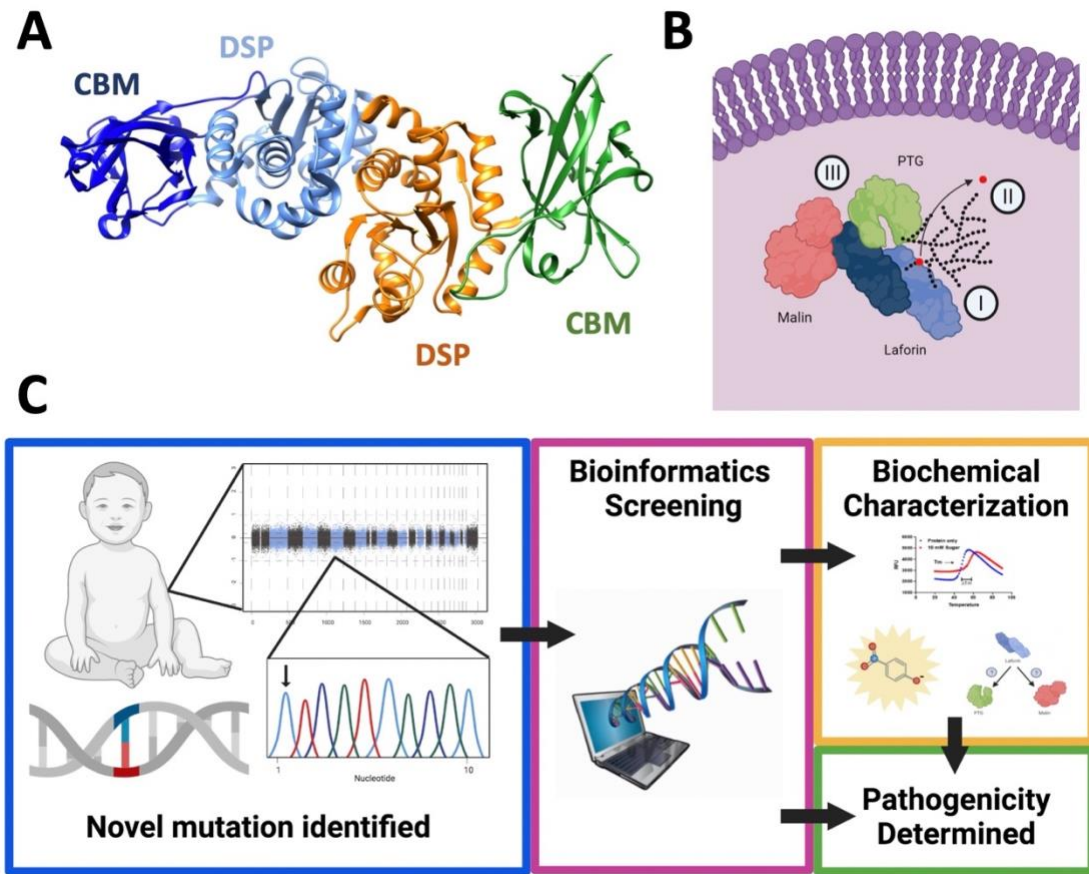


Figure 3.1 Laforin Function and Pipeline Overview

A) Laforin cartoon ribbon structure (pdb 4rkk) shown as an anti-parallel dimer, with each monomer containing a CBM and DSP domain.

B) Representation of the three critical functions of laforin being quantified in our pipeline.

C) Schematic of pipeline for pathogenic determination. Novel SNPs are identified through genetic testing, then screened through bioinformatics analysis. Based on those results, the SNP can either be directly characterized as benign or pathogenic, or submitted to the pipeline for further testing of three critical functions of laforin.

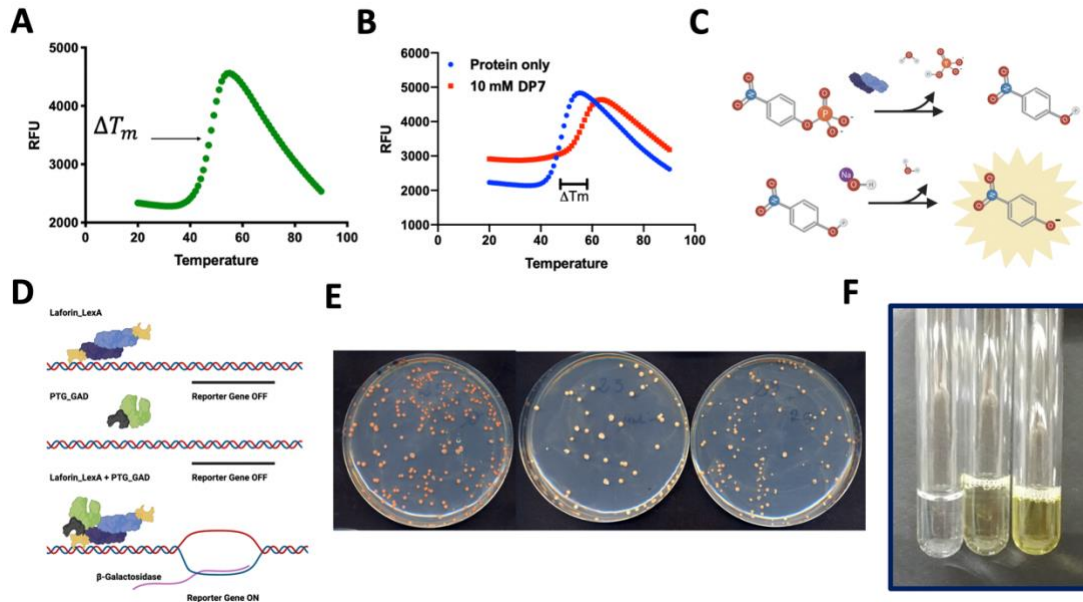


Figure 3.2 Methods Utilized in Pipeline Analysis

A) Representative data from DSF thermal assay of WT laforin, the arrow indicates the point of inflection that defines the protein melting temperature.

B) Representation of DSF thermal shift assay for WT laforin, where the addition of a ligand that binds to the protein, like DP7, produces a change in the protein melting temperature.

C) Schematic of the pNPP assay reaction to report phosphatase activity

D) Representative schematic of constructs used for the yeast two-hybrid (Y2H) assay, producing the colorimetric change that can be visually observed in yeast colonies (E) and quantified through spectrophotometry (F).

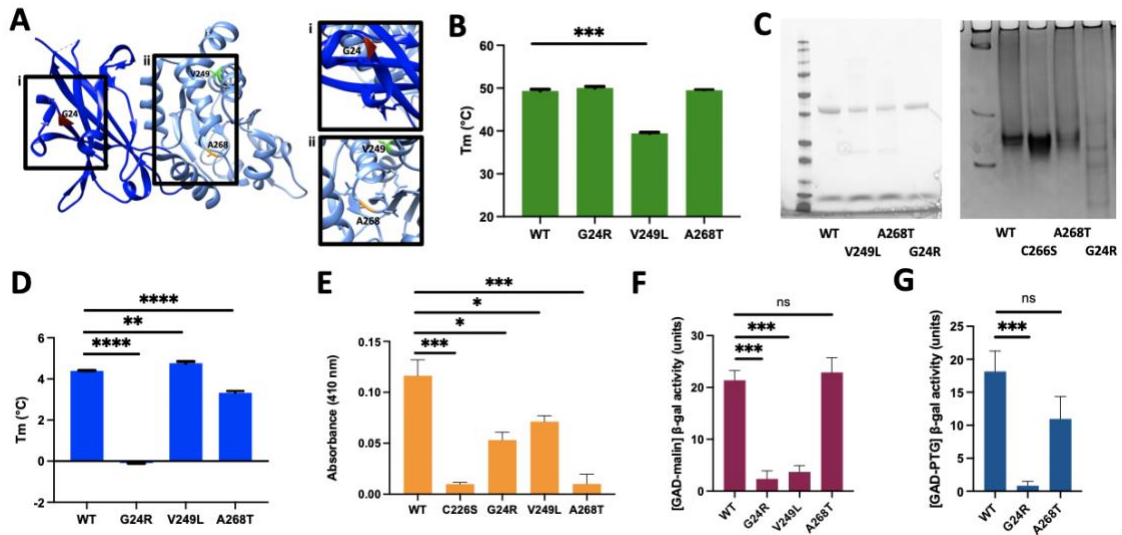


Figure 3.3 Pipeline Analysis of Laforin Patient Mutations

A) Laforin structure showing the location of G24R in the β -sheet sandwich motif (i), the location of A268T in the DSP active site and V249L in the core of the DSP (ii).

B) Melting temperature calculated from DSF analysis for each mutant compared to wildtype (WT), as a measure of protein stability.

C) SDS-Page (left) and Native Affinity Gel Electrophoresis (right) for purification of mutants, with the native gel revealing multiple bands in the lane of purified G24R, indicating proteolytic cleavage.

D) Interaction with DP7 substrate as demonstrated by changes in melting temperature through the DSF assay.

E) Phosphatase activity of each mutant as demonstrated by the pNPP assay. C266S is the phosphatase inactive mutant of laforin.

F) Yeast two-hybrid (Y2H) assay showing interaction between malin and each laforin mutant.

G) Y2H assay showing interaction between PTG and each laforin mutant.

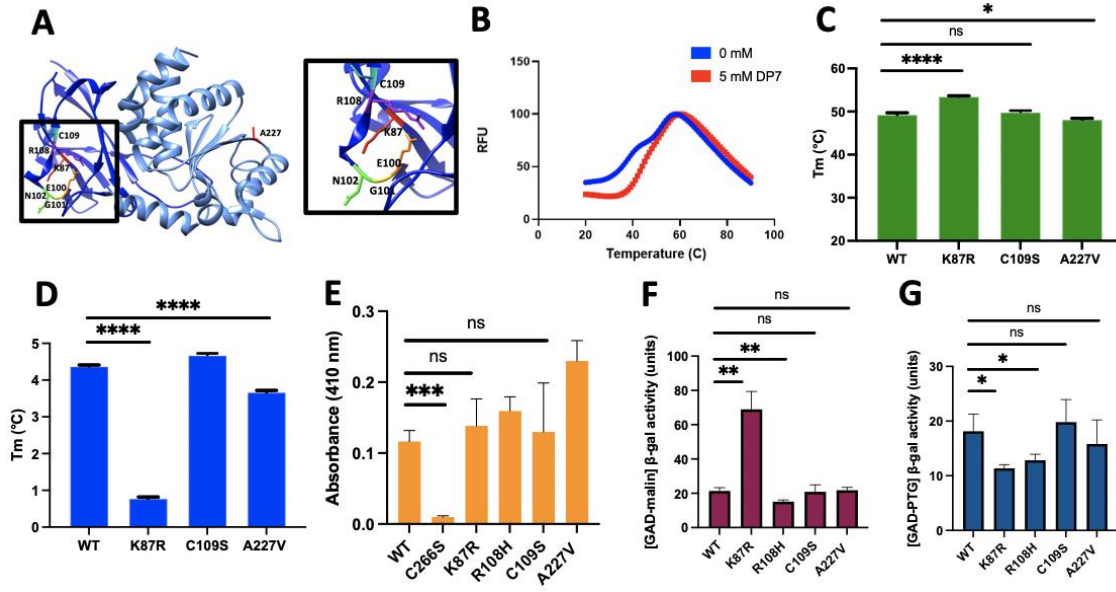


Figure 3.4 Pipeline Analysis of Laforin SNPs with Clear Pathogenicity Predictions via Bioinformatics

A) Ribbon cartoon of laforin monomer structure, callout to the right focuses on the edge of the CBM, between the beta-sheets, where the majority of the SNPs are clustered.

B) Raw curve from DSF analysis for R108H, showing two separate melting states in the absence of DP7.

C) Melting temperature calculated from DSF analysis for each mutant compared to wildtype, as a measure of protein stability. Note that the asterisk demonstrates a significant difference in terms of pathogenicity.

D) Interaction with DP7 substrate as demonstrated by changes in melting temperature through the DSF assay. For R108H, the change in stability could not be accurately measured due to its two-state melting profile.

E) Phosphatase activity of each SNP as demonstrated by the pNPP assay. C266S is the phosphatase inactive mutant of laforin.

F) Yeast two-hybrid (Y2H) assay showing interaction between malin and each laforin SNP.

G) Y2H assay showing interaction between PTG and each laforin SNP.

*P < 0.05; ** P < 0.01; *** P < 0.001; **** P < 0.0001

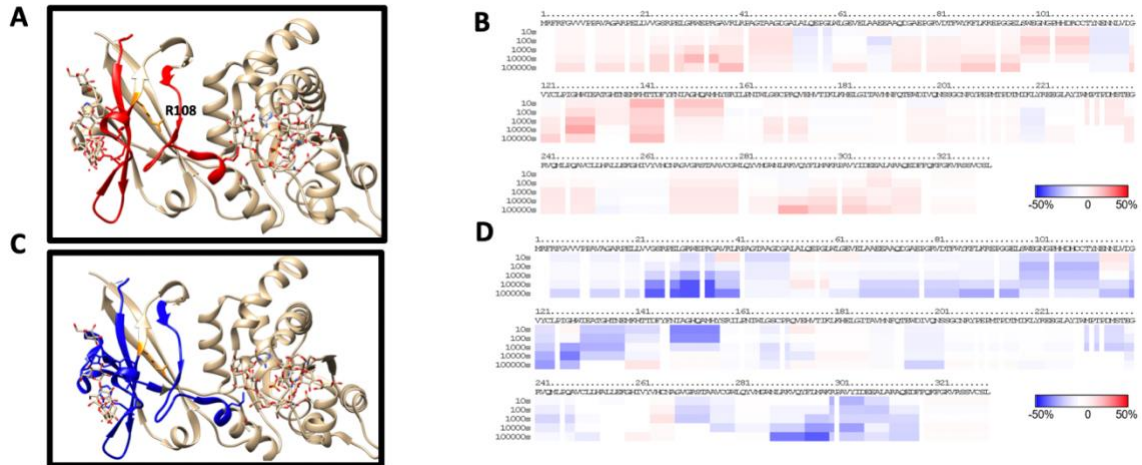


Figure 3.5 HDX Analysis of R108H Laforin Compared to WT Laforin

A) Illustration of laforin structure (PDB 4rkk) with R108 highlighted near the CSM-DSP Interface. Ribbons in red correspond with the amino acids that showed greater surface exposure through HDX analysis compared to WT

B) Change in amino acid deuteration in WT laforin compared to R108H laforin. The increased deuteration in the CBM region (amino acids 1-124) suggests that R108H destabilizes the CBM, particularly along the CBM-DSP interface.

C) Ribbons in blue correspond with the amino acids that showed less surface exposure when R108H was incubated with glycogen

D) Change in deuteration in R108H laforin bound to rabbit liver glycogen compared to R108H alone. The binding site for glycogen shows decreased deuteration, as well as the amino acids along the CBM-DSP interface, suggesting that the mutant can still bind to glycogen.

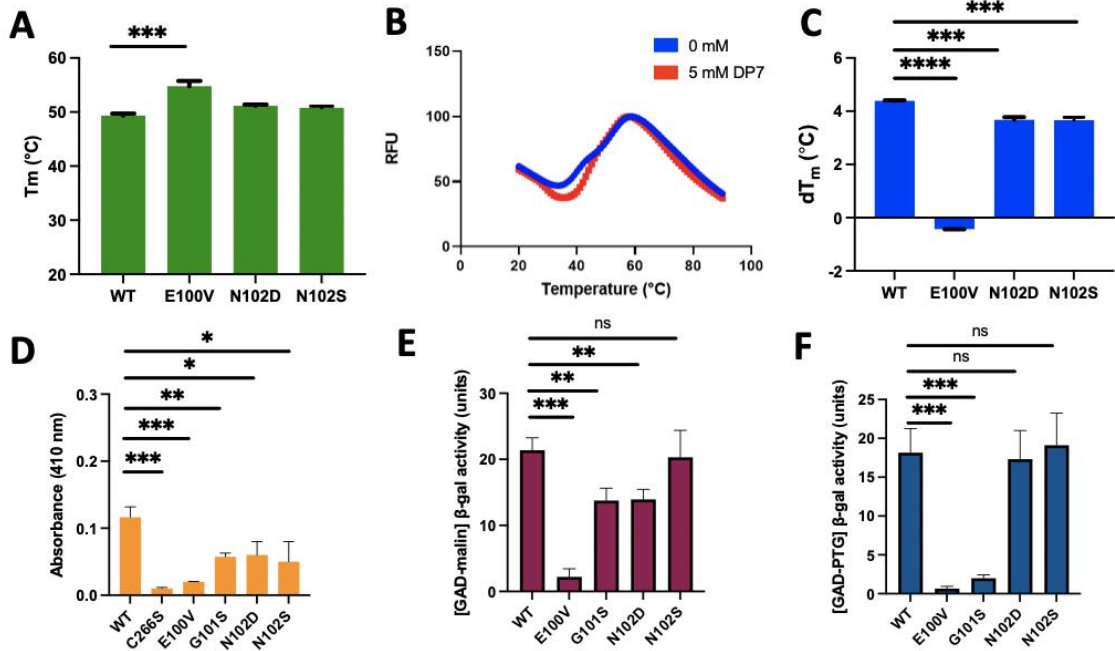


Figure 3.6 Pipeline Analysis of Laforin Mutations with Uncertain Pathogenicity Predictions via Bioinformatics

A) Melting temperature calculated from DSF analysis for each mutant compared to wildtype, as a measure of protein stability.

B) Raw curve from DSF analysis for G101S, showing two separate melting states in the absence of DP7.

C) Interaction with DP7 substrate as demonstrated by changes in melting temperature through the DSF assay. For G101S, the change in stability could not be accurately measured due to its two-state melting profile.

D) Phosphatase activity of each SNP as demonstrated by the pNPP assay. C266S is the phosphatase inactive mutant of laforin.

E) Yeast two-hybrid (Y2H) assay showing interaction between malin and each laforin SNP.

F) Y2H assay showing interaction between PTG and each laforin SNP.

* $P < 0.05$; ** $P < 0.01$; *** $P < 0.001$; **** $P < 0.0001$

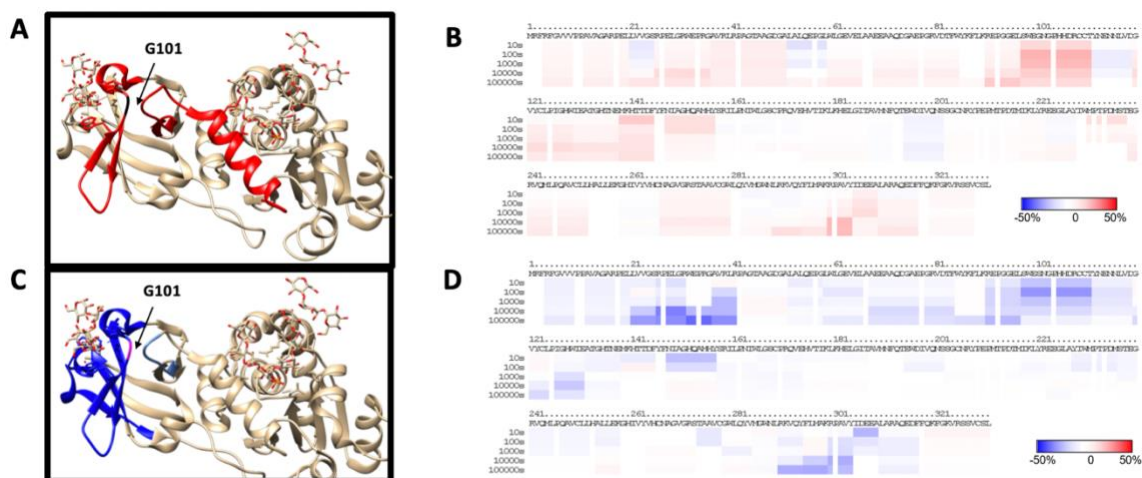


Figure 3.7 HDX Analysis of G101S Laforin Compared to WT Laforin

A) Illustration of laforin structure (PDB 4rkk) with G101 highlighted near the CSM-DSP Interface. Ribbons in red correspond with the amino acids that showed greater surface exposure through HDX analysis compared to WT

B) Change in amino acid deuteration in WT laforin compared to G101S laforin. The increased deuteration in the CBM region (amino acids 1-124) suggests that G101S destabilizes the CBM, particularly along the CBM-DSP interface.

C) Ribbons in blue correspond with the amino acids that showed less surface exposure when G101S was incubated with glycogen

D) Change in deuteration in G101S laforin bound to rabbit liver glycogen compared to G101S alone. The binding site for glycogen shows decreased deuteration, as well as the amino acids along the CBM-DSP interface, suggesting that the mutant can still bind to glycogen.

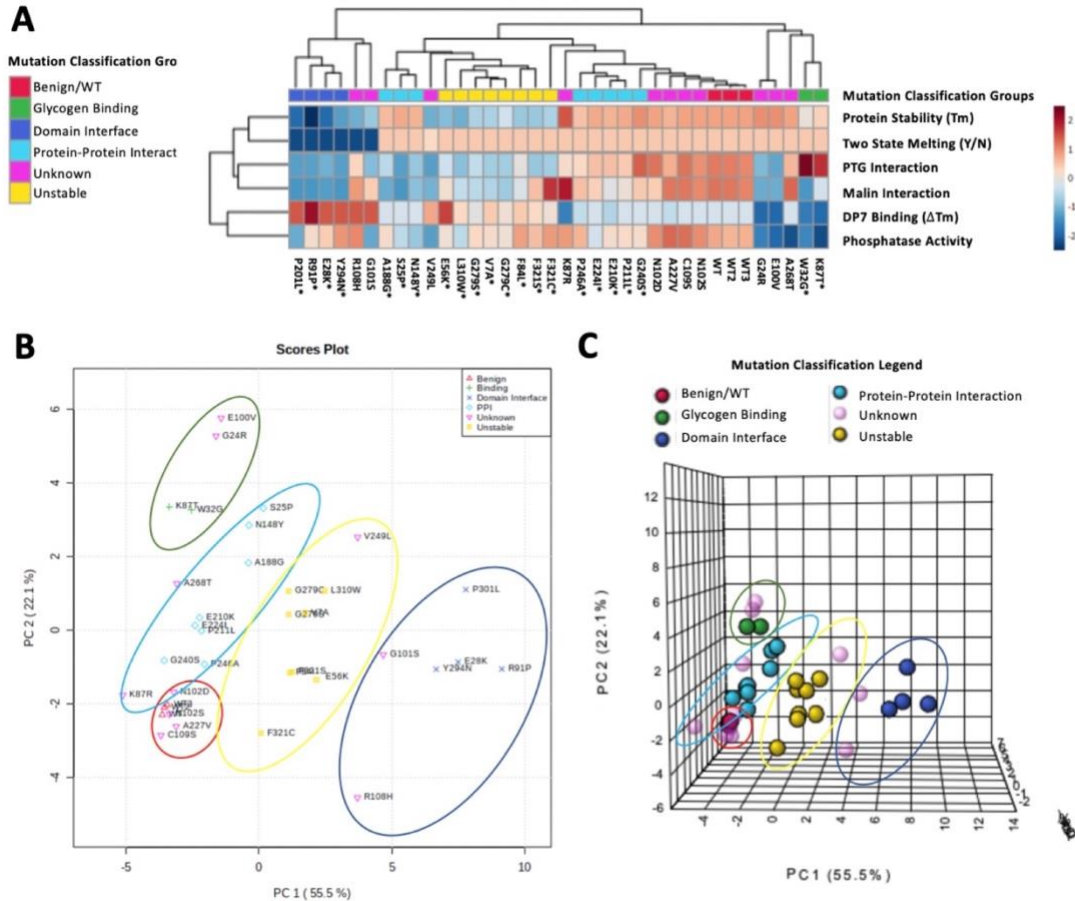


Figure 3.8 Multivariate Analysis of SNP Pipeline Results and Pathogenicity Assignments

A) Heatmap (Euclidian, average clustering) aligning the novel SNP profiles with previously characterized patient mutations (* indicates data from Brewer et al. iScience 2021).

B) Two-dimensional supervised PCA showing patient mutations and novel SNPs clustered according to their primary functional defect. Colored circles reflect the relationship clusters from the Heatmap.

C) Three-dimensional representation of (B), with SNPs of unknown pathogenicity in translucent pink, showing their tentative clustering near either WT laforin or patient mutation groups.

CHAPTER 4. DEFINING DRIVER-GENE CHARACTERISTICS FOR LAFORA DISEASE IN MOUSE MODELS

4.1 Introduction

The genetic drivers of Lafora Disease (LD) were discovered in the late 1990s and early 2000s [48, 51, 128, 129]. EPM2A (epilepsy, progressive myoclonus 2A) was the first driver-gene identified for LD, and was later shown to code for the glycogen phosphatase laforin [53, 129]. A second genetic driver, EPM2B (epilepsy, progressive myoclonus 2B), was identified a few years later, and was shown to code for an E3 ubiquitin ligase, malin [51, 54]. Laforin knock-out (LKO) and malin knock-out (MKO) mouse models were developed to study disease progression [107, 130]. Both models accumulated Lafora bodies (LBs), which were later demonstrated to drive disease progression, and exhibited neurological defects [107, 130]. For several decades, LKO and MKO models have been used interchangeably to investigate disease progression and treatment options. However, over the past two decades, certain clinical reports have suggested that LD patients with missense mutations in EPM2B have a less rapid disease progression compared to patients with missense EPM2A mutations [70, 73, 75, 76, 131-133]. While patients with LD exhibit the same phenotypic disease progression regardless of the driver-gene, clinical data suggests that specific mutation(s) in laforin or malin can influence the rapidity of progression [68, 73, 76, 78, 131]. For laforin, we have demonstrated a genotype-phenotype correlation between the type and degree of functional loss in the laforin mutant and the rapidity of disease progression [112]. A genotype-phenotype correlation for mutations in malin has not yet been established, however, we hypothesize that a similar correlation would emerge based on the degree and type of functional loss.

Both laforin and malin perform multiple interactions required to regulate glycogen metabolism. Laforin binds to glycogen and is thought to act as a scaffold, allowing other glycogen-regulating proteins, such as Protein Targeting to Glycogen (PTG) and malin, to interact. In addition, laforin can remove phosphate from glycogen and is the only known mammalian glycogen phosphatase [53, 106, 119]. However, the pathogenicity of loss of phosphatase activity has been brought into question in recent years, as a mouse model expressing phosphatase-inactive laforin, laforin C266S (LCS), did not form LBs [57]. While the functions of laforin have been well-characterized, the functions of malin as an E3 ligase are still being elucidated and characterized. Malin is thought to regulate glycogen metabolism through the ubiquitination of other glycogen-regulating enzymes [54, 105, 134]. It has been shown to ubiquitinate laforin, PTG, glycogen debranching enzyme (AGL), AMP-activated protein kinase (AMPK) and glycogen phosphorylase (GP), although the effect of malin ubiquitination is not fully understood for each of these interactions [54, 56, 125, 134-136]. Data suggest that malin-directed ubiquitination of laforin and PTG targets them for degradation, while malin-directed ubiquitination of GP has been shown to translocate the enzyme to the nucleus, where it participates in nuclear glycogen metabolism and promotes histone acetylation [54, 56, 125, 137]. When there is a loss of function in either laforin or malin, aberrant glycogen forms, characterized by poor branching, extended linear chain lengths, and hyperphosphorylation, leading to LB aggregation [59, 60].

While tools and assays are still being developed to elucidate the mechanisms of laforin and malin in glycogen metabolic regulation, our lab has developed a suite of analyses using immunohistochemistry (IHC) and mass spectrometry to spatially define glycogen aggregation throughout the brain and determine metabolic profiles resulting from the loss of enzymatic function [98, 138]. Using these tools, we can define the impact of loss of laforin, loss of laforin phosphatase activity, or loss of malin on the rate of LB accumulation, providing critical insights into the rate of disease progression based on the driver-gene. In this chapter, we establish the differences in LB accumulation and metabolic profiles between the LKO, LCS, and MKO mouse models.

4.2 Results

4.2.1 LKO mouse model shows rapid glycogen accumulation compared to LCS and MKO mouse models

Using IHC and MALDI analyses, we sought to explain a phenomenon observed in the LCS mouse model. Laforin C266S is the catalytically inactive form of laforin where the glycogen phosphatase activity is completely abolished. Interestingly, when an overexpression of laforin C266S was introduced into an LKO mouse model, no LB aggregates were observed [57]. This led to the suggestion that phosphatase activity is not necessary to prevent pathogenicity in LD patients. Previous work from our lab established that the Laforin C266S mutant has a gain-of-function in binding to glycogen in addition to the loss of phosphatase activity [86, 139]. To further investigate the impact this has on glycogen accumulation, we used IHC with an anti-glycogen antibody to visualize glycogen accumulation in brain, skeletal muscle, and heart tissue from 10-month old WT, LCS, and LKO mice. While LCS mice did not show the characteristic LB aggregates found in the LKO mice, there was diffuse staining throughout multiple tissue types compared to WT, suggesting that overall glycogen levels may still be increased (Figure 4.1A). To clarify this observation, 3 brain slices from each mouse model were treated with isoamylase to cut apart the branched glycogen into its linear components and run through MALDI analysis to quantify glycogen abundance in the hippocampus, one of the brain regions that shows the greatest accumulation of LBs in LKO mice (Figure 4.1B). While LKO had the highest abundance of glycogen accumulation, the LCS levels of glycogen were elevated compared to WT. To determine the impact of laforin C266S on glycogen chain length, the distribution of chain lengths was graphed. Surprisingly, the LKO and LCS mice showed a similar increase in linear glucose chain-lengths DP7 – DP11 compared to the WT mice. This suggests that phosphatase activity does play a role in regulating glycogen architecture.

In order to track the aggregation of LBs and spatially define glycogen accumulation in the brain as the disease progresses for both driver-genes, 3-, 6-, and 9-month WT, LKO, and MKO mice (n=3) were analyzed for glycogen content using MALDI mass spectrometry, allowing for the spatial analysis of linear chain lengths of glycogen. Maltoheptaose (DP7), a linear oligosaccharide composed of seven glucose moieties, is one

of the most abundant chain lengths in glycogen and provides a good measure of glycogen content (Figure 4.2A). At 3-months, LKO mice show an increase in glycogen levels in the hippocampus and cerebellum, while 3-month MKO mice look similar to the WT mice in terms of glycogen abundance. Strikingly, while LKO mice showed global accumulation of glycogen throughout nearly all brain regions by 6 months, 6-month MKO mice showed aggregation primarily in the hippocampus and cerebellum. At 9 months, both LKO and MKO mice show global accumulation of glycogen, although the glycogen abundance levels in MKO mice appear lower compared to the LKO mice (Figure 4.2A). A similar visual survey was performed for the DP15 chain length of glycogen. Previous studies of LB composition revealed a higher composition of long chain lengths (>DP12) compared to WT glycogen architecture. Therefore, one would expect to see a pronounced difference in abundance of DP15 between the WT and LD mouse models. The same trends observed in DP7 are present in the analysis of DP15 abundance, with a particular concentration of DP15 in the hippocampus and cerebellum for both LKO and MKO mice (Figure 4.2B).

The regional differences observed in the MALDI spatial analysis provide some insight into the regions of the brain likely to be most affected by the aggregation of LBs. To tease apart this relationship, the slices were annotated to isolate the hippocampus, cerebellum, cerebral cortex, and hindbrain and quantify the glycogen accumulation in those regions (Figures 4.3 and 4.4). At 3 months of age, MKO mice show similar levels of glycogen abundance compared to WT mice in all regions of the brain (Figure 4.3A). LKO mice, by contrast, show increased glycogen abundance in the hippocampus, cerebellum, and hindbrain regions. However, the LKO glycogen abundance in the cerebral cortex is similar to abundance levels in WT mice (Figure 4.3A). To examine the changes in glycogen architecture, the percent of chain length distribution was graphed (Figure 4.3B). In the cerebellum and hippocampus, the LKO mice show a distinct chain length distribution compared to the WT and MKO mice. The same analysis was performed on the 9-month brain slices. Both the 9-month LKO and MKO mice show increased glycogen abundance compared to WT in all four regional analyses, however, the glycogen accumulation in the MKO model is consistently lower compared to the abundance of glycogen in the LKO mice (Figure 4.4A). An analysis of the glycogen architecture through graphing the chain length distribution reveals that the glycogen in LKO and MKO mice contain a greater prevalence of long chain lengths compared to the WT mice (Figure 4.4B).

4.2.2 Metabolomics profiles are driver-gene dependent in LD mouse models

Glycogen is the primary energy storage polysaccharide for mammals, and glycogen synthesis and degradation are tightly regulated in relationship to the cytosolic energy levels that drive central carbon metabolism, particularly in the brain [140, 141]. Previous work in our lab demonstrated that LKO mice show a significant decrease in the abundance of central carbon metabolites in brain tissue, suggesting that aberrant glycogen alters brain metabolism [61]. Since the LCS mice produced an aberrant glycogen architecture similar to the LKO mice, we took frozen brain tissue samples from 12-month old mice, extracted the polar metabolites, and used Gas Chromatography Mass Spectrometry (GCMS) in order to compare their levels of central carbon metabolites (Figure 4.5A). Both LCS and LKO

mice showed a similar decrease in abundance of central carbon metabolites compared to the WT mice. Having compared the LCS and LKO mice, we then compared the metabolic profile of 12-month-old MKO mice against a WT cohort. Surprisingly, the MKO mice did not show a significant change in central carbon metabolites compared to the WT mice (Figure 4.5B).

4.2.3 Glycosylation defects differ between LKO and MKO mouse models

Recent work from our lab identified a glycosylation defect in LKO mice [100]. The data suggest that glycogen in the brain acts as a repository for sugars other than glucose which are needed for synthesizing glycans for protein glycosylation [100]. Since the LBs cannot be degraded, the sugars needed to synthesize glycans become inaccessible, leading to a widespread glycosylation defect. Given the differences observed in the rates of glycogen accumulation in LKO versus MKO mice, we sought to characterize glycosylation defects in the MKO mice. 3-, 6-, and 9-month WT, LKO, and MKO mice were analyzed using MALDI mass spectrometry. Brain slices were mounted on slides and treated with PNGase to release the glycan decorations from glycoproteins. Figure 4.6 shows MALDI imaging from two different glycans detected in each mouse model, which demonstrated a significant change in levels depending on the mouse model. At 3-months, there is no significant change in glycan levels observed between the WT, LKO, and MKO mice. At 6 and 9 months, however, the LKO mice exhibit a dramatic decrease in glycan levels compared to the WT mice. Surprisingly, this pattern is not observed in the MKO mice, and no significant decrease in glycosylation is detected compared to WT. The levels of 18 different glycans were quantified and assessed for changes in relative abundance in the hippocampus in the 9-month-old mice. Glycan levels were consistently decreased in LKO mice compared to the WT and MKO cohorts (Figure 4.6C-E).

4.3 Discussion

As we work toward the goal of personalized medicine and defining patient cohorts in LD, it will be important to define the relationship between the specific loss of enzymatic function and the accumulation of LBs, which drives the etiology of the disease. In this chapter, we utilized mouse models to determine the changes in glycogen accumulation and LB aggregation given the complete loss of laforin, laforin phosphatase activity, or malin. We demonstrated that all three mouse models produced aberrant glycogen. However, the rate of accumulation differed significantly between the three models.

Past studies have shown that mice expressing Laforin C266S, the phosphatase inactive form of laforin, do not form LBs, which calls into question the contribution of laforin phosphatase activity toward preventing LD [57]. These studies confirmed that the resulting glycogen was hyperphosphorylated, but that hyperphosphorylation did not lead to LB aggregation [57]. Our analyses of glycogen chain length distribution showed that LCS mice produce aberrant glycogen chain length patterns similar to LKO mice,

suggesting that glycogen chain lengths are extended in the LCS mouse model compared to WT mice. Given the aberrant architecture, one would expect LBs to form, but at 12 months of age, no LBs were observed in any of the LCS mouse tissues. MALDI analysis of the LCS mouse tissue does show elevated levels of glycogen accumulation compared to WT mice, but the accumulation does not reach the same level as the LKO mice. One hypothesis for this phenomenon is the impact of the C266S mutation on glycogen binding. Past work in our lab demonstrated that laforin C266S exhibits greater stability when interacting with long linear glucose chains compared to WT laforin [86, 139]. Therefore, it is possible that this preference for the longer chain lengths provides the LCS mice with a gain of function that allows them to degrade glycogen through upregulation of an alternate pathway such as glycolysis. Assessment of glycolysis markers in LCS mice compared to WT and LKO mice could provide some insight into the viability of this hypothesis. Additionally, a recently identified patient mutation, A268T, shows complete loss of phosphatase activity but no significant loss or gain of other laforin functions. Creating an A268T mouse model would provide a more accurate assessment of the contribution of glycogen hyperphosphorylation to LB aggregation.

Having characterized the glycogen architecture and aggregation in LKO and LCS mice, we then sought to compare the glycogen aggregation between the two different driver-genes for LD using the LKO and MKO mouse models. Patients with LD present the same phenotype regardless of the driver-gene. However, multiple clinical reports suggest that the driver-gene could impact the rapidity of disease progression [68, 70, 73, 75, 76, 133]. While the mechanism through which malin contributes to Lafora Disease remains unclear, studies from multiple labs have shown that the LB aggregations arising from loss of laforin or malin drive the disease progression [60, 61, 63, 67, 142]. Therefore, we defined the spatial aggregation of LBs in the brain in 3-, 6-, and 9-month MKO mice and compared it against age-matched LKO and WT mice. Several patterns emerged from this analysis. First, glycogen aggregated more slowly in MKO mice compared to LKO mice across all brain regions. If this trend holds true in LD patients, then a slower rate of glycogen aggregation could explain the slower progression through the disease. Second, with the slower aggregation rate in MKO mice, it becomes clear that the rate of aggregation changes depending on the brain region. Most IHC studies in LD focus on the hippocampus, which has a high prevalence of LBs. This time-course analysis shows that aggregation becomes detectable first in the hippocampus and cerebellum, followed by aggregation in the hindbrain. It was only in the 9-month old MKO mice that aggregation in the cerebral cortex was detectable. In previous time-course studies focused on LKO mice, this regional variation was harder to visualize because of more rapid glycogen accumulation [143]. Further studies on the role of malin will be required to elucidate why the glycogen accumulation is slower. However, this difference between the two mouse models presents an opportunity to compare faster and slower rates of disease progression, providing a tool for testing the efficacy of therapies on different patient cohorts.

In addition to variation in the rate of glycogen accumulation, there are significant differences between the metabolic profiles of the LKO, LCS, and MKO mouse models. The LKO metabolic profile has been characterized previously, and consistently shows a decrease in the abundance of central carbon metabolites in brain tissue past the age of 6 months [143]. Therefore, 12-month old LKO, LCS, and MKO mice were selected for

metabolic analyses. Surprisingly, given the lack of LB aggregation in LCS mice, they displayed a similar decrease in central carbon metabolites compared to the LKO mice. One possible explanation for this is the similarity of the glycogen architecture between the LKO and LCS mice. The hyperphosphorylation and increased chain lengths would decrease the solubility and enzyme accessibility of the glycogen. Even if that aberrant glycogen was degraded through the glycolysis pathway before it could aggregate into LBs, it is possible that glycogen degraded through glycolysis does not have the same metabolic fate as glycogen degraded in the cytosol. Analysis of other metabolic pathways could help to further distinguish the LKO and LCS metabolic profiles and perhaps elucidate a metabolic role for the phosphorylation of glycogen.

In contrast to the LKO and LCS mice, the MKO mouse model did not exhibit a significant change in central carbon metabolite levels compared to the WT cohort. It is possible that the slower aggregation of glycogen in the MKO model simply delays the decrease in central carbon metabolism. Older MKO mice could be analyzed to determine if the metabolic profile changes after reaching similar levels of LB aggregation to those found in the 6-month LKO mice. Another possible explanation could involve malin's regulation of GP localization. Since malin-directed ubiquitination of GP localizes GP to the nucleus, a loss of malin could theoretically lead to an increase of GP activity in the cytosol. Increased activity of GP could potentially slow the aggregation of glycogen and release more glucose from aberrant glycogen before it becomes insoluble, offsetting some of the impact of trapping glucose in LBs. However, additional studies will be needed to determine if either hypothesis has merit.

A final point of variation from our mouse model characterization is the difference in glycosylation levels between the LKO and MKO mice. In the LKO mouse model, a global decrease in protein glycosylation is observed. However, while some glycan levels in the MKO mouse model are decreased compared to WT mice, the difference is not statistically significant. It is possible that the glycosylation defect only emerges once LB aggregation has reached a certain stage. If that is the case, then perhaps older MKO mice would exhibit a glycosylation defect. Further experimentation is necessary to test that hypothesis. An alternate hypothesis is that laforin plays a regulatory role in the integration and release of sugars for glycan synthesis – a role that it could fulfil independently of malin. This hypothesis could be tested through an analysis of the LB carbohydrate composition between LKO and MKO mouse models. If the MKO LBs have higher glucose content percentage-wise compared to the LKO LBs, then it is possible that the MKO model would not exhibit a glycosylation defect regardless of stage of disease progression. If this trend replicated in patients, then it would be an important distinction for determining therapy options for patients with the laforin driver-gene compared to the malin driver-gene. These results highlight the necessity of testing therapeutics on both LKO and MKO mouse models to determine their efficacy, which is the focus of the next chapter.

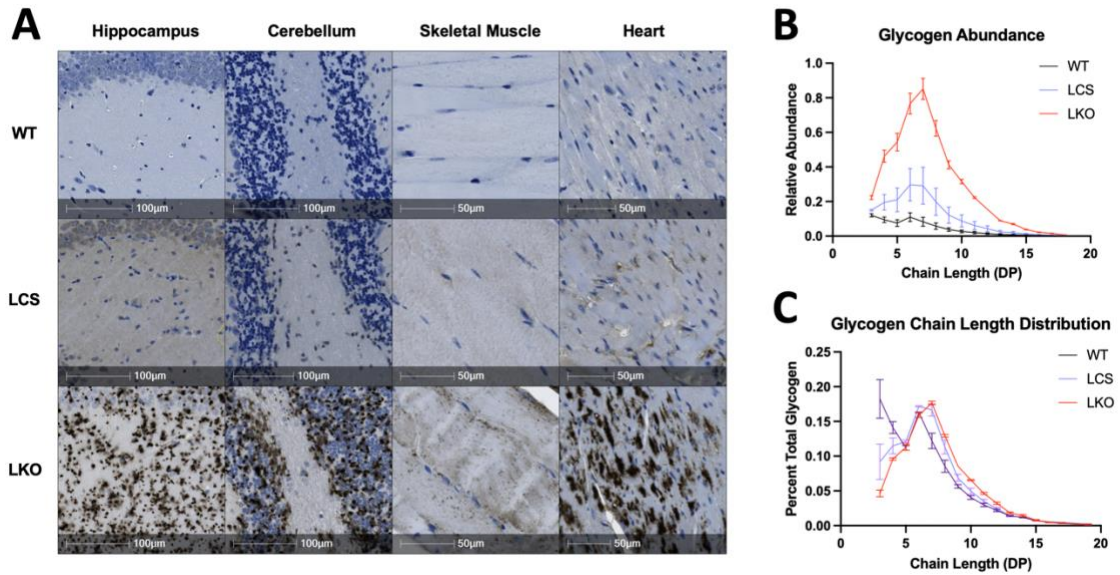


Figure 4.1 IHC and MALDI Analysis of Glycogen Content in LKO and Laforin C266S (LCS) Mice Compared to WT

A) IHC staining for glycogen using antibody IV58B6 in the hippocampus, cerebellum, skeletal muscle, and heart of LKO, Laforin C266S and WT mice.

B) MALDI analysis of the relative abundance of linear glycogen chain lengths in brain tissue from WT, LCS, and LKO mice.

C) MALDI analysis showing the percent abundance of each linear chain length in brain tissue compared between the WT, LCS, and LKO mouse models.

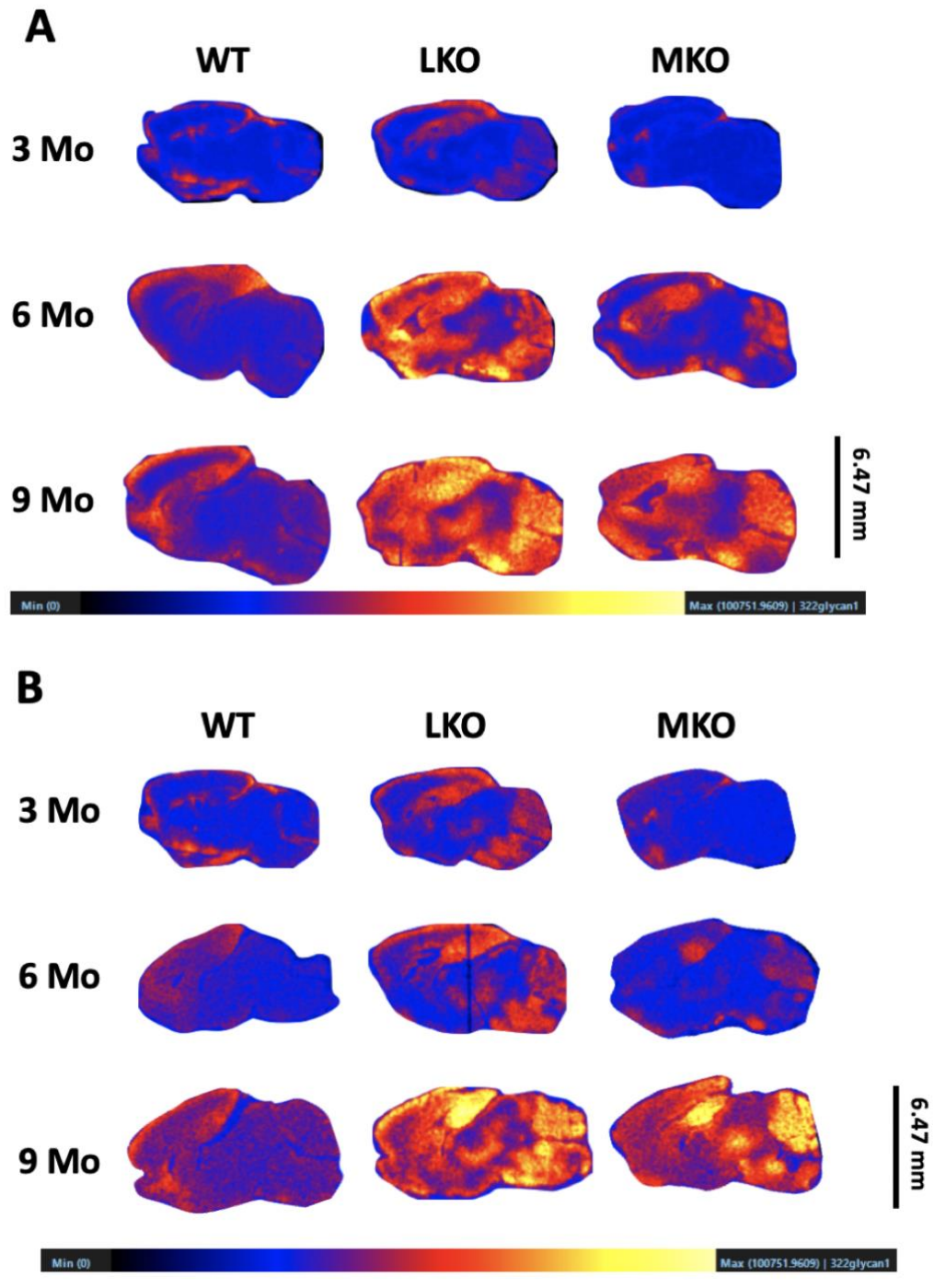


Figure 4.2 MALDI Analysis of Glycogen Content in WT, LKO, and MKO Mice
 A) Representative images of maltoheptaose (DP7) concentration in brain tissue from WT, LKO, and MKO mice at 3, 6, and 9 months.
 B) Representative images of DP15 concentration in brain tissue WT, LKO, and MKO mice at 3, 6, and 9 months.

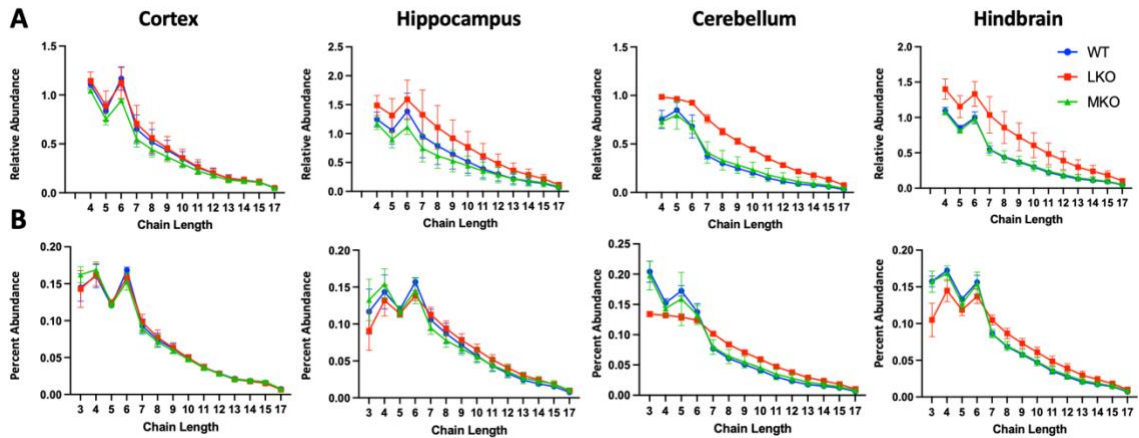


Figure 4.3 Quantification of MALDI Analysis of Glycogen Content in WT, LKO, and MKO Mice at 3 Months of Age

A) Plots of relative abundance for each chain length of glycogen in WT (blue), LKO (red), and MKO (light green) mice. Brain regions analyzed (from left to right) were the cortex, hippocamps, cerebellum, and hindbrain.

B) Plots of percent abundance for each chain length of glycogen in WT (blue), LKO (red), and MKO (light green). Brain regions analyzed (from left to right) were the cortex, hippocamps, cerebellum, and hindbrain. Three mice were analyzed for each group, and the mean and SEM plotted in the figures.

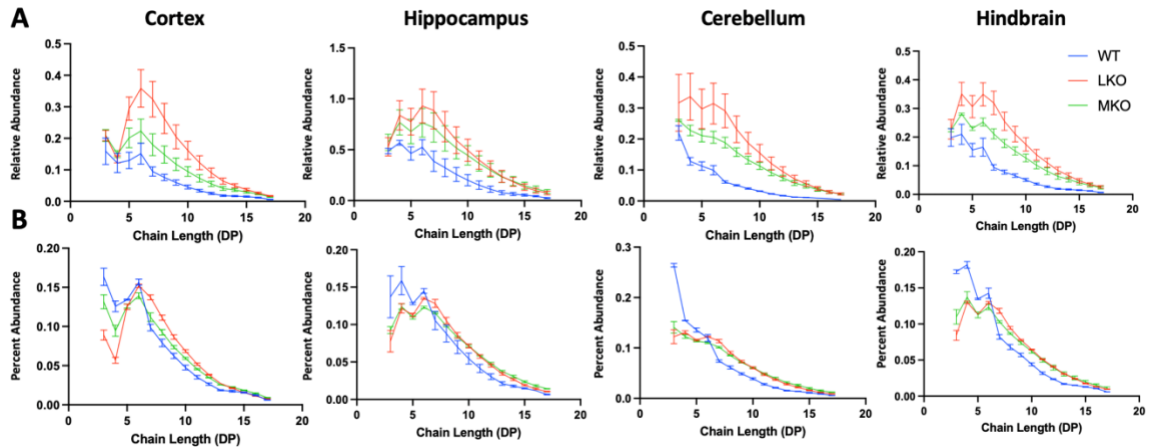


Figure 4.4 Quantification of MALDI Analysis of Glycogen Content in WT, LKO, and MKO Mice at 9 Months of Age

A) Plots of relative abundance for each chain length of glycogen in WT (blue), LKO (red), and MKO (light green) mice. Brain regions analyzed (from left to right) were the cortex, hippocamps, cerebellum, and hindbrain.

B) Plots of percent abundance for each chain length of glycogen in WT (blue), LKO (red), and MKO (light green). Brain regions analyzed (from left to right) were the cortex, hippocamps, cerebellum, and hindbrain. Three mice were analyzed for each group, and the mean and SEM plotted in the figures.

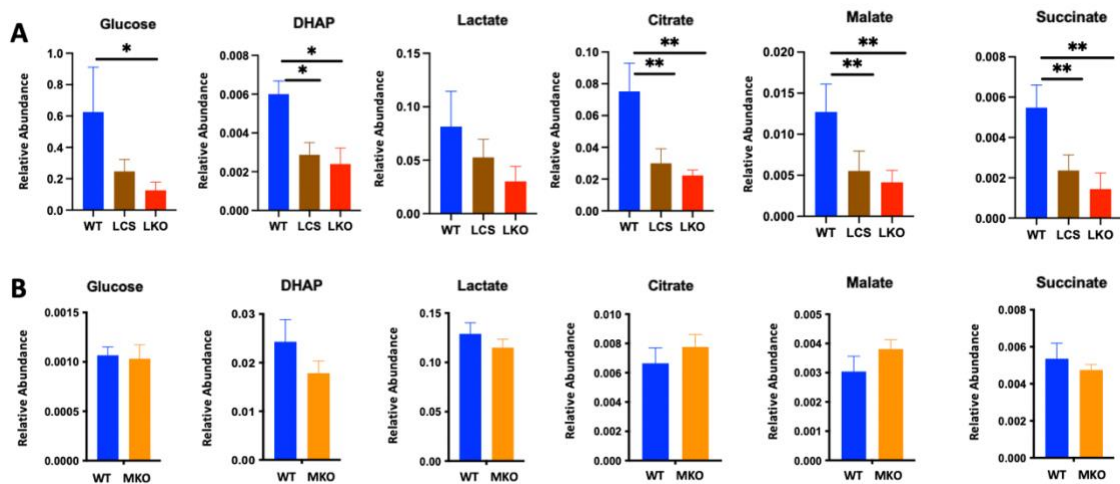


Figure 4.5 Metabolomics analysis of WT, LCS, LKO, and MKO mouse models

A) Relative abundance of select central carbon metabolites in brain tissue from 12-month WT, LCS and LKO mice.

B) Relative abundance of select central carbon metabolites in brain tissue from 12-month WT, MKO mice.

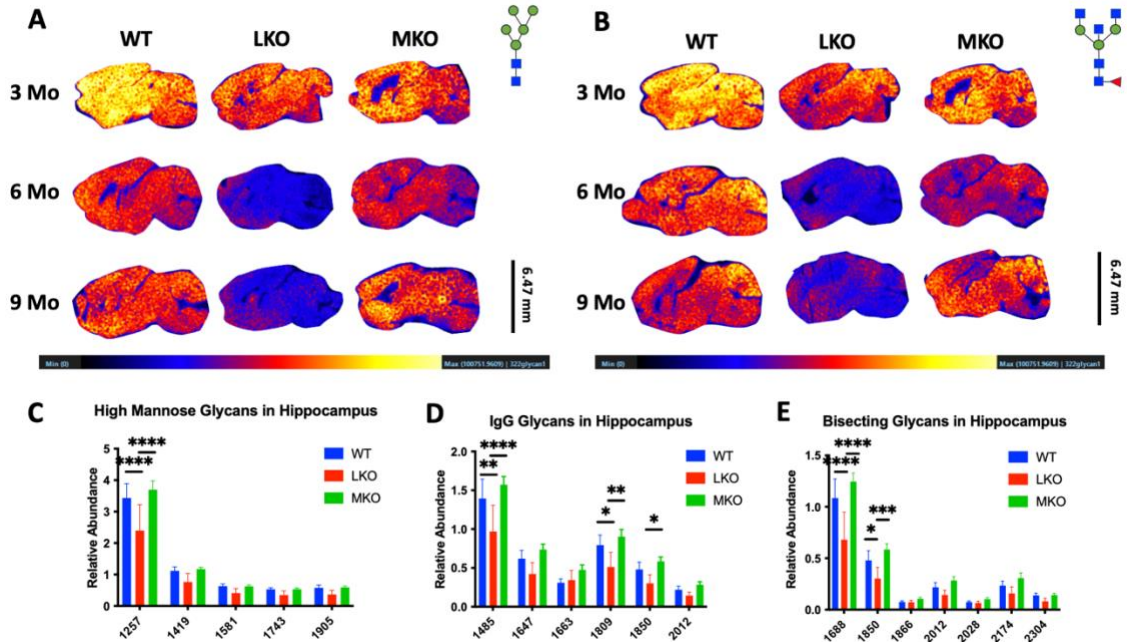


Figure 4.6 MALDI Analysis of Glycosylation in WT, LKO, and MKO Mice.

A) Representative images of glycan 1257 concentration in WT, LKO, and MKO mice at 3, 6, and 9 months. Glycan schematic pictured in top right corner, blue squares are N-acetylglucosamine and green circles are mannose.

B) Representative images of glycan 1688 concentration in WT, LKO, and MKO mice at 3, 6, and 9 months. Glycan schematic pictured in top right corner, blue squares are N-acetylglucosamine, green circles are mannose, and red triangle is fucose.

C) Quantification of high mannose glycans in the hippocampus for 9-month-old WT, LKO, and MKO mice.

D) Quantification of IgG glycans in the hippocampus for 9-month-old WT, LKO, and MKO mice.

E) Quantification of bisecting glycans in the hippocampus for 9-month-old WT, LKO, and MKO mice.

* $P < 0.05$; ** $P < 0.01$; *** $P < 0.001$; **** $P < 0.0001$

CHAPTER 5. GYS1 ANTISENSE THERAPY PREVENTS DISEASE-DRIVING AGGREGATES AND EPILEPTIFORM DISCHARGES IN A LAFORA DISEASE MOUSE MODEL

5.1 Introduction

Lafora Disease (LD) is a devastating childhood epilepsy and dementia, brought on by autosomal recessive mutations in either *EPM2A* or *EPM2B*, which encode for the glycogen phosphatase laforin and E3 ubiquitin ligase malin, respectively [48-54, 102, 144]. These two enzymes regulate glycogen storage in tissues throughout the body. When the function of either protein is impaired, aberrant glycogen with hyperphosphorylation and extended glucose chains form and aggregate into Lafora Bodies (LBs) [57, 60, 108, 145-147]. Patients with LD develop seemingly normal until early adolescence, when they experience seizures with increasing frequency and severity, coupled with neuroinflammation and neurodegeneration that is accompanied by rapid childhood dementia [58, 101, 148, 149]. There is currently no approved therapy for LD, and the progression of the disease proves fatal after approximately 11 years from the onset of symptoms [69, 71].

Among LD patients, about half exhibit a mutation in *EPM2A*, while the other half present with a mutation in *EPM2B* [71]. Therefore, an ideal therapeutic should demonstrate efficacy in LD patients regardless of which gene is mutated. While the precise mechanism of the disease is not fully understood, particularly in regards to the contribution of malin ubiquitination, the loss of malin or laforin function yields aberrant glycogen and subsequent LB aggregation that drives very similar disease progression in patients with mutations in either gene. Multiple studies have demonstrated that LBs are the driving agent behind disease progression [63, 150-152]. Multiple laboratories hypothesized that reducing glycogen synthesis would slow LB aggregation and therefore slow disease progression. Subsequent studies in multiple murine models from numerous laboratories demonstrated that when glycogen synthesis is reduced by 50% in LD mice, LBs do not form and disease symptoms are reduced or abrogated [63, 109, 151, 152]. Therefore, glycogen synthase 1 (*GYS1*), the enzyme that drives glycogen synthesis in the brain, was selected as a target for LD therapeutics.

A *Gys1* anti-sense oligonucleotide (ASO) was recently developed that successfully decreased *Gys1* expression in the brain for LD mouse models [65]. The efficacy of the *Gys1*-ASO treatment was tested in young *Epm2a*^{-/-}, laforin knock-out (LKO), LD mice compared to treatment efficacy of older mice and with varied length of treatment [65]. Treatment was more effective the earlier the *Gys1*-ASO was administered. Although *Gys1*-ASO treatment did not clear existing LBs, the *Gys1*-ASO did halt LB formation and reduce neuroinflammation in LKO mice [65].

Given the promising results in long-term administration to LKO mice, we sought to determine if the *Gys1*-ASO therapy produced similar results in the *Epm2b*^{-/-}, malin knock-out (MKO), mouse model and to define if the *Gys1*-ASO modulated neuronal excitability. Therefore, we treated a cohort of MKO mice with the same *Gys1*-ASO and assessed the impact of treatment on *Gys1* expression and glycogen accumulation

throughout the brain in both male and female cohorts. Using histological and mass spectrometry analyses, Gys1-ASO treatment significantly reduced the expression of Gys1 and synthesis of glycogen in the brain, reducing glycogen accumulation in LBs. Furthermore, brain slices from the malin KO mice were analyzed for neuronal excitability, and slices treated with Gys1-ASO exhibited a reduction to near WT levels of excitability, suggesting that treatment with the Gys1-ASO could decrease seizure potential in LD. Cumulatively, our analyses, coupled with previous results, demonstrate critical proof of concept data that this Gys1-ASO is effective for LD caused by mutations in *Epm2a* or *Epm2b*.

5.2 Results

5.2.1 Gys1-ASO Decreases *Gys1* mRNA and Gys1 Protein Expression

As previously demonstrated, a Gys1-ASO was developed to knock down glycogen synthase expression in the brain and validated it as a therapeutic agent in LKO mice [65] (Figure 5.1A). To test the Gys1-ASO as a therapeutic approach in MKO mice, we assigned male and female mice into groups (n=5 per group) for no surgery or surgery with vehicle, control scrambled ASO, or Gys1-ASO via intracerebroventricular (ICV) injections. Mice were administered treatment at 4-, 7-, and 10-months of age, and were sacrificed at 13-months (Figure 5.1B). Brain hemispheres were divided via sagittal dissection with the side ipsilateral to the ICV injection flash frozen and the side contralateral to the ICV injection fixed in formalin and embedded in paraffin for analysis.

To evaluate the efficacy of the Gys1-ASO, levels of *Gys1* mRNA and protein expression were analyzed. The frozen brain tissue was pulverized, cells lysed, RNA was extracted from the lysate, and qRT-PCR was performed to quantify mRNA expression of *Gys1*. For both the female and male cohorts, *Gys1* mRNA decreased significantly in the Gys1-ASO treated cohort (Figure 5.2A, F). The lysate was then immunoblotted to assess Gys1 protein expression. Gys1-ASO treatment dramatically decreased Gys1 protein levels compared to control animals in both sexes (Figure 5.2B-C, G). To assess spatial Gys1 reduction, anti-GYS1 immunohistochemistry (IHC) was performed and revealed a striking decrease in Gys1 levels in all brain regions for both female and male mice treated with the Gys1-ASO (Figure 5.2D-E, H-I).

5.2.2 Gys1-ASO Treatment Reduces Glycogen Accumulation

Historically, Periodic Acid-Schiff (PAS) staining was the primary method used to assess LB accumulation. PAS staining targets carbohydrate macromolecules, like glycogen and LBs by using periodic acid to break their carbon-carbon bonds and oxidize the hydroxyl groups to produce two aldehyde groups, and then Schiff reagent reacts with the aldehyde group to produce a fuchsia or deep purple staining [153]. In LD murine models,

the hippocampus exhibits significant accumulation of LBs via PAS staining. Therefore, hippocampal regions from each of the MKO treatment groups were analyzed by PAS staining [102, 105]. (Figure 5.3A, C). HALO software was used to quantify the number of LBs in the hippocampus and plot the number of LBs in each size bracket. In both females and males, we observed a significant decrease in the number of larger LB aggregates (area $>5\mu\text{m}^2$) in the Gys1-ASO treatment group compared to the controls (Figure 5.3B, D).

While PAS staining allows comparison to previous studies, the IV58B6 anti-glycogen antibody exhibits increased specificity for glycogen and decreased variability [154]. We performed IHC using IV58B6 to assess glycogen accumulation in each MKO treatment group (Figure 5.3E, G). IHC of IV58B6 staining in the hippocampus was significantly lower in the Gys1-ASO treated group compared to the controls (Figure 5.3F, H).

A method utilizing Matrix Assisted Laser Desorption/Ionization (MALDI) coupled with mass spectrometry was recently developed to define the spatial glucose chain length distribution of glycogen [99]. In LD mouse models, glucose chain length is extended compared to wildtype glycogen, which promotes LB aggregation [57, 59]. Sagittal slices from paraffin blocks were treated with a citraconic acid buffer for antigen retrieval, then sprayed with an isoamylase matrix to hydrolyze glycogen at α -1,6-branch points to produce linear glucose chains. The treated slices then underwent MALDI coupled with time-of-flight detection to profile the quantity of these linear glucose chain distribution from glycogen among different brain regions, which can be used to quantify glycogen levels. The MKO mice treated with Gys1-ASO displayed significantly less glycogen accumulation in all brain regions compared to the control groups, in agreement with the IHC staining (Figure 5.4A). Quantification of the glucose chain lengths in both the hippocampal and cerebellum regions confirmed a reduction in glycogen levels for Gys1-ASO treated mice compared to the control groups (Figure 5.4B-C).

5.2.3 Gys1-ASO Treatment Decreases Neuronal Excitability in MKO Mice

Multiple studies have demonstrated that LBs drive disease progression. Indeed, crossing LD mouse models with genetic models that reduce glycogen levels eliminates early-onset neurodegeneration and normalizes seizure susceptibility [61, 63, 109, 151, 152]. Recently, multiple groups have developed pre-clinical LD therapies that include enzyme therapy to degrade LBs, and both Gys1-ASO and AAV-based therapies to down-regulate Gys1 [64-66, 111, 155, 156]. To date, no study has tested if treatment impacts epileptiform activity, which is a key hallmark of the disease. Since administration of the Gys1-ASO halted the progression of LB aggregation, we sought to test the impact on epileptiform discharges (ED). 4-month-old MKO and wildtype littermates were administered either vehicle or Gys1-ASO via ICV. After 3 months, the mice were sacrificed and slices from their hippocampi were placed on electrodes for multi-electrode analysis (MEA) analyzed for synaptic firing and epileptiform discharge activity (Figure 5.5A-B). Slices from the contralateral side were probed to define the effect of Gys1-ASO treatment. When compared to wildtype vehicle-injected mice, the MKO vehicle-injected

mice displayed a significantly higher rate of synaptic firing when averaged over a 5-minute time period (Figure 5.5C). Additionally, the MKO vehicle-injected mice displayed higher rates of ED compared to the wildtype controls (Figure 5.5D-E). Conversely, MKO mice treated with Gys1-ASO exhibited a significant decrease in both synaptic firing and ED over the same time period when compared to the vehicle-injected MKO mice (Figure 5.5C-E).

5.3 Discussion

LD impacts seemingly previously healthy teens with progressive epilepsy and childhood dementia. There is currently no treatment for this devastating disease, but targeting glycogen synthesis via Gys1-ASO administration is a promising pre-clinical strategy. ASO treatment is a safe and well-tolerated technique that has been utilized in the pre-clinical settings for more than 50 years [157]. There are ten ASO drugs that have received FDA approval to date, and more than 100 ASO drugs at multiple stages of clinical trials for a number of diseases [157, 158]. In this study, we demonstrate that the Gys1-ASO treatment is effective at decreasing glycogen synthase levels. The reduction in Gys1 protein levels corresponds to decreased glycogen accumulation and reduced ED in an MKO model of LD, suggesting that slowing glycogen aggregation into LBs reduces neuronal excitability.

The mechanism of the Gys1-ASO works by binding to *Gys1* mRNA at a target site that activates RNase H1, which accelerates the degradation rate of the target mRNA [65, 159]. While only a marginal decrease in *Gys1* mRNA was observed, the treatment with Gys1-ASO led to a significant decrease in Gys1 protein expression. This phenomenon has been observed in multiple studies, where a small change in *Gys1* mRNA results in a significant change Gys1 protein expression [111, 152]. If this phenomenon holds true in humans, then patients would only need to see a small decrease in mRNA levels to experience significant knock-down of GYS1 activity and halt glycogen aggregation into LBs.

Aggregation and dysregulation of glycogen has been linked to multiple neurological diseases in recent years, including Pompe Disease, Amyotrophic Lateral Sclerosis, and Alzheimer's Disease [104, 140, 160-163]. Therefore, the ability to target and control glycogen synthesis in the brain is a potential therapeutic strategy for multiple diseases. Indeed, Maze Therapeutics recently demonstrated promising pre-clinical results for small molecule inhibition of Gys1 to treat Pompe Disease in murine and canine models [164, 165]. Gys1 is responsible for driving glycogen synthesis in all tissues except the liver, which utilizes Gys2. While glycogen is an important energy source in many organs, multiple groups have demonstrated that 50% reduction in glycogen levels does not produce adverse health effects in mouse models or in humans. Indeed, Gys1-heterozygous animals do not exhibit abnormalities despite synthesizing only 50% of wildtype levels of glycogen [166]. Several studies with Gys1-heterozygous mice demonstrate that they maintain similar weight to their wildtype counterparts, normal levels of serum glucose and lactate, normal lifespan, and no significant change in locomotor activity, balance, or gait [167, 168].

In addition to studying the impact of decreased glycogen synthase activity, multiple studies have examined the impact of a mutations in another gene that leads to decreased glycogen synthesis [169, 170]. The *PPP1R3A* gene encodes a positive regulator of glycogen synthesis, but there is a truncating mutation of *PPP1R3A* that results in ~65% reduction of glycogen synthesis [169]. When this mutation was introduced into a mouse model, the same ~65% decrease in glycogen synthesis occurred and no cardiac or other disease phenotype was identified in the mice [169]. A recent study quantified the health outcomes in humans with this truncation mutation using UK Biobank data [170]. Their study reported ventricular ejection fraction, wall thickness, maximum heart rate, and maximum workload, finding no association between *PPP1R3A* truncation and cardiac defects. They also did not observe changes in serum metabolites or glucose levels [170]. These data strongly suggest that a 65% reduction in glycogen synthesis is well tolerated. Given these data, it is not surprising that the Gys1-ASO was well-tolerated with no adverse symptoms in the current study. Similar to *PPP1R3A*, reduction of glycogen accumulation by Gys1-ASO was well-tolerated with no adverse symptoms in the current study.

The results with MKO mice demonstrate similar efficacy in reducing LB levels as a previous study that utilized LKO mice and the same Gys1-ASO. Of the patients with LD, about half of them have a mutation in *EPM2A* while the other half have a mutation in *EPM2B* [71, 101, 112]. The results from this study suggest that the Gys1-ASO is a potential long-term treatment for LD patients regardless of the driver gene. Therefore, patients who are screened for epilepsy genes and identify mutations in *EPM2A* or *EPM2B* could potentially receive this treatment to prevent glycogen accumulation and LD aggregation in the brain.

Equally important, the Gys1-ASO in this study achieved broad brain biodistribution and exhibits significant reduction of Gys1 throughout all brain regions. The Gys1 reduction resulted in decreased LB aggregates in all brain regions examined, including the hippocampus and cerebellum, where LBs are most prevalent in LD. Previous work demonstrated that a 50% knock-down of Gys1 activity was sufficient to prevent LB aggregation in murine models, and the data from this study supports that finding [62, 63, 109, 152].

Early screening could also be key for treatment efficacy given disease progression. LD is a progressive disease where LD patients and LD mouse models develop seemingly normally, indicating that there is no primary epileptic circuit in the LD brain [86, 101, 102, 149]. In both LD mice and patients, LB formation precedes symptomatic disease [102, 171-173]. Initial symptoms arise in the teen years for patients and at 3-4 months of age in LD mice, while LBs are detectable in mice that are weeks old [61, 67, 105, 149, 174]. Several laboratories utilizing multiple mouse models have demonstrated that LBs cause disease sequela, including myoclonus, perturbed synapse electrophysiology, increased susceptibility to seizure-inducing drugs, and progressive loss of both neuronal cells and cognitive function [61, 63, 67, 101, 109, 151, 152, 175]. Current data suggest that early treatment may reduce total LB accumulation.

While the specific regulation of glycogen by laforin and malin remains controversial, loss of function in either protein results in aberrant glycogen with increased phosphorylation and extended glucose chain lengths [59, 61, 125, 176, 177]. Previous

studies have demonstrated that extended glucose chains form helices that decrease water-solubility and increase glycogen aggregation to become LBs [60, 178]. Recent LB characterization revealed that this aberrant glycogen exhibits starch-like properties, with spontaneous formation of B-crystallinity, leading to insolubility and sequestration, forming LB aggregates [59]. Normally, there are two primary pathways for degrading glycogen in the brain: the brain isoform of Glycogen Phosphorylase (PYGB) is the primary enzyme responsible for degrading soluble glycogen in the brain, and alpha-glycosidase (GAA) is an enzyme expressed in the lysosome, responsible for degrading brain glycogen via glycophagy [107, 140, 162]. Neither of these degradation pathways successfully degrade or inhibit LBs in LD. As the aberrant glycogen aggregates into LBs, PYGB can no longer access the glucose moieties for degradation, and the rate of glycogen synthesis surpasses the ability of the glycophagy pathway to clear all the aggregates through normal GAA activity [156]. However, if one can reduce the rate of glycogen synthesis, then theoretically, these pathways could clear more of the aberrant glycogen before it aggregates into LBs. Our data, and previous work, support this hypothesis. Using multiple glycogen detection methods, we have demonstrated that treatment with Gys1-ASO significantly reduces glycogen accumulation throughout the brain in the MKO LD mouse model. Combined with previous work from the Minassian laboratory showing similar results in the laforin KO LD model, we have demonstrated that the Gys1-ASO therapy successfully reduces LB accumulation regardless of the driver gene.

Another important hallmark of LD is epilepsy. Patients display progressive myoclonus epilepsy, experiencing seizures of increasing frequency and severity. In mouse models, mice display increased susceptibility to kainite-induced seizures. However, even before seizures are evident in patients, they display abnormal EEG readings with epileptiform activity. Both LKO and MKO mouse models recapitulate this epileptiform activity as early as 3 months old [102, 179]. Importantly, the electrophysiology data suggests that the prevention of LB formation through Gys1-ASO administration reduces levels of epileptiform in the MKO murine model. Multiple studies suggest a link between glycogen metabolism and epilepsy [141, 180, 181]. While the precise mechanism or mechanisms remain to be elucidated, several compelling hypotheses have been presented. Glycogen is an important storage molecule in the brain, not just for energy, but other critical substrates. Our recent work demonstrated that brain glycogen stores glucosamine, a critical sugar for protein glycosylation [100]. Glycosylation disorders have been linked to neuronal degradation and epilepsy [81]. Glycogenolysis is also linked with glutamine synthase activity. Glycogenolysis has been shown to promote K^+ and glutamate uptake, and thereby glutamine synthesis, which play a critical role in neuronal excitability [141, 180, 181]. By reducing the rate of glycogen synthesis, it is possible that more glycogen remains accessible to degradation pathways, allowing glycosylation and glutamatergic neurotransmission to be less perturbed, thereby leading to a reduction in neuronal excitability and ED.

ASO treatment halts LB accumulation and reduces neuronal excitability, but it does not appear to clear pre-existing LBs. However, other therapies are in development that degrade the LB aggregates. Extensive pre-clinical evaluation has been completed of antibody-enzyme fusions that employ antibody fragments as a delivery vehicle to transport enzymes capable of degrading LBs into the cytoplasm of neurons and astrocytes

[66, 80, 81, 155]. This opens the possibility for a combination therapy, where existing LBs could be cleared with an antibody-enzyme fusion and then prolonged treatment with Gys1-ASO to prevent the formation of new LBs. Taken together, these therapies would have the potential to allow patients to live free from the devastating seizures and neurodegeneration driven by LB aggregation.

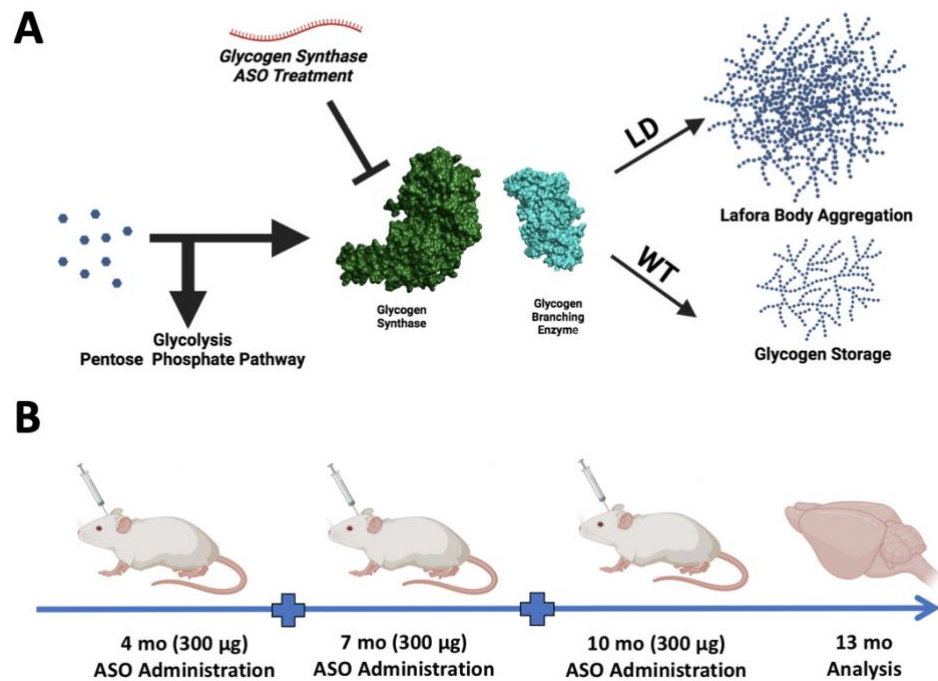


Figure 5.1 Using Antisense Oligonucleotide (ASO) Administration to Halt Lafora Body Aggregation.

A) Schematic showing the fate of glucose in a Lafora Disease (LD) patient compared to wildtype (WT) and the predicted impact of GYS1 ASO administration.

B) Schematic showing timeline for drug administration and testing in malin knock-out (MKO) mouse model.

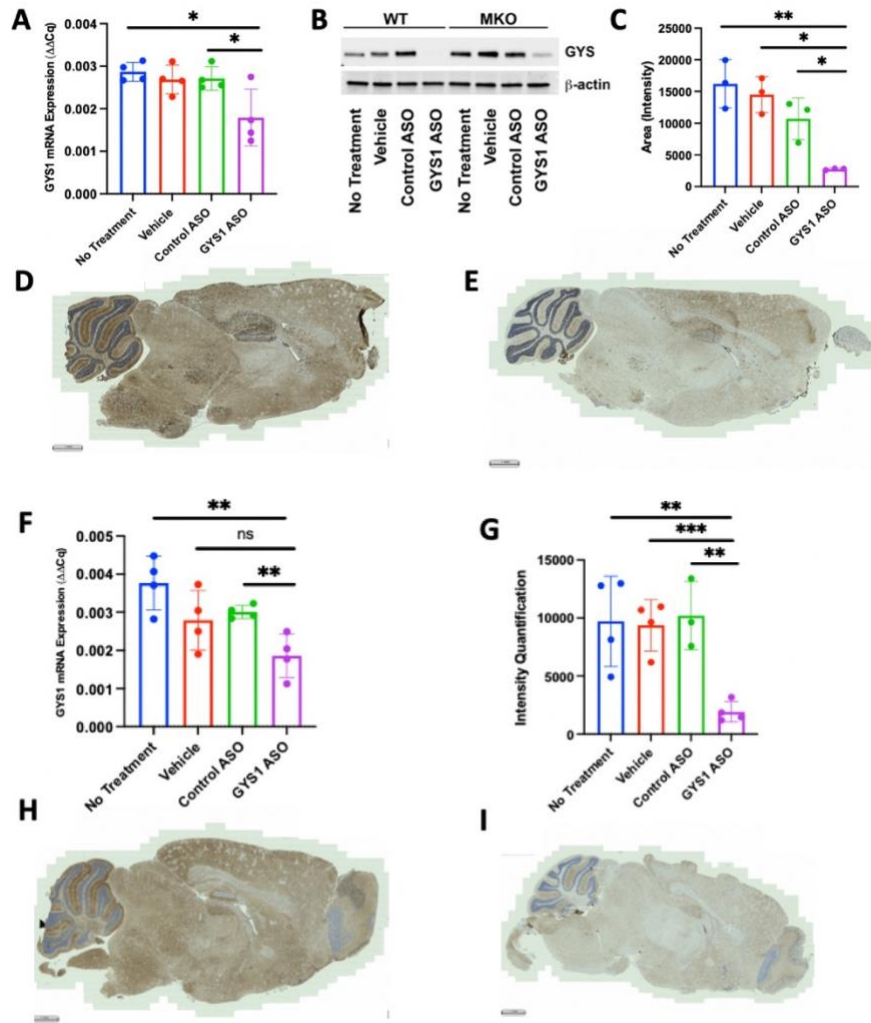


Figure 5.2 Confirming Knock-Down of Glycogen Synthase (GYS1).

A) mRNA transcription levels of *Gys1* in brain tissue for the MKO female mouse cohorts.

B) Representative blot of Gys1 protein expression in brain tissue in WT and MKO female mouse cohorts.

C) Quantitation of Western Blots for Gys1 protein expression in MKO female mouse cohorts.

D) Representative IHC stain for Gys1 in scramble ASO treated mouse.

E) Representative IHC stain for Gys1 in Gys1-ASO treated mouse.

F) mRNA transcription levels of *Gys1* for male mouse cohorts.

G) Quantitation of Gys1 protein expression in male mouse cohorts.

H) Representative IHC stain for Gys1 in scramble ASO treated male mouse.

I) Representative IHC stain for Gys1 in Gys1-ASO treated male mouse.

Statistical significance was calculated using unpaired student T-test, where * indicates $P < 0.05$, ** $P < 0.01$, *** $P < 0.001$

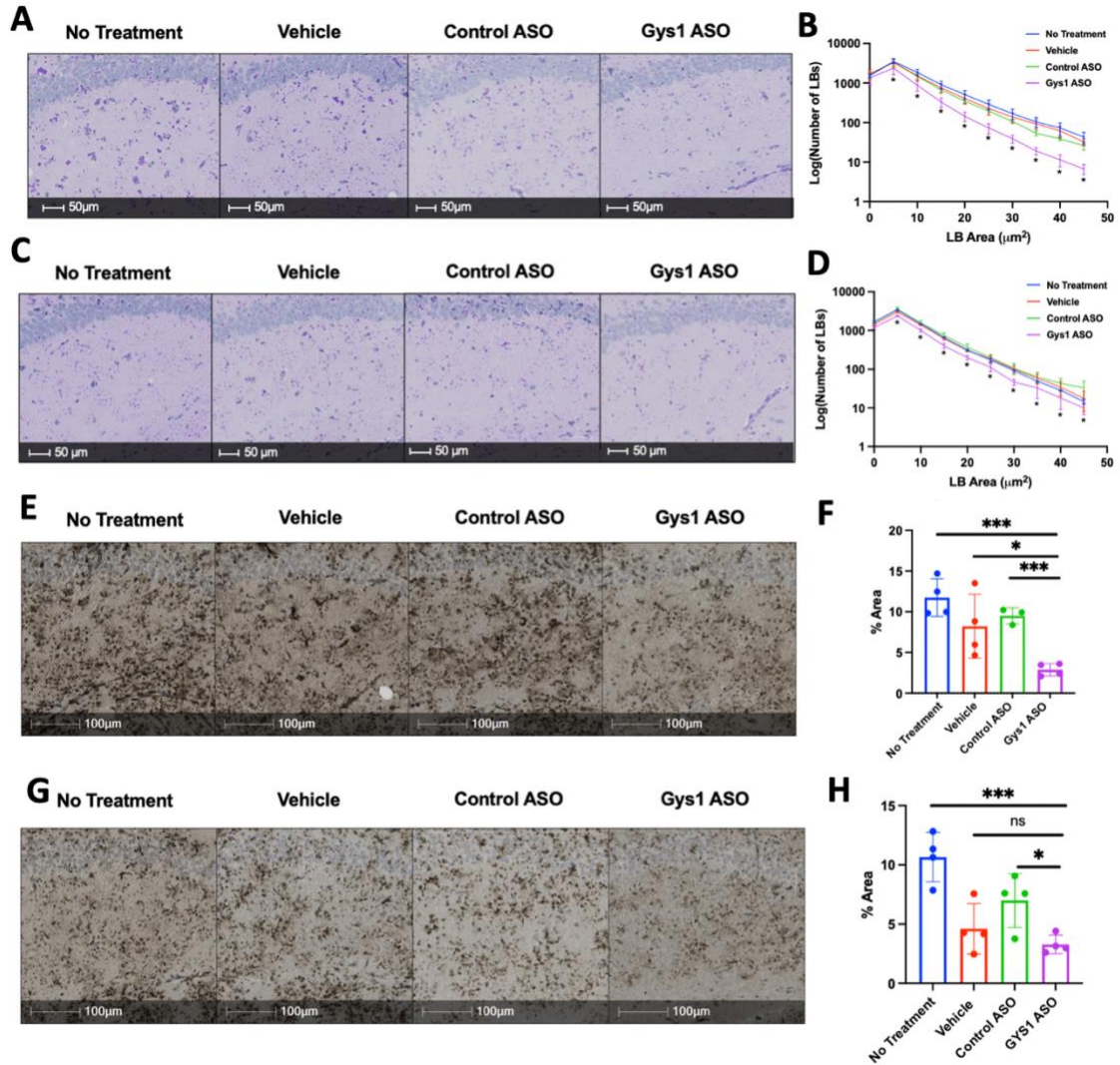


Figure 5.3 Quantifying Lafora Body Aggregation in the Hippocampus

A) Representative images of PAS-stained hippocampi in female MKO mice.
 B) Quantitation of percent area of Lafora bodies in PAS-stained hippocampi of female MKO mice.
 C) Representative images of IHC using the IV58B6 α -glycogen antibody to stain hippocampi of female MKO mice.
 D) Percent area of hippocampi staining of female MKO mice with the IV58B6 antibody.
 E) Representative images of PAS-stained hippocampi in male MKO mice.
 F) Quantitation of percent area of Lafora bodies in PAS-stained hippocampi of male MKO mice.
 G) Representative images of IHC using the IV58B6 α -glycogen antibody to stain hippocampi of male MKO mice.
 H) Percent area of hippocampi staining of male MKO mice with the IV58B6 antibody. Statistical significance was calculated using unpaired student T-test, where * indicates $P < 0.05$, ** $P < 0.01$, *** $P < 0.001$

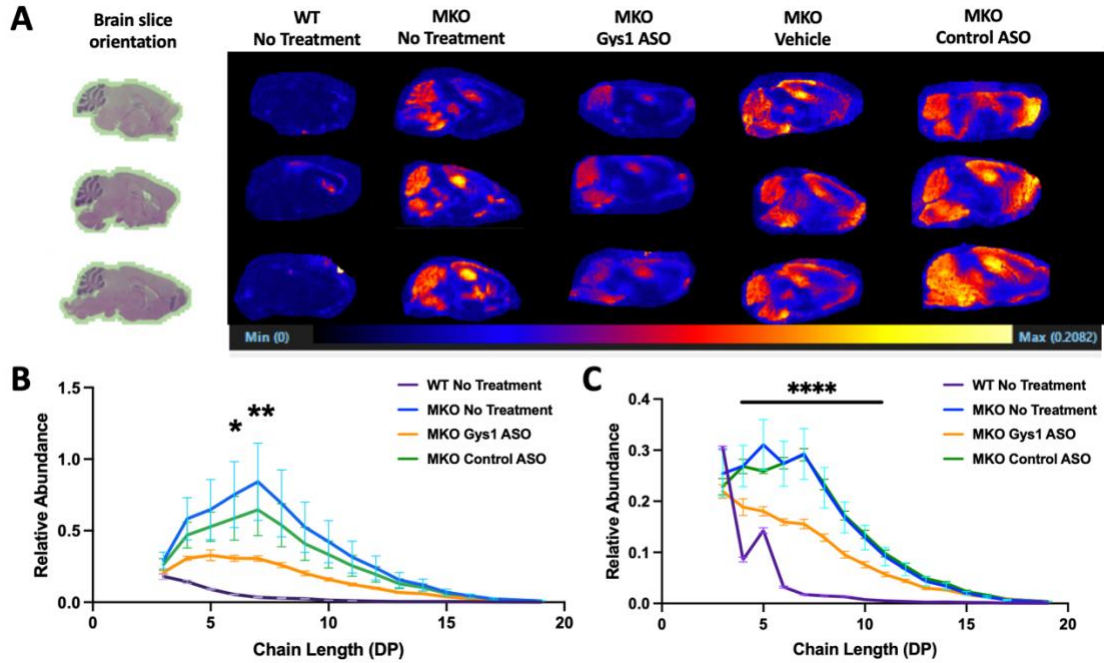


Figure 5.4 Representative Images of MALDI Analysis Showing Glycogen Accumulation in Female Mouse Cohorts

A) Three sagittal slices from each cohort were treated with CHCA matrix to allow for identification and analysis of glycogen-derived polymers. These images show the concentration of maltoheptaose (DP7) throughout the brain, the most common glycogen-derived polymer.

B) CHCA matrix treatment allows glycogen-derived polymers to be detected through MALDI analysis. The relative abundance of each polymer from triose through DP19 was quantified in the hippocampus and plotted. N=3

C) Quantification of glycogen-derived polymers in the Cerebellum. N=3

Statistical significance was calculated using unpaired student T-test, where * indicates P<0.05, ** P<0.01, *** P<0.001

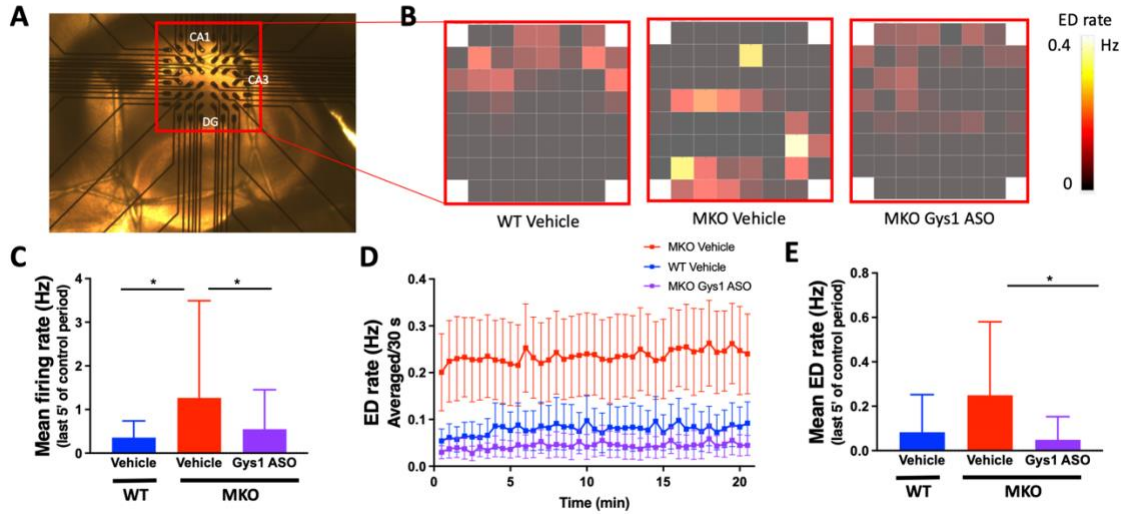


Figure 5.5 Electrophysiology Analysis of Hippocampus Using Multi-Electrode Array

A) Representative picture of hippocampal slice on the electrode grid with regions CA1, CA3, and DG labelled.

B) Representative heatmap depicting spontaneous firing average from hippocampal slices in WT vehicle, MKO vehicle, and MKO Gys1-ASO treated mice.

C) Mean firing rate quantified for the last 5 minutes of the control period.

D) Quantification of epileptiform discharge (ED) rate averaged over 30-second intervals for a 20-minute control period.

E) Quantified mean ED rate averaged over the last five minutes of the control period.

* indicates $P < 0.05$

CHAPTER 6. ADAPTING THE PERSONALIZED MEDICINE PIPELINE FOR GLUT1 DEFICIENCY SYNDROME

6.1 Introduction

Glut1 Deficiency Syndrome (Glut1DS) results from mutations in the *SLC2A1* gene, which encodes for glucose transporter 1 (Glut1) [182]. Glut1 is a 12-membrane spanning, bidirectional transporter, and one of the GLUT family transporters, which are responsible for facilitating glucose uptake into cells [183]. Glut1 is ubiquitously expressed in all tissues, however, it is highly expressed in the plasma membrane of endothelial cells and astrocytes and plays a critical role in transporting glucose across the blood-brain barrier (Figure 6.1) [184]. First described in 1991, patients with a deficiency in Glut1 expression or function were characterized by seizures, developmental delays, and low glucose concentration in the cerebrospinal fluid (CSF) [182]. Recent estimates predict approximately 1:50,000 people have mutations in *SLC2A1* [185]. 90% of diagnoses are due to heterozygous *de novo* mutations that are autosomal dominant [184, 186]. The current recommended treatment for Glut1DS is the ketogenic diet [187]. While the diet does lessen the severity of symptoms in most patients, it is not a cure. The diet is challenging to maintain and some patients do not respond to the diet [187-189]. Additionally, patient phenotypes vary greatly between patients, making it difficult for them to be accurately diagnosed [187, 190]. In fact, there is an average of 6.6 years between symptom onset and diagnosis for Glut1DS patients [190]. The longer it takes for a patient to be correctly diagnosed, the longer they have to wait to start the ketogenic treatment, which likely negatively impacts clinical symptoms. Recent innovations to rapidly detect Glut1 in red blood cells could help reduce time to diagnosis, however, the variability between patients continues to make it challenging to identify patients and predict the severity of disease progression [191, 192].

Over the past thirty years a number of patient case reports have been published, highlighting a broad spectrum of patient phenotypes [190, 193-195]. However, a large-scale study has not been attempted to identify genotype-phenotype correlations. The Cystic Fibrosis (CF) Community performed a similar study almost a decade ago to categorize patient mutations in the CFTR chloride transporter based on the predicted functional impact. They used the mutation groups to define patient cohorts and identify novel therapeutic targets for each cohort [43]. There are now two CF patient cohorts that have FDA approved therapies: potentiators to open channels with gating mutations, and correctors for protein trafficking mutations [44]. If patient cohorts for Glut1 can be identified based on the genetic mutation, physicians can tailor treatment to individual patients and researchers could identify novel therapeutic targets. A genotype-phenotype correlation could also identify patients who would not respond well to the ketogenic diet. Drawing on lessons learned from building a personalized medicine pipeline for Lafora Disease (LD), we used a combination of bioinformatics mutation analyses and structural analyses reported in literature to propose a set of mutation groups for Glut1. Then, we utilized patient case studies reported in literature to define Glut1 phenotype classes. Finally, we analyzed previously unpublished data from a cohort of 47 German patients to assess the efficacy of our genotype-phenotype predictions. Taken together, we offer

insights gleaned from analyzing and categorizing mutations in patients with Glut1DS, presenting a workflow that could be more broadly adapted for studying rare diseases.

6.2 Results

6.2.1 Identifying mutations groups for Glut1

Currently, there is no consensus on how to categorize Glut1DS patients into cohorts based on their individual mutation. It has been suggested that frameshift mutations, truncations, and complete loss of a Glut1 copy result in the most severe phenotypes [193]. However, the spectrum of missense mutations has been largely unexplored. Using a PubMed literature search, 90 unique patient missense mutations were identified [190-192, 196-199]. Of those mutations, 60 were detailed as case studies for patient phenotypes [190, 193, 196, 197]. To determine the usefulness of bioinformatics engines in predicting mutation class, all 90 missense mutations were processed through seven separate pathogenicity prediction engines. CUPSAT and SDM were utilized to predict the mutation impact on Glut1 stability, PANTHER and SIFT to predict pathogenicity based on sequence homology, SNAP to account for allelic frequency of the mutation, along with PhD-SNP and Meta-SNP, which use a combination of bioinformatics engines to predict pathogenicity [88, 89, 92, 126, 200, 201]. The results of the bioinformatics analyses are displayed in Table 6.1.

As discussed in Chapter 3, bioinformatics analyses are limited in their ability to group mutations based on the degree of functional loss. Therefore, to account for this limitation, published structural analyses of Glut1 were used to identify amino acids with key functional properties in the transporter. The SCL2A1 gene is composed of 10 exons and 9 introns [202]. Glut1DS can be caused by missense, frameshift, and stop mutations throughout these 10 exons. We first compiled amino acids shown to regulate membrane orientation of the transporter. A series of arginine and glutamate amino acids along the cytoplasmic end of the transporter control the orientation or conformation of Glut1 (Figure 6.2A). The amino sequences R89-R93 and R330-R333 are mutational hot spots in Glut1DS and are responsible for regulating inward/outward orientation of the transporter [183, 202]. The c-terminus of Glut1 also contains a targeting sequence for the plasma membrane [202]. Next, we searched for amino acids known to regulate glucose uptake by the transporter. Glut1 has a cytoplasmic loop between transmembrane (TM) helices TM6 and TM7 [203]. This loop contains R223, which is reported to regulate glucose uptake [204]. Other amino acids in the loop play a role in forming a pocket for glucose entry into the transporter [204]. Finally, we reviewed published molecular dynamics simulations that predicted the amino acids that facilitate glucose transport [204-206]. The molecular dynamics simulations predicted that Q161, Q282, N288, and W388 all directly interact with the glucose molecule as the confirmation changes from inward to outward-facing (Figure 6.2B) [204]. Additionally, these simulations identified the amino acids critical for maintaining the shape and structure of the glucose channel, allowing for transport. A summary of all the amino acids with critical functions identified from literature have been compiled in Table 6.2.

Using this structural information, we then grouped the mutations using Cystic Fibrosis CFTR mutation groupings as a template, where mutations resulting in partial versus full loss of transport, decreased transporter localization and expression, and decreased stability define groups based on the type of functional loss. We identified five mutation groups for Glut1 (Figure 6.3). Group 1 represents what we predict to be the most severe mutation. Mutations within this Group 1 are frameshift or nonsense mutations, resulting in significant truncation of the final protein product. Group 1 could also include intronic mutations that affect splicing. Thus, it could lead to the complete loss of one copy of the Glut1 allele. Group 2 mutations are located within membrane orientation motifs, which could decrease plasma membrane expression, or result in incorrect orientation in the plasma membrane. Group 2 also includes mutations that disrupt targeting of the transporter to the plasma membrane. Group 3 encompasses mutations that are directly involved in glucose transport, leading to a large decrease or complete loss in glucose transport. Group 3 also includes mutations that lock the transporter in the inward or outward conformation. In Group 3, mutant transporters are correctly targeted to the plasma membrane, but glucose transport is abolished. Group 4 mutations are amino acids directly adjacent to those responsible for glucose transport, where mutations are likely to decrease, but not abolish, transport. Group 4 also includes mutations in the cytoplasmic loop, such as R223, which could lead to a decrease in transporter activity. In Group 5, the missense mutations are predicted to reduce protein stability. These produced proteins may therefore be subjected to increased turnover, impacting glucose transport levels. Each of these groups has the potential for a unique treatment strategy, and the degree of loss in glucose transport could be tested for correlation with phenotype profiles.

6.2.2 Mapping phenotypes to elucidate a genotype-phenotype correlation for Glut1DS

To better aid in diagnosis, multiple researchers and clinicians have sought to develop a phenotypic spectrum for Glut1DS [193, 195, 207]. Building on their framework, we conducted a literature search for articles clinically evaluating Glut1DS patient mutations and their resulting phenotype. To allow for comparison between recordings, we utilized publications that reported on seizures, movement disorders, and intellectual disability in patients [190, 193, 196, 197]. Microcephaly is a common phenotype for Glut1 patients, but reporting between publications was not consistent enough to allow for comparison. For seizures, the most commonly reported categories were absence, focal, and generalized tonic-clonic seizures. The most consistently reported movement disorders were ataxia, hypotonia, dystonia, and spasticity. The reports of development disorders were most variable between publications. Some reports only specified mild or moderate retardation, while others reported specific language, mental, or movement retardation, but did not specify if it was mild or moderate. To determine phenotype groups for patients, their phenotypes were clustered according to the similarity of their profiles (**Figure 6.4**). From this clustering, a few defining features emerged: presence and degree of developmental disability, and the manifestation of seizure and movement disorders together or separately.

We assigned a phenotype class to each patient based on the following profiles: Class 1 is the most severe phenotype, with seizures, movement disorders, and moderate-

severe developmental disability. Class 2 patients had seizures, movement disorders, and mild developmental disability. Class 3 patients had both seizures and movement disorders, but no reported developmental disability. Class 4 is the least severe phenotype, where patients have movement disorders or seizures, but not both (Figure 6.5).

6.2.3 Elucidating genotype-phenotype correlations from patient data

One of the challenges of elucidating genotype-phenotype correlation is consistency in data reporting. Therefore, we wanted to optimize our genotype-phenotype predictions using uniformly collected patient data. We collaborated with Dr. Jeorg Klepper, one of the leading physicians worldwide for his expertise in treating Glut1DS patients. Dr. Klepper provided anonymized data from 47 Glut1DS patients with uniform phenotype reporting. First, we analyzed the patient mutations and assigned them a mutation group based on their predicted functional impact. Second, we assigned the patient phenotype classification based on our previous system. Perhaps because of the long-term uniform reporting, almost all the patients exhibited developmental disability, putting most of the patients in phenotype Class 1 or 2, even though all five mutation groups were represented. Since we had detailed phenotype reporting, we used the same clustering algorithm to test if any other patient profiles emerged. To help further distinguish between patient groups, we added a “score” for each of the three main categories to aggregate the number and severity of reported symptoms (Figure 6.6). The clustering revealed a cohort of patients with movement retardation separate from speech and cognition retardation, suggesting that specifying the type of developmental delays will be important for establishing patient cohorts. There was also some additional clustering around hypotonia, absence seizures, and focal seizures, illustrating the need for specific reporting on the manifestations of the seizure or movement disorder.

It is important to note that sorting patient mutation severity based solely on phenotypic data can be influenced by many factors, even if one attempts to control for uniformity of symptom reporting. Since the ketogenic diet can greatly reduce phenotype severity, it becomes a confounding variable in data analysis [189, 208]. The ketogenic diet has even been shown to improve microcephaly in some Glut1DS patients [193]. Therefore, it appears that patients who start the ketogenic diet earlier in life might have milder phenotypes in the future regardless of the severity of their mutation. Since Dr. Klepper provided uniform reporting on age of diagnosis for his patients and the age a patient began the ketogenic diet, we were able to tease apart some of that effect. We excluded all patients who began the ketogenic diet prior to two years of age and re-ran the clustering of patient profiles. In this analysis, the most severe mutations in Groups 1 and 2 largely clustered together. Mutation Groups 3-5 did not separate into individual clusters, however, this initial assessment opens the door to further refinement of the genotype groups and illustrates the need for biochemical pipeline to clarify mutations with an uncertain impact on transporter function.

6.3 Discussion

Patients with Glut1DS display a broad spectrum of phenotypes, making diagnosis and prognosis challenging [187, 190, 193, 195]. Once diagnosed, patients can be treated with the ketogenic diet. Research suggests that the earlier patients begin the ketogenic diet, the better their prognosis, making it critical to be able to correctly identify Glut1DS patients despite the wide variation in phenotype [193, 208]. While the ketogenic diet may help alleviate some of the phenotypic severity, it is challenging to maintain and it does not fix the underlying mechanistic problem of the disease [187, 188, 209]. This is where strategies for developing personalized medicine can benefit Glut1DS patients. Defining a genotype-phenotype correlation could lead to the discovery of new therapeutic targets and identify which patients would benefit most from the proposed therapy.

In a rare disease like Glut1DS where the genetic driver has been identified, the first step toward a personalized medicine platform is to aggregate the structural data of the mutated protein and reported patient phenotypes. This survey of the literature creates a framework for future research and collaboration: it identifies gaps in current knowledge of Glut1 structure-function and reveals which phenotype data should be uniformly reported. In this chapter, we demonstrate that patient mutations can be clustered based on the predicted structural and functional impact on Glut1. These data can then be compared with reported patient phenotypes to identify correlations between the groups. While the model can be further refined, the current findings create a starting framework for defining patient cohorts and suggests follow-up analyses that would help elucidate a genotype-phenotype correlation.

The most severe group of mutations, where Glut1 expression or localization to the membrane is lost, clustered strongly with the most severe phenotype class, both in the literature-reported phenotypes and the patient cohort from Dr. Klepper. There were a few outliers that required further examination. In the literature-reported phenotypes, an important confounding variable was the patient's starting age for the ketogenic diet. Without this information, it was impossible to address the impact it had on the genotype-phenotype correlation. That is why Dr. Klepper's patient cohort with uniform data on age of diagnosis and ketogenic diet allowed for better refinement of the model. A few outliers from the initial genotype-phenotype clustering, like Q305X, c.679ins2, and s213fc, could be explained by their early diagnosis and subsequent use of the ketogenic diet, which mitigates symptoms. After controlling for the age of starting keto treatment, the remaining outliers were the L169 deletion and the c.467dupT frameshift mutation. For the frameshift mutation, the patient began the ketogenic diet at 2 years of age, right at the cut-off age for the group of patients receiving early treatment with the ketogenic diet. This could suggest that starting the ketogenic diet up through two years of age has a significant impact on the observed phenotype, however, more systematic data analysis would be needed to confirm this hypothesis. For the L169 deletion, we predicted it would be in the most severe mutation group because it falls in the middle of TM5, which plays an important role in conformation changes of the transporter and contains multiple amino acids that directly interact with glucose. However, it is possible that this deletion does not severely impact the structure. Indeed, the patient's reported glucose CSF levels were 42 mg/dL, which, while lower than normal, was higher than most other patients in the cohort. An *in vitro* assay could be

developed to test for glucose transport activity in this mutation, and allow it to be appropriately classified if it retains partial glucose transport.

For Groups 2-5, the clustering was not as pronounced as originally expected. If the phenotype is largely driven by loss or reduction in glucose transport, then you would expect Groups 2&3 to cluster together, perhaps close to the Group 1 mutations, since they are predicted to block glucose transport. Similarly, we expected Groups 4 and 5 to cluster together because they are predicted to result in a partial loss of glucose transport. Instead, about half of the mutations in Group 2 clustered with Group 1, while the rest mixed together with Groups 3-5 clustered. While the age of starting the ketogenic diet could have some impact on the data clustering, it is more likely that some of the mutations predicted to be in Groups 2 or 3 reduce the transport of glucose, rather than abolishing it completely. To strengthen the predictive capacity of the model, it will be necessary to develop a biochemical pipeline for functional analysis, much like we did with Lafora Disease. Indeed, there are already several research groups working on high-throughput methods for measuring glucose transport in mutated Glut1 [210]. Utilizing these methods to assess uncertain pathogenic predictions for the Glut1 mutations would allow for better genotype-phenotype correlation.

With more comprehensive phenotypic data, our model could be expanded upon to better represent the phenotypic clustering of Glut1DS patients. Our current model was developed from parameters most commonly reported in literature, but could be greatly improved by increasing sample size and adding additional phenotype parameters. First, researcher and clinicians should reach an understanding of which parameters need to be recorded. Based on this analysis, we recommend that at a minimum, developmental disorders in speech, cognition, and movement should be universally reported. For seizures, it would be helpful to distinguish at a minimum if a patient has focal or generalized seizures, although it would also be useful to further report simple versus complex focal seizures and absence versus tonic-clonic generalized seizures. With movement disorders, it would be helpful to unify the language used to describe the various disorders. At a minimum, ensuring that clinical reports detail the presence or absence of ataxia, PED, hypotonia, dystonia, and spasticity would be helpful. Additionally, creating a uniform measure of reporting for microcephaly would allow for that parameter to be included in future analyses. In current clinical summaries, when any of these parameters are excluded from the data table, it is impossible to know whether patients did not exhibit those symptoms or if clinicians simply did not report them. In addition to universal reporting of symptoms, potentially confounding variables, like age of diagnosis and age of starting treatment with the ketogenic or similar diet should be reported. A uniform data reporting system would increase the accuracy of a Glut1DS phenotypic spectrum and therefore provide better predictions based on individual patient mutations, resulting in faster diagnoses and personalized treatment plans.

While increasing the number of reported parameters for Glut1DS patient phenotypes, further refinement could be achieved with uniform reporting of frequency and severity of symptoms. It would also help to have reporting on glucose and lactate CSF levels in all Glut1DS patients, as these biomarkers are reported to be the most consistent predictors of Glut1DS. Understandably, there is a limit to how detailed clinical reports can get, but there is significant room for improvement. For example, determining a uniform set

of parameters for mild, moderate, and severe movement retardation would help further distinguish between patient cohorts. Currently, the designation of mild or severe is highly subjective, making comparisons difficult. Also, technological innovations in the healthcare system could eventually improve phenotype reporting. Already, diseases that require regular blood glucose monitoring have developed smart phone apps to facilitate 24/7 tracking [211]. Other apps are useful for continuous monitoring of patient diets and heart rates [212, 213]. As these innovations expand to include phenotypes important for Glut1DS patients, we should incorporate their use as quickly as possible to further refine patient phenotype clustering. With more data, we can begin to pick apart environmental, lifestyle, and genetic contributions to patient phenotypes. This will improve patient treatment recommendations, and as therapies are developed, the patients most likely to benefit can be quickly identified. In this way, our framework for establishing genotype-phenotype correlations can be easily adapted to improve patient outcomes not only for Glut1DS, but other rare diseases.

Table 6.1 Bioinformatics Analysis and Mutation Group Classification Based on Structural Analysis from Literature

Results from nine separate bioinformatics engines to predict pathogenicity. The results were matched with the location of the mutation in the Glut1 structure and the predicted loss of function from previous structure-function analyses of the transporter to determine if bioinformatics would be sufficient to predict severity of patient mutations.

	CUPSAT	SDM	PhD-SNP	SIFT	Panther	SNAP	Meta-SNP	Location	Mutation Group Predicted
Mutation	$\Delta\Delta G$	Probability (benign positive, pathogenic negative)						Region	(1 is most severe)
F434I	-1.81	-0.29	-0.831	-0.01	NA	-0.76	-0.779	T12	5
V165I	-0.56	-0.2	0.477	-0.05	0.452	0.485	0.48	T5	5
T310N	2.01	-0.23	-0.556	0.23	-0.878	0.39	-0.639	T8	5
S324P	-1.49	-1.84	-0.609	-0.1	-0.848	-0.57	-0.715	T8	5
S324L	-1.04	0.35	-0.81	-0.02	-0.836	-0.725	-0.715	T8	5
S313T	-1.68	-0.58	0.075	0.46	0.243	0.185	0.272	T8	5
S313P	-2.35	-2	-0.679	-0.04	0.434	-0.56	-0.702	T8	5
R232C	-2.21	-1.74	-0.812	-0.04	-0.791	-0.515	-0.711	L6-7	5
R218H	-0.08	0.19	0.453	0.06	-0.589	0.19	-0.607	L6-7	5
P431T	-1.33	0.34	0.59	0.59		0.37	0.2	L12	5
M180K	-1.25	-0.63	-0.719	-0.04	0.464	-0.71	-0.602	L5-6	5
L231P	-4.45	-3.68	-0.8548	0	-0.856	-0.675	-0.777	L6-7	5
L169P	4.76	-2.23	-0.918	0	-0.93	-0.7	-0.829	T5	5
L101S	0.5	-1.41			-0.521	0.26	0.496	T3	5
K183Q	-1.67	0.3	0.216	0.43	0.066	0.14	0.325	T5	5
G419R	0.96	-1.05	-0.853	-0.1	NA	-0.705	-0.782	T11	5
G314S	0.02	-2.03	-0.763	-0.04	-0.977	-0.6	-0.798	T8	5
G134S	1.49	-1.87	-0.897	0	-0.963	-0.775	-0.858	T4	5
G130S	1.63	-2.32	-0.895	-0.01	-0.984	-0.735	-0.831	T4	5
G130R	1.21	-2.2	-0.949	-0.01	-0.992	-0.83	-0.899	T4	5
C421R	-5.04	0.75	-0.617	0.34	NA	-0.605	-0.717	T11	5
A342T	2.01	-1.53	-0.609	-0.01	-0.848	-0.57	-0.715	T9	5
A275T	-2.45	-2.85	0.403	0.18	0.341	0.49	0.468	T7	5
T295M	1.47	0.83	-0.558	0.05	-0.939	-0.615	-0.791	L7-8	4
V140M	-0.63	-0.56	0.453	-0.05	-0.659	-0.555	-0.655	T4	4
T295M	1.47	0.83	-0.558	-0.05	-0.939	-0.615	-0.791	L7-8	4
S294P	-0.88	-1.18	-0.874	-0.01	-0.862	-0.73	-0.829	L7-8	4

R212C		-1.64	-0.867	0	-0.9596	-0.73	-0.84	L6-7	4
R153C	3.8	-0.71	-0.862	0	-0.989	-0.91	-0.894	L4-5	4
M142K	-2.82	-0.28	-0.799	0	-0.984	-0.77	-0.875	T4	4
L278P	-6.36	-4.14	-0.879	-0.03	-0.897	-0.73	-0.804	T7	4
L215F	-0.94	-1.14	0.446	0.21	-0.587	0.21	-0.605	L6-7	4
L162R	1.66	-0.29	-0.927	0	-0.934	-0.71	-0.839	T5	4
I287L	-1.2	0.77	-0.657	-0.02	-0.563	-0.635	-0.515	T7	4
G75R	2.32	-2.27	-0.871	0	-0.992	-0.815	-0.91	T2	4
G286H	-2.31	-3.34	-0.897	0	-0.996	-0.835	-0.891	T7	4
G286D	-4.64	-3.7	-0.908	0	-0.991	-0.845	-0.896	T7	4
R400L	-1.21	0.08	-0.897	0	NA	-0.805	-0.817	L10-11	3
E243V	0.06	-0.61	-0.779	-0.05	-0.77	-0.505	-0.607	L6-7	3
E247V	-0.65	-0.61	-0.627	0.15	-0.978	0.44	0.832	L6-7	3
E393K	0.12	-0.27	-0.86	0	NA	-0.885	-0.816	L10-11	3
G18R	-3.99	-0.76	-0.679	0.35	0.356	-0.68	-0.745	N term	3
H160Q	0.84	0.64	0.332	0.3	0.499	0.445	0.14	T5	3
L12F	1.92	-1.26	0.474	0.12	-0.777	0.38	-0.611	N term	3
M1T	NA	NA	0.16	0.56		0.34	0.177	N term	3
M96C	-4.11	-1.25	-0.904	0.09	-0.925	0.46	-0.798	T3	3
N34I	0.29	0.34	-0.856	0	-0.995	-0.755	-0.883	L1-2	3
N34S	-1.2	-0.95	0.225	0.37	-0.978	-0.57	-0.625	L1-2	3
N34Y	0.93	-0.2	-0.865	0	-0.993	-0.785	-0.919	L1-2	3
N411S	-1.91	-0.67	-0.801	0.13		0.465	-0.511	L12	3
Q283R	-1.33	-1.56	-0.921	0	-0.817	-0.815	-0.836	T7	3
R11S	0.07	-0.77	0.323	0.4	0.268	0.4	0.446	N term	3
R126C	2.3	-2.41	-0.923	0	-0.995	-0.87	-0.882	T4	3
R126H	-0.85	-0.87	-0.955	0	-0.988	-0.84	-0.897	T4	3
R126L	0.72	0.63	-0.893	0	-0.991	-0.875	-0.889	T4	3
R153C	3.8	-0.71	-0.862	0	-0.989	-0.91	-0.894	L4-5	3
R153H	1.27	-0.07	-0.822	0	-0.976	-0.91	-0.871	L4-5	3
R153L	1.77	0.26	-0.89	0	-0.971	-0.89	-0.843	L4-5	3
R153P	2.67	-2.25	-0.875	0	-0.976	-0.9	-0.869	L4-5	3
R212C	-0.91	-1.64	-0.867	0	-0.956	-0.73	-0.84	L6-7	3
R212H	-1.23	-2.02	-0.811	-0.02	-0.896	-0.615	-0.743	L6-7	3
R400C	-0.54	-0.65	-0.883	0	NA	-0.825	-0.837	L10-11	3
R400H	-2.96	-1.1	-0.804	0	NA	-0.825	-0.793	L10-11	3

S226V	-0.64	0.77	0.22	0.24	0.421	0.21	0.415	L6-7	3
T9M	-5.09	0	-0.517	0	-0.933	-0.685	-0.754	N term	3
V328L	-1.78	0.09	0.42	0.13	0.367	0.45	0.466	T8	3
V391L	-5.62	0.23	0.165	0.64		0.29	0.194	L10-11	3
R400H	-2.96	-1.1	-0.804	0		-0.825	-0.793	L10-L11	3
R333Q	0.29	-1.34	-0.937	0	-0.922	-0.855	-0.877	L8-9	2
R333W	-0.37	0.13	-0.894	0	-0.616	-0.85	-0.847	L8-9	2
R223W	-1.1	-0.06	-0.658	-0.1	-0.696	0.455	-0.515	L6-7	2
S95I	1.37	1.47	-0.869	0.15	-0.754	0.445	-0.625	T3	2
R93W	0.53	-0.14	-0.892	-0.01	-0.843	-0.59	-0.765	T3	2
R92W	-6.29	0.4	-0.908	0	-0.976	-0.74	-0.841	T3	2
G91D	-4.01	-2.85	-0.913	0	-0.991	-0.85	-0.897	T3	2
E209D	-0.63	-0.82	-0.62	-0.03	-0.855	-0.605	-0.562	L6-7	2
A224G	-3.4	-2.21	-0.711	0.05	-0.786	0.285	-0.57	L6-7	2
E209D	-0.63	-0.82	-0.62	-0.03	-0.855	-0.605	-0.562	L6-7	2
A224G	-3.4	-2.21	-0.711	0.05	-0.786	0.285	-0.57	L6-7	2
R223P	-3.73	-2.07	-0.808	0.11	0.343	-0.525	-0.731	L6-7	2
R458W	NA	NA	-0.842	0		-0.68	-0.767	L12	2
M96V	-4.72	-0.97	-0.772	0	-0.993	-0.785	-0.919	T3	2
E329Q	NA	NA	-0.583	0	-0.811	-0.66	-0.717	L8-L9	2
M96V	-4.72	-0.97	-0.772	0	-0.993	-0.785	-0.919	T3	2
E329Q	NA	NA	-0.583	0	-0.811	-0.66	-0.717	L8-L9	2
R333W	-0.61		-0.937	0	-0.922	-0.855	-0.877	L8-L9	2
V328L	-1.78	0.09	0.42	0.13	0.367	0.45	0.466	T8	2
M96V	-4.72	-0.97	-0.772	0.12	-0.676	0.45	-0.574	T3	2
R93Q	-0.47	-0.51	-0.782	-0.02	0.416	-0.575	-0.723	T3	2
P485L			0.217	0.75		0.265	0.242	L12	2
L169 del								T5	1
E380*								L10-11	1
K256 del								L6-7	1
Q304*								L7-8	1
Q161*								T5	1
S368*								L10-11	1
R330*								L8-L9	1
L169del								T5	1

Table 6.2 List of Amino Acids in Glut1 Critical for Transporter Function Based on Structural Analysis from Literature.

Sorted by predicted contribution to Glut1 function, the following amino acids were shown or predicted to disrupt transporter orientation/conformation, glucose uptake, or glucose transport when mutated.

Transporter Orientation	Glucose Uptake Regulation	Glucose Transport Interaction	
R89-R93	F26	S23	E247
E209	F72	T30	Q282
I287-A289	R223	N34	Q283
Y293-T295	F291	S73	N288
E329	W292	R126	Y292
R330-R333	W388	T137	W388
E393	F409	P141	F389
R400	W412	R153	E393
E454		H160	R400
		Q161	I404
		R212	N411
		E243	N415

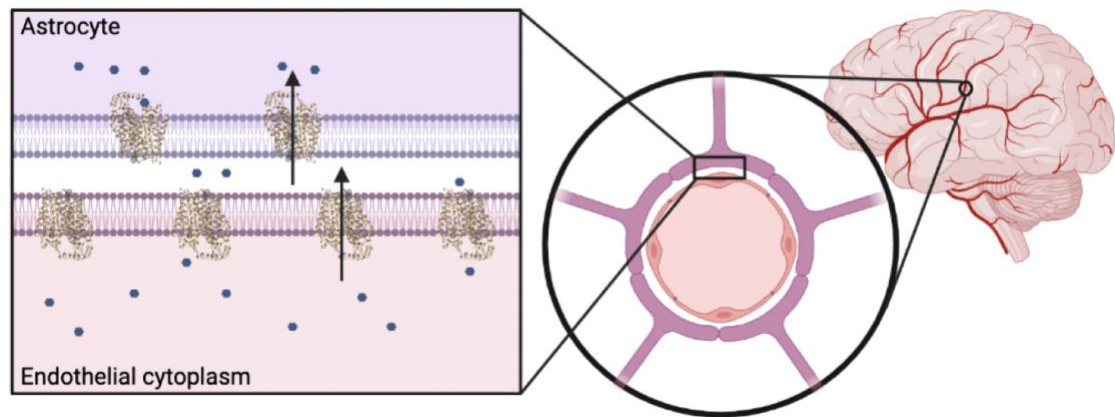


Figure 6.1 Schematic of Glut1 localization and function

While expressed in all tissue types, this is an illustration of the critical function of Glut1 at the blood-brain barrier, where the bidirectional transporters are highly concentrated in endothelial cells and astrocytic feet to regulate glucose concentration across the blood-brain barrier. (Glut1 structure from PDB 4pyp)

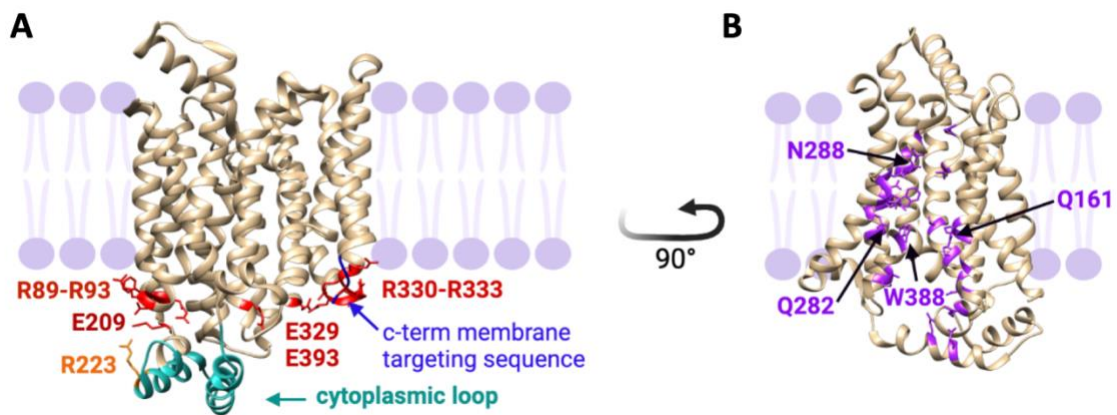


Figure 6.2 Key Structural Features Reported in Glut1 Literature

A) Determined structure of Glut1 from the Protein Data Base (PDB: 4pyp) with amino acids associated with membrane orientation and inward-outward conformation regulation are highlighted in red. The c-terminus sequence, responsible for targeting to the membrane, is highlighted in blue. The cytoplasmic loop associated with regulating glucose transport is highlighted in teal, with R223 highlighted in orange as it is reported to play a critical role in transport regulation.

B) A cut-away of the Glut1 structure with the amino acids predicted by molecular dynamics simulations to facilitate glucose transport across the membrane are highlighted in purple. Key amino acids predicted to directly interact and stabilize an intermediate conformation of Glut1 are labeled.

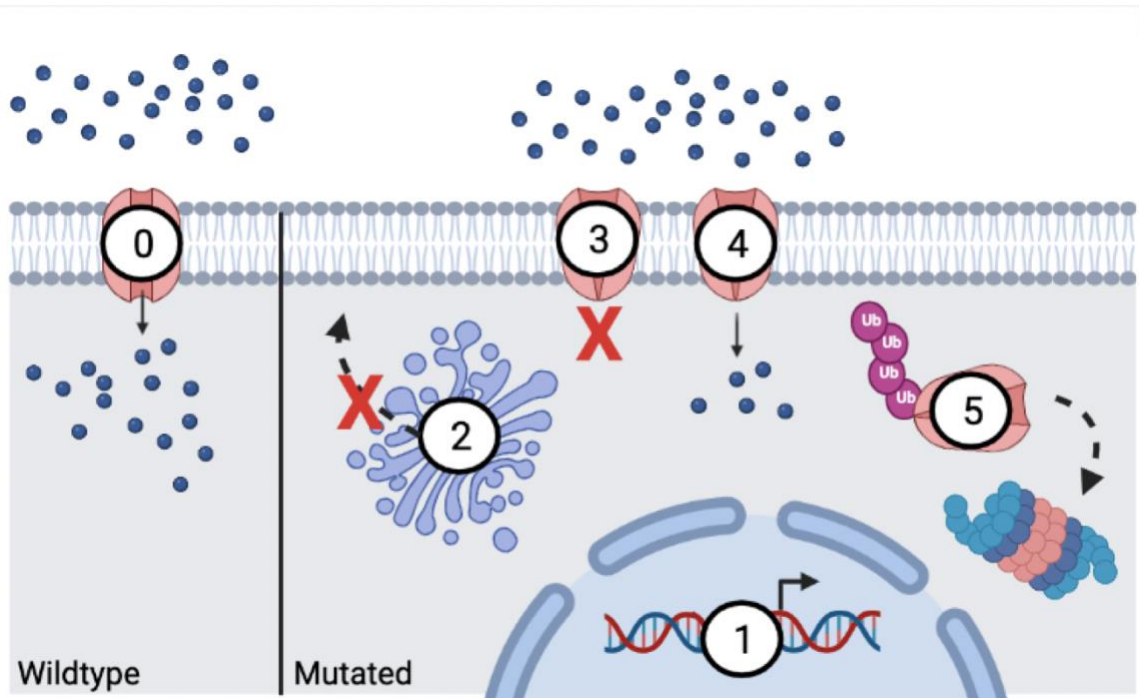


Figure 6.3 Glut1 Proposed Mutation Groups

Group 0 depicts fully-functional Glut1. Group 1 represents mutations impacting transcription, along with nonsense and frameshift mutations that result in a truncated protein. Group 2 mutations impact folding, targeting to the membrane, or orientation within the membrane, preventing glucose transport. Group 3 mutations localize correctly to the membrane, but the mutation either prevents conformational change of Glut1, or completely blocks the transport of glucose across the membrane. Group 4 mutations result in a reduction of glucose transport. Group 5 mutations are defined by a loss in stability, leading to increased protein turn-over.

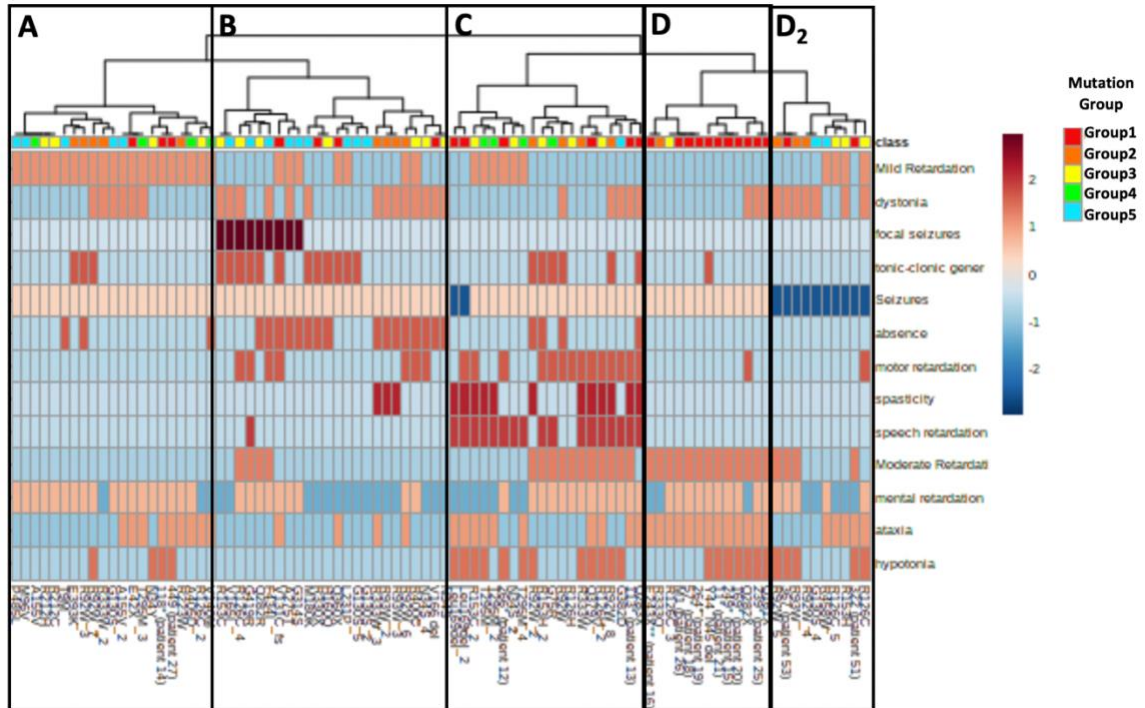


Figure 6.4 Glut1 Genotype-Phenotype Clustering from Literature-Reported Cases
 Phenotype markers were recorded as present (1), absent (0) or not reported (NA). Patient phenotype clustering was then composed using MetaboAnalyst Heatmap function with Euclidean distance measuring and Ward clustering algorithm. The mutations clustered in box A share reporting of seizures and mild retardation. The majority of mutations in box B had reported focal or absence seizures. Box C matches with the most severe phenotypes showing moderate-severe retardation with seizures and movements disorders. Box D highlights a group of patients with moderate-severe retardation with no or few movement disorder markers. Note that in box D₂, the mutations where seizure absence or presence was not reported clustered together.

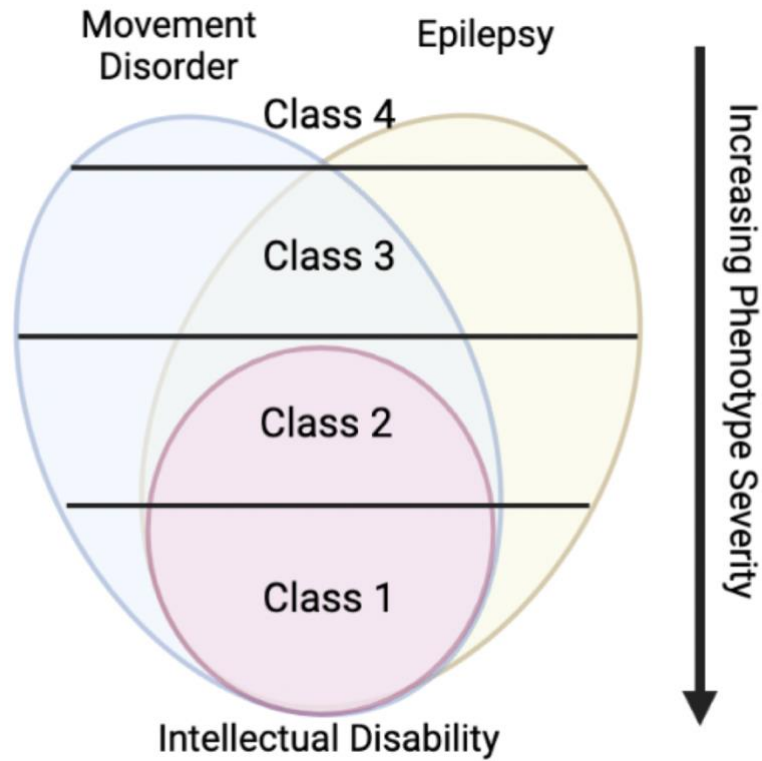


Figure 6.5 Glut1 Proposed Phenotype Classifications

In order of increasing severity, phenotype classes are defined as: Class 4, patients have movement disorder or seizures, rarely both and often treatable; Class 3, patients display both movement disorders and seizures, but no developmental decline; Class 2 patients have mild developmental delays in addition to seizures and movement disorders; Class 1 patients have moderate-severe developmental delays along with seizures and movement disorders.

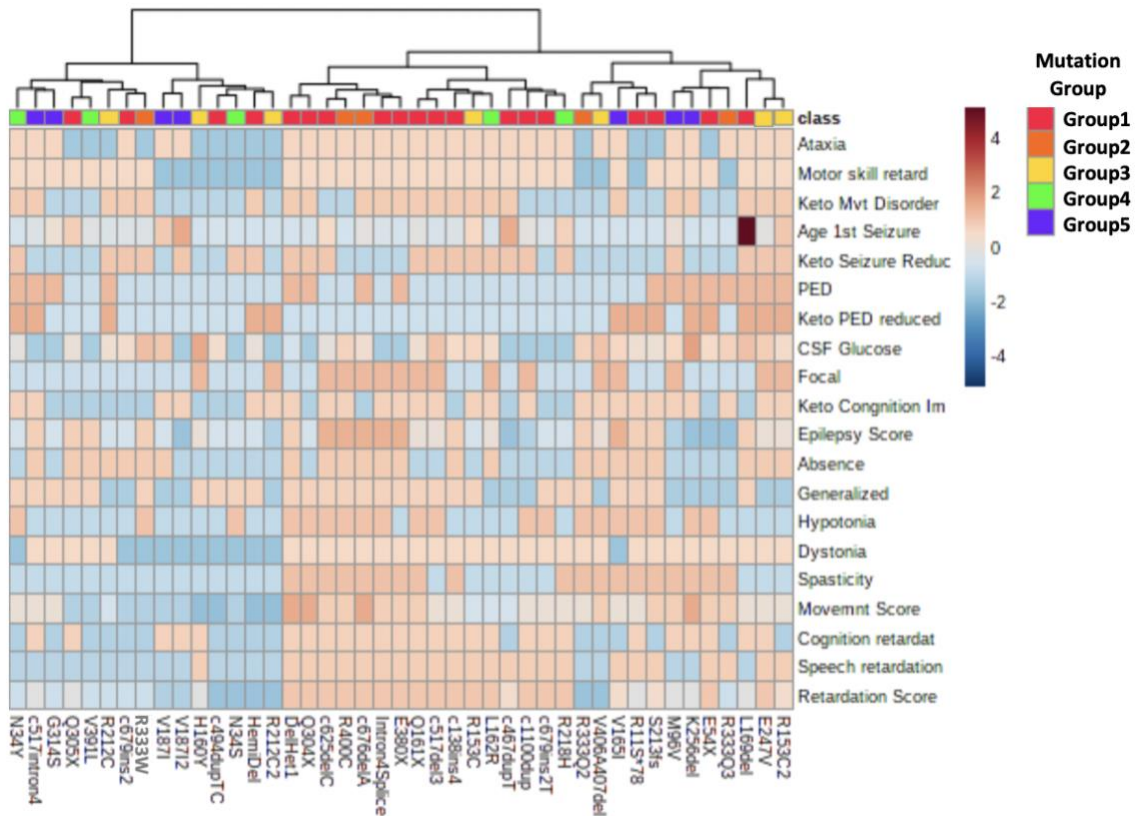


Figure 6.6 Glut1 Genotype-Phenotype Analysis from Uniformly-Reported Patient Data.

Using the same process described in Figure 6.4, patient phenotypes were run through a clustering algorithm. Key features that emerged from the clustering include movement retardation alone versus all three measures of development delay and the efficacy of the keto diet on reducing seizure frequency movement disorder severity.

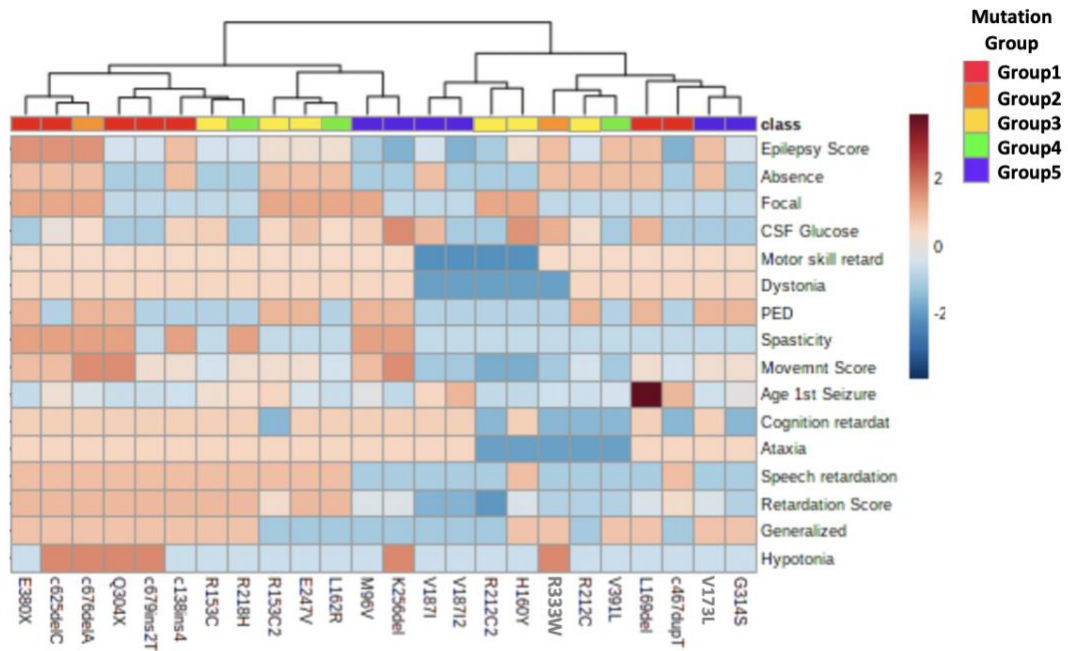


Figure 6.7 Glut1 Genotype-Phenotype Analysis from Patients who Started KDT After 2 Years of Age

Using the same clustering algorithm from Figure 6.4, patients who started the ketogenic diet after 2 years of age were clustered. Generally, mutations predicted to be most severe cluster together, while mutations predicted to only partially disrupt glucose transport cluster separately.

CHAPTER 7. CONCLUDING REMARKS

7.1 Overall Summary

Personalized Medicine (PM) is shifting the focus of therapy development away from a one-size-fits-all approach toward a nuanced understanding of the individual genetic, lifestyle, and environmental factors that contribute to disease. This approach holds particular promise for rare diseases where the patient community is small. The Cystic Fibrosis (CF) Community successfully implemented a PM approach to identify novel therapeutic targets based on the type of mutation in the patient's *CFTR* gene. While there are still CF patients with mutations that do not yet have access to treatment, the PM approach led to FDA approved drugs for two of the patient cohorts defined by their genotype-phenotype analyses [44].

Lafora Disease (LD) patients are good candidates for the PM approach. While all patients present a similar phenotype of progressive myoclonus epilepsy, the rate of progression through the disease varies significantly, and data suggest this variation is primarily explained by the patient's mutation. Importantly, multiple therapy modalities are in development for LD. These therapies can either degrade the Lafora Body (LB) aggregates that drive the disease, or prevent the aggregation from occurring by reducing glycogen synthesis. As several of these therapies are approaching clinical trials, it is important to identify the best candidates for each therapy modality. In Chapter 3, we presented a rapid assessment pipeline for predicting pathogenicity and grouping *EPM2A* patient mutations according to the loss of function in laforin. Through a combination of in silico and in vitro analyses, novel patient mutations can be matched with similar function loss profiles of known mutations, allowing for more accurate prognosis of the patient's disease progression.

LD patients display mutations in one of two driver genes: *EPM2A*, which encodes for the glycogen phosphatase laforin, and *EPM2B*, which encodes for the E3 ubiquitin ligase, malin. Together, malin and laforin regulate glycogen architecture and metabolism. While patients exhibit the same phenotypic progression regardless of the driver-gene, multiple reports suggest that *EPM2B* mutations are associated with a slower disease progression [70, 131]. In Chapter 4, we used MALDI imaging and mass spectrometry analyses to characterize the rate aggregation of LBs in the two LD mouse models: laforin knock-out (LKO) and malin knock-out (MKO) mice. The analysis revealed a slower rate of glycogen aggregation in the MKO model compared to the LKO model, if this trend holds true in LD patients, this could explain the slower progression rate identified by clinicians. While the differences between the MKO and LKO models require further exploration, this characterization suggests that the MKO mice could be used to model a slow rate of disease progression, while the LKO mice could represent the rapid disease progression cohort, highlighting the need for therapies to be tested in both LKO and MKO mice.

Given the differences uncovered between the two mouse models, we sought to assess the impact of a *Gys1* Antisense Oligonucleotide (ASO) therapy developed by Ionis Therapeutics in the MKO mouse model. Previous work demonstrated that the ASO halted LB progression in LKO mice and led to a significant decrease in LB diameters compared

to the control groups. Given the slower accumulation of glycogen in the MKO mouse, we wanted to evaluate the efficacy of long-term *Gys1*-ASO administration in the MKO model. Our analyses revealed that ICV administration of the *Gys1*-ASO significantly reduces *Gys1* expression throughout all brain regions and results in decreased LB diameters, as shown in the LKO model. Excitingly, we were also able to demonstrate that the *Gys1*-ASO treatment also reduced neuronal excitability in the hippocampus. With this data, we concluded that the *Gys1*-ASO therapy would be a viable therapy modality for LD patients regardless of their driver-gene.

While more work is required to expand PM opportunities for LD patients, we wanted to take the lessons learned from our genotype-phenotype characterizations and demonstrate how the process can be adapted for other rare diseases. We selected the brain metabolic disorder Glut1 Deficiency Syndrome (Glut1DS) as a proof-of-concept for adapting our PM framework in LD to another rare disease. As with LD and CF, patients with Glut1DS can have mild or severe disease progression. Using published structural data and clinical patient reports, we applied our approach for defining patient cohorts in LD. First, we used reported structural data to predict a set of mutation groups that would result in similar function loss. Next, we correlated the mutation groups with reported patient phenotypes. The resulting framework can now be further refined to produce genotype-phenotype correlations and perhaps lead to the discovery of novel therapeutic targets. It also demonstrates the flexibility of the PM approach between different rare disease modalities (Figure 7.1).

7.2 Limitations and Future Directions

This dissertation presents a framework for better integration of basic science research, pharmaceutical development, and clinical evaluation to accelerate the development of personalized therapies. It is our hope that this framework provides a path for other rare diseases to follow. However, there are still many opportunities for expanding PM for LD and the broader Rare Disease Community.

In the LD Community, about 50% of patients have mutations in *EPM2A*, while the other half display mutations in *EPM2B*. Initially, we hoped to present an *in vitro* pipeline for both laforin and malin, however, we were unable to express recombinant malin *in vitro* in large enough quantities for functional analysis. In the future, cell culture assays should be developed to aid in the rapid assessment of *EPM2B* patient mutations. Immunoprecipitation or biotinylation assays could tease apart the impact of specific mutations on protein-protein interactions, and immunofluorescence assays could be employed to define changes in the localization of malin-ubiquitinated substrates. Additionally, isotopic tracing with labeled glucose and metabolomics analyses could be utilized in these cell culture assays to define changes in metabolic regulation for specific patient mutations. As the assays define these functional parameters for malin, it will allow for a better understanding of which amino acids play critical roles in maintaining protein function and ultimately, better clustering of genotypic profiles.

One limitation for the basic science approach to PM is resources required to develop enzyme-specific tools to evaluate the functional impact of mutations *in vitro* when

bioinformatics analyses are not sufficient. One potential gamechanger for this limitation is the recent release of AlphaFold [214]. Already, the accuracy of AlphaFold's protein structure predictions presents an opportunity for rapid drug design. As future versions of the platform seek to predict the impact of mutations on the protein structure, it may prove to be a useful tool for defining patient cohorts in proteins that are challenging to express or purify *in vitro*. Even without that functionality, the model of the WT version of the enzyme may be helpful in predicting the site of specific protein-protein interactions, thereby improving the accuracy of predicted function loss.

Animal models provide an alternative pathway to characterize disease progression. For LD, the two mouse models, LKO and MKO, develop LB aggregates in the cytoplasm of most tissue types. These models were instrumental in demonstrating the role of LBs in driving disease progression. While these two models are often used interchangeably, the work in this dissertation highlights key differences in the rate of LB aggregation and other metabolic hallmarks of LD. This presents an opportunity to define laforin- and malin-specific contributions to disease progression in LD. Future studies can utilize isotopic tracing with labeled glucose to perform flux analysis and compare the alterations in central carbon metabolism between the two models. Additional longitudinal studies could extend the ages analyzed for this dissertation in order to determine if the differences in glycosylation and metabolism are the result of delayed LB accumulation, or the functional impairment of a different regulatory pathway.

While animal models provide important insights into disease mechanism and progression, there are limitations to using the LKO and MKO models to draw conclusions about LD patients. One issue is the lack of spontaneous seizures in the mouse model. LD patients display increasingly severe tonic-clonic seizures as the disease progresses. As this phenotype is not observed in the mice, other methods must be used to define the link between LB aggregation and seizure onset. LD patients develop seemingly normal into their teen years, and yet the function of laforin or malin is impaired from birth. This suggests that there is a threshold of LB aggregation required to trigger the seizures. The exact mechanism of seizure induction in LD remains unknown. Several theories involve glutamate transport dysregulation, neurodegeneration, and inflammation, but the way that links back to LB aggregation must still be elucidated. Metabolomics analyses of LD patient serum and CSF samples may provide additional insight toward the link between LB aggregation and LD progression. New methods are in development to allow for imaging of glycogen *in vivo* [215, 216]. As these techniques become more accessible, patients could be recruited to monitor both the rate of LB accumulation and the changes in their metabolic profiles, elucidating the metabolic impact of LB accumulation in patients.

In all of these areas, from bioinformatics, to *in vitro* and cell culture experiments, mouse models, and patient data, collaboration between patients, researchers, and clinicians is critical to the success in applying PM to treat LD. As the toolkit for implementing PM expands, more rare disease communities will be able to define patient cohorts to improve patient care and accelerate therapy development for these devastating diseases.

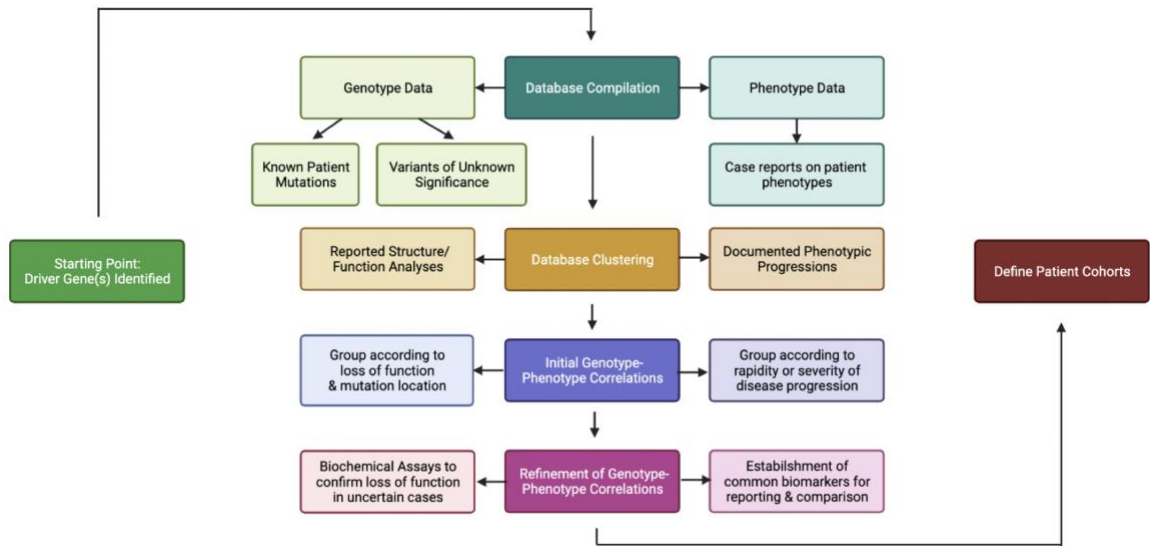


Figure 7.1 Roadmap for Building Genotype-Phenotype Correlations in Rare Disease Communities

The schematic above illustrates the proposed roadmap for analyzing genotypic and phenotypic data in rare disease communities to build genotype-phenotype correlations. After gathering all available genotype and phenotype data, each set of data is processed separately to cluster similar profiles. The genotype and phenotype clusters can then be compared to look for correlations. These clusters can then be further refined through the development of biochemical pipelines to better characterize function-loss tied to specific patient mutations.

REFERENCES

1. Sykiotis, G.P., A.G. Kallioliou Gd Fau - Papavassiliou, and A.G. Papavassiliou, *Pharmacogenetic principles in the Hippocratic writings*. (0091-2700 (Print)).
2. Pappas, G., I.J. Kiriaze, and M.E. Falagas, *Insights into infectious disease in the era of Hippocrates*. *International Journal of Infectious Diseases*, 2008. **12**(4): p. 347-350.
3. Visvikis-Siest, S., et al., *Milestones in Personalized Medicine: From the Ancient Time to Nowadays-the Provocation of COVID-19*. (1664-8021 (Print)).
4. Phillips, C.J., *Precision Medicine and its Imprecise History*. *Harvard Data Science Review*, 2020. **2.1**(Winter 2020).
5. Jørgensen, J.A.-O., *Twenty Years with Personalized Medicine: Past, Present, and Future of Individualized Pharmacotherapy*. (1549-490X (Electronic)).
6. *Precision Medicine Initiative (PMI) Working Group. The Precision Medicine Initiative Cohort Program—building a research foundation for 21st century medicine*. 2015. [cited 29 August 2021; Available from: <https://www.nih.gov/sites/default/files/research-training/initiatives/pmi/pmi-working-group-report-20150917-2.pdf> .
7. Schee Genannt Halfmann, S., et al., *Personalized Medicine: What's in it for Rare Diseases?* (0065-2598 (Print)).
8. *PerMed: Shaping Europe's View of Personalized Medicine. Strategic Research and Innovation Agenda (SRIA)*. 2015 [cited 15 June 2022; Available from: https://www.icpermed.eu/media/content/PerMed_SRIA.pdf.
9. Collins, F. *Personalized Medicine, National Human Genome Research Institute*. 2022 [cited 2 September 2022; Available from: <https://www.genome.gov/genetics-glossary/Personalized-Medicine>.
10. *Precision Medicine, US Food and Drug Administration*.
11. Coalition, P.M., *Personalized Medicine at the FDA: The Scope and Significance of Progress in 2021*. 2021.
12. Health, N.I.o., *The Promise of Precision Medicine*. 12 February 2020.
13. Tsimberidou, A.M., et al., *Review of precision cancer medicine: Evolution of the treatment paradigm*. *Cancer Treatment Reviews*, 2020. **86**: p. 102019.
14. Maciejko, L., M. Smalley, and A. Goldman, *Cancer Immunotherapy and Personalized Medicine: Emerging Technologies and Biomarker-Based Approaches*. *LID - 350 [pii] LID - 10.4172/2155-9929.1000350 [doi]*. (2155-9929 (Print)).
15. Gülbakan, B., et al., *Discovery of biomarkers in rare diseases: innovative approaches by predictive and personalized medicine*. (1878-5077 (Print)).
16. Tsimberidou, A.M., P. Müller, and Y. Ji, *Innovative trial design in precision oncology*. (1096-3650 (Electronic)).
17. Slamon Dj Fau - Clark, G.M., et al., *Human breast cancer: correlation of relapse and survival with amplification of the HER-2/neu oncogene*. (0036-8075 (Print)).
18. Carter, P., et al., *Humanization of an anti-p185HER2 antibody for human cancer therapy*. (0027-8424 (Print)).

19. Doroshow, D.B. and J.H. Doroshow, *Genomics and the History of Precision Oncology*. (1558-5042 (Electronic)).
20. Stockley, T.L., et al., *Molecular profiling of advanced solid tumors and patient outcomes with genotype-matched clinical trials: the Princess Margaret IMPACT/COMPACT trial*. *Genome Medicine*, 2016. **8**(1): p. 109.
21. Tsimberidou, A.M., et al., *Precision medicine: preliminary results from the Initiative for Molecular Profiling and Advanced Cancer Therapy 2 (IMPACT2) study*. *npj Precision Oncology*, 2021. **5**(1): p. 21.
22. Pich, O., et al., *The translational challenges of precision oncology*. *Cancer Cell*, 2022. **40**(5): p. 458-478.
23. Dobosz, P. and T. Dzieciatkowski, *The Intriguing History of Cancer Immunotherapy*. (1664-3224 (Electronic)).
24. Decker, W.K., et al., *Cancer Immunotherapy: Historical Perspective of a Clinical Revolution and Emerging Preclinical Animal Models*. (1664-3224 (Print)).
25. Styczyński, J., *A brief history of CAR-T cells: from laboratory to the bedside*. *Acta Haematologica Polonica*, 2020. **51**(1): p. 2-5.
26. Chung, B.H.Y., J.F.T. Chau, and G.K.-S. Wong, *Rare versus common diseases: a false dichotomy in precision medicine*. *npj Genomic Medicine*, 2021. **6**(1): p. 19.
27. Kaufmann, P., A.R. Pariser, and C. Austin, *From scientific discovery to treatments for rare diseases – the view from the National Center for Advancing Translational Sciences – Office of Rare Diseases Research*. *Orphanet Journal of Rare Diseases*, 2018. **13**(1): p. 196.
28. Melnikova, I., *Rare diseases and orphan drugs*. *Nature Reviews Drug Discovery*, 2012. **11**(4): p. 267-268.
29. Whitcomb, D.C., *Barriers and Research Priorities for Implementing Precision Medicine*. (1536-4828 (Electronic)).
30. Selker, H.P., et al., *A Useful and Sustainable Role for N-of-1 Trials in the Healthcare Ecosystem*. (1532-6535 (Electronic)).
31. Bellomo, F., et al., *Drug Repurposing in Rare Diseases: An Integrative Study of Drug Screening and Transcriptomic Analysis in Nephropathic Cystinosis*. *International Journal of Molecular Sciences*, 2021. **22**(23): p. 12829.
32. Ingber, D.E., *Human organs-on-chips for disease modelling, drug development and personalized medicine*. *Nature Reviews Genetics*, 2022. **23**(8): p. 467-491.
33. Amaral, M.D., *Precision medicine for rare diseases: The times they are A-Changin'*. *Current Opinion in Pharmacology*, 2022. **63**: p. 102201.
34. Andersen Dh Fau - Hodges, R.G. and R.G. Hodges, *Celiac syndrome; genetics of cystic fibrosis of the pancreas, with a consideration of etiology*. (0096-8994 (Print)).
35. Sheppard, D.N. and M.J. Welsh, *Structure and function of the CFTR chloride channel*. (0031-9333 (Print)).
36. Schwiebert, E.M., et al., *Chloride channel and chloride conductance regulator domains of CFTR, the cystic fibrosis transmembrane conductance regulator*. *Proceedings of the National Academy of Sciences*, 1998. **95**(5): p. 2674-2679.
37. Lyczak, J.B., G.B. Cannon Cl Fau - Pier, and G.B. Pier, *Lung infections associated with cystic fibrosis*. (0893-8512 (Print)).

38. Bobadilla, J.L., et al., *Cystic fibrosis: A worldwide analysis of CFTR mutations—correlation with incidence data and application to screening*. *Human Mutation*, 2002. **19**(6): p. 575-606.
39. McCague, A.F., et al., *Correlating Cystic Fibrosis Transmembrane Conductance Regulator Function with Clinical Features to Inform Precision Treatment of Cystic Fibrosis*. (1535-4970 (Electronic)).
40. Welsh, M.J. and A.E. Smith, *Molecular mechanisms of CFTR chloride channel dysfunction in cystic fibrosis*. (0092-8674 (Print)).
41. Boyle, M.P. and K. De Boeck, *A new era in the treatment of cystic fibrosis: correction of the underlying CFTR defect*. (2213-2600 (Print)).
42. Sloane, P.A. and S.M. Rowe, *Cystic fibrosis transmembrane conductance regulator protein repair as a therapeutic strategy in cystic fibrosis*. (1531-6971 (Electronic)).
43. Marson, F.A.L., C.S. Bertuzzo, and J.D. Ribeiro, *Classification of CFTR mutation classes*. (2213-2619 (Electronic)).
44. Boyle, M.P., et al., *A CFTR corrector (lumacaftor) and a CFTR potentiator (ivacaftor) for treatment of patients with cystic fibrosis who have a phe508del CFTR mutation: a phase 2 randomised controlled trial*. *The Lancet Respiratory Medicine*, 2014. **2**(7): p. 527-538.
45. De Boeck, K. and M.D. Amaral, *Progress in therapies for cystic fibrosis*. (2213-2619 (Electronic)).
46. Micallef, J. and O. Blin, *Orphan drug designation in Europe: A booster for the research and development of drugs in rare diseases*. (1958-5578 (Electronic)).
47. Lafora, G.R. and B. Glueck, *Beitrag zur Histopathologie der myoklonischen Epilepsie*. *Zeitschrift für die gesamte Neurologie und Psychiatrie*, 1911. **6**(1): p. 1-14.
48. Serratosa, J.M., et al., *The gene for progressive myoclonus epilepsy of the Lafora type maps to chromosome 6q*. (0964-6906 (Print)).
49. Serratosa, J.M., et al., *The molecular genetic bases of the progressive myoclonus epilepsies*. (0091-3952 (Print)).
50. Minassian, B.A., et al., *Mutations in a gene encoding a novel protein tyrosine phosphatase cause progressive myoclonus epilepsy*. *Nature Genetics*, 1998. **20**(2): p. 171-4.
51. Chan, E.M., et al., *Genetic mapping of a new Lafora progressive myoclonus epilepsy locus (EPM2B) on 6p22*. *Journal of medical genetics*, 2003. **40**(9): p. 671-675.
52. Serratosa, J.M., et al., *A Novel Protein Tyrosine Phosphatase Gene Is Mutated in Progressive Myoclonus Epilepsy of the Lafora Type (EPM2)*. *Human Molecular Genetics*, 1999. **8**(2): p. 345-352.
53. Worby, C.A., J.E. Gentry Ms Fau - Dixon, and J.E. Dixon, *Laforin, a dual specificity phosphatase that dephosphorylates complex carbohydrates*. *Journal of biological chemistry*, 2006. **281**(41): p. 30412-8.
54. Gentry, M.S., C.A. Worby, and J.E. Dixon, *Insights into Lafora disease: Malin is an E3 ubiquitin ligase that ubiquitinates and promotes the degradation of laforin*. *Proceedings of the National Academy of Sciences of the United States of America*, 2005. **102**(24): p. 8501-8506.

55. Worby, C.A., M.S. Gentry, and J.E. Dixon, *Malin decreases glycogen accumulation by promoting the degradation of protein targeting to glycogen (PTG)*. *J Biol Chem*, 2008. **283**(7): p. 4069-76.
56. Sun, R.C., et al., *Nuclear Glycogenolysis Modulates Histone Acetylation in Human Non-Small Cell Lung Cancers*. *Cell Metabolism*, 2019. **30**(5): p. 903-916.e7.
57. Nitschke, F., et al., *Abnormal glycogen chain length pattern, not hyperphosphorylation, is critical in Lafora disease*. *EMBO molecular medicine*, 2017. **9**(7): p. 906-917.
58. Turnbull, J., et al., *Glycogen hyperphosphorylation underlies lafora body formation*. *Annals of Neurology* 2010. **68**(6): p. 925-33.
59. Brewer, M.K., et al., *Polyglucosan body structure in Lafora disease*. (1879-1344 (Electronic)).
60. Sullivan, A.M., et al., *Pathogenesis of Lafora Disease: Transition of Soluble Glycogen to Insoluble Polyglucosan*. *International Journal of Molecular Sciences*, 2017. **18**(8): p. 1743.
61. Duran, J.A.-O., et al., *Astrocytic glycogen accumulation drives the pathophysiology of neurodegeneration in Lafora disease*. (1460-2156 (Electronic)).
62. Duran, J., et al., *Deleterious effects of neuronal accumulation of glycogen in flies and mice*. *EMBO molecular medicine*, 2012. **4**(8): p. 719-29.
63. Duran, J., et al., *Glycogen accumulation underlies neurodegeneration and autophagy impairment in Lafora disease*. *Human molecular genetics*, 2014. **23**(12): p. 3147-56.
64. Gumusgoz, E., et al., *AAV-Mediated Artificial miRNA Reduces Pathogenic Polyglucosan Bodies and Neuroinflammation in Adult Polyglucosan Body and Lafora Disease Mouse Models*. *LID - 10.1007/s13311-022-01218-7 [doi]*. (1878-7479 (Electronic)).
65. Ahonen, S., et al., *Gys1 antisense therapy rescues neuropathological bases of murine Lafora disease*. (1460-2156 (Electronic)).
66. Brewer, M.K., et al., *Targeting Pathogenic Lafora Bodies in Lafora Disease Using an Antibody-Enzyme Fusion*. (1932-7420 (Electronic)).
67. Valles-Ortega, J., et al., *Neurodegeneration and functional impairments associated with glycogen synthase accumulation in a mouse model of Lafora disease*. *EMBO molecular medicine*, 2011. **3**(11): p. 667-681.
68. Lesca, G., et al., *Novel mutations in EPM2A and NHLRC1 widen the spectrum of Lafora disease*. (1528-1167 (Electronic)).
69. Nitschke, F., et al., *Lafora disease - from pathogenesis to treatment strategies*. (1759-4766 (Electronic)).
70. Gómez-Abad, C., et al., *Lafora disease due to EPM2B mutations: a clinical and genetic study*. (1526-632X (Electronic)).
71. Pondrelli, F., et al., *Natural history of Lafora disease: a prognostic systematic review and individual participant data meta-analysis*. *Orphanet Journal of Rare Diseases*, 2021. **16**(1): p. 362.

72. Jansen, A.C. and E. Andermann, *Progressive Myoclonus Epilepsy, Lafora Type*. *BTI - GeneReviews*(®).
73. Singh, S. and S. Ganesh, *Lafora progressive myoclonus epilepsy: a meta-analysis of reported mutations in the first decade following the discovery of the EPM2A and NHLRC1 genes*. *Human mutation*, 2009. **30**(5): p. 715-23.
74. Ianzano, L., et al., *Lafora progressive Myoclonus Epilepsy mutation database- EPM2A and NHLRC1 (EPM2B) genes*. (1098-1004 (Electronic)).
75. Lanoiselée, H.M., et al., *Are c.436G>A mutations less severe forms of Lafora disease? A case report*. (2213-3232 (Print)).
76. Ferlazzo, E., et al., *Mild Lafora disease: clinical, neurophysiologic, and genetic findings*. (1528-1167 (Electronic)).
77. Jara-Prado, A., et al., *Late onset Lafora disease and novel EPM2A mutations: breaking paradigms*. (1872-6844 (Electronic)).
78. Zutt, R., et al., *Unusual Course of Lafora Disease*. (2470-9239 (Print)).
79. Brewer, M.K. and M.S. Gentry, *The 3rd International Lafora Epilepsy Workshop: Evidence for a cure*. *Epilepsy & behavior : E&B*, 2018. **81**: p. 125-127.
80. Gentry, M.S., et al., *The 5th International Lafora Epilepsy Workshop: Basic science elucidating therapeutic options and preparing for therapies in the clinic*. *Epilepsy Behav*, 2020. **103**(Pt A): p. 106839.
81. Markussen, K.H., et al., *The 6th International Lafora Epilepsy Workshop: Advances in the search for a cure*. *Epilepsy & Behavior*, 2021. **119**: p. 107975.
82. Wilkens, C., et al., *Plant α -glucan phosphatases SEX4 and LSF2 display different affinity for amylopectin and amylose*. *FEBS Letters*, 2015. **590**(1): p. 118-128.
83. Sherwood, A.R., et al., *A bioassay for Lafora disease and laforin glucan phosphatase activity*. *Clinical biochemistry*, 2013. **46**(18): p. 1869-76.
84. Roma-Mateo, C., et al., *Laforin, a dual-specificity phosphatase involved in Lafora disease, is phosphorylated at Ser25 by AMP-activated protein kinase*. *The biochemical journal*, 2011. **439**(2): p. 265-75.
85. Garcia-Gimeno, M.A., et al., *A novel EPM2A mutation yields a slow progression form of Lafora disease*. *Epilepsy Res*, 2018. **145**: p. 169-177.
86. Raththagala, M., et al., *Structural mechanism of laforin function in glycogen dephosphorylation and lafora disease*. (1097-4164 (Electronic)).
87. Adzhubei la Fau - Schmidt, S., et al., *A method and server for predicting damaging missense mutations*. (1548-7105 (Electronic)).
88. Parthiban, V., D. Gromiha Mm Fau - Schomburg, and D. Schomburg, *CUPSAT: prediction of protein stability upon point mutations*. (1362-4962 (Electronic)).
89. Pandurangan, A.P., et al., *SDM: a server for predicting effects of mutations on protein stability*. (1362-4962 (Electronic)).
90. Johnson, A.D., et al., *SNAP: a web-based tool for identification and annotation of proxy SNPs using HapMap*. (1367-4811 (Electronic)).
91. Capriotti, E. and P. Fariselli, *PhD-SNPg: a webserver and lightweight tool for scoring single nucleotide variants*. (1362-4962 (Electronic)).
92. Capriotti, E., Y. Altman Rb Fau - Bromberg, and Y. Bromberg, *Collective judgment predicts disease-associated single nucleotide variants*. (1471-2164 (Electronic)).

93. Pei, J. and N.V. Grishin, *AL2CO: calculation of positional conservation in a protein sequence alignment*. (1367-4803 (Print)).
94. Hall, M., et al., *The WEKA data mining software: an update*. SIGKDD Explor. Newsl., 2009. **11**(1): p. 10–18.
95. Young, L.E.A., et al., *Accurate and sensitive quantitation of glucose and glucose phosphates derived from storage carbohydrates by mass spectrometry*. Carbohydr Polym, 2020. **230**: p. 115651.
96. Sun, R.C., et al., *Nuclear glycogenolysis modulates histone acetylation in human non-small cell lung cancers*. Cell metabolism, 2019. **30**(5): p. 903-916. e7.
97. Andres, D.A., et al., *Improved workflow for mass spectrometry-based metabolomics analysis of the heart*. J Biol Chem, 2020. **295**(9): p. 2676-2686.
98. Stanback, A.E., et al., *Regional N-glycan and lipid analysis from tissues using MALDI-mass spectrometry imaging*. (2666-1667 (Electronic)).
99. Hawkinson, T.R. and R.C. Sun, *Matrix-Assisted Laser Desorption/Ionization Mass Spectrometry Imaging of Glycogen Glycogen In Situ*, in *Mass Spectrometry Imaging of Small Molecules: Methods and Protocols*, Y.-J. Lee, Editor. 2022, Springer US: New York, NY. p. 215-228.
100. Sun, R.C., et al., *Brain glycogen serves as a critical glucosamine cache required for protein glycosylation*. (1932-7420 (Electronic)).
101. Gentry, M.S., et al., *Lafora disease offers a unique window into neuronal glycogen metabolism*. J Biol Chem, 2018. **293**(19): p. 7117-7125.
102. Ganesh, S., et al., *Targeted disruption of the Epm2a gene causes formation of Lafora inclusion bodies, neurodegeneration, ataxia, myoclonus epilepsy and impaired behavioral response in mice*. Human Molecular Genetics, 2002. **11**(11): p. 1251-1262.
103. Serratosa, J.M., et al., *A novel protein tyrosine phosphatase gene is mutated in progressive myoclonus epilepsy of the Lafora type (EPM2)*. (0964-6906 (Print)).
104. Molares-Vila, A., et al., *Biomarkers in Glycogen Storage Diseases: An Update*. International journal of molecular sciences, 2021. **22**(9): p. 4381.
105. DePaoli-Roach, A.A., et al., *Genetic depletion of the malin E3 ubiquitin ligase in mice leads to lafora bodies and the accumulation of insoluble laforin*. Journal of biological chemistry, 2010. **285**(33): p. 25372-81.
106. Fernández-Sánchez, M.E., et al., *Laforin, the dual-phosphatase responsible for Lafora disease, interacts with R5 (PTG), a regulatory subunit of protein phosphatase-1 that enhances glycogen accumulation*. Hum Mol Genet, 2003. **12**(23): p. 3161-71.
107. Criado, O., et al., *Lafora bodies and neurological defects in malin-deficient mice correlate with impaired autophagy*. Human Molecular Genetics, 2011. **21**(7): p. 1521-1533.
108. Nitschke, F., et al., *Hyperphosphorylation of glucosyl C6 carbons and altered structure of glycogen in the neurodegenerative epilepsy Lafora disease*. Cell Metabolism, 2013. **17**(5): p. 756-67.
109. Pederson, B.A., et al., *Inhibiting glycogen synthesis prevents Lafora disease in a mouse model*. (1531-8249 (Electronic)).
110. Tang, B., et al., *Discovery and Development of Small-Molecule Inhibitors of Glycogen Synthase*. J Med Chem, 2020. **63**(7): p. 3538-3551.

111. Gumusgoz, E., et al., *Targeting Gys1 with AAV-SaCas9 Decreases Pathogenic Polyglucosan Bodies and Neuroinflammation in Adult Polyglucosan Body and Lafora Disease Mouse Models*. *Neurotherapeutics*, 2021. **18**(2): p. 1414-1425.
112. Brewer, M.K., et al., *An empirical pipeline for personalized diagnosis of Lafora disease mutations*. (2589-0042 (Electronic)).
113. Montenegro, L.A.-O., et al., *Performance of mutation pathogenicity prediction tools on missense variants associated with 46,XY differences of sex development*. (1980-5322 (Electronic)).
114. Ahmad, A., et al., *Clinical and genetic studies in patients with Lafora disease from Pakistan*. (1878-5883 (Electronic)).
115. Lynch, D.S., N.W. Wood, and H. Houlden, *Late-onset Lafora disease with prominent parkinsonism due to a rare mutation in EPM2A*. *Neurology. Genetics*, 2016. **2**(5): p. e101-e101.
116. Ganesh, S., et al., *Laforin, defective in the progressive myoclonus epilepsy of Lafora type, is a dual-specificity phosphatase associated with polyribosomes*. *Human Molecular Genetics*, 2000. **9**(15): p. 2251-2261.
117. Kuchtová, A., M. Gentry, and Š. Janeček, *The unique evolution of the carbohydrate-binding module CBM20 in laforin*. *FEBS letters.*, 2018. **592**(4).
118. Irimia, J.M., et al., *Muscle glycogen remodeling and glycogen phosphate metabolism following exhaustive exercise of wild type and laforin knockout mice*. *Journal of Biological Chemistry*, 2015. **290**(37): p. 22686-98.
119. Gentry, M.S., P. Roma-Mateo C Fau - Sanz, and P. Sanz, *Laforin, a protein with many faces: glucan phosphatase, adapter protein, et alii*. *The FEBS Journal*, 2013. **280**(2): p. 525-37.
120. IA, A., et al., *A method and server for predicting damaging missense mutations*. (1548-7105 (Electronic)).
121. Vivoli, M., et al., *Determination of protein-ligand interactions using differential scanning fluorimetry*. (1940-087X (Electronic)).
122. Wright, T.A., et al., *Extraction of Thermodynamic Parameters of Protein Unfolding Using Parallelized Differential Scanning Fluorimetry*. *The Journal of Physical Chemistry Letters*, 2017. **8**(3): p. 553-558.
123. Wang, J., et al., *A unique carbohydrate binding domain targets the lafora disease phosphatase to glycogen*. *Journal of biological chemistry*, 2002. **277**(4): p. 2377-80.
124. Meekins, D.A., et al., *Mechanistic Insights into Glucan Phosphatase Activity against Polyglucan Substrates*. (1083-351X (Electronic)).
125. Worby, C.A., M.S. Gentry, and J.E. Dixon, *Malin decreases glycogen accumulation by promoting the degradation of protein targeting to glycogen (PTG)*. *The Journal of biological chemistry*, 2008. **283**(7): p. 4069-4076.
126. Miosge, L.A., et al., *Comparison of predicted and actual consequences of missense mutations*. (1091-6490 (Electronic)).
127. Niroula, A. and M. Vihinen, *How good are pathogenicity predictors in detecting benign variants?* *PLOS Computational Biology*, 2019. **15**(2): p. e1006481.
128. Minassian, B.A., et al., *Genetic locus heterogeneity in Lafora's progressive myoclonus epilepsy*. *Ann Neurol*, 1999. **45**(2): p. 262-5.

129. Serratosa, J.M., et al., *A novel protein tyrosine phosphatase gene is mutated in progressive myoclonus epilepsy of the Lafora type (EPM2)*. Human Mol Genet, 1999. **8**.
130. Wang, W., et al., *Glycogen metabolism in tissues from a mouse model of Lafora disease*. Archives of biochemistry and biophysics, 2007. **457**(2): p. 264-269.
131. Baykan, B., et al., *Late-onset and slow-progressing Lafora disease in four siblings with EPM2B mutation*. (0013-9580 (Print)).
132. Franceschetti, S., et al., *Clinical and genetic findings in 26 Italian patients with Lafora disease*. (0013-9580 (Print)).
133. Singh, S., et al., *Novel NHLRC1 mutations and genotype-phenotype correlations in patients with Lafora's progressive myoclonic epilepsy*. (1468-6244 (Electronic)).
134. Romá-Mateo, C., P. Sanz, and M.S. Gentry, *Deciphering the role of malin in the Lafora progressive myoclonus epilepsy*. IUBMB life, 2012. **64**(10): p. 801-808.
135. Moreno, D., et al., *The laforin-malin complex, involved in Lafora disease, promotes the incorporation of K63-linked ubiquitin chains into AMP-activated protein kinase beta subunits*. Mol Biol Cell, 2010. **21**(15): p. 2578-88.
136. Cheng, A., et al., *A role for AGL ubiquitination in the glycogen storage disorders of Lafora and Cori's disease*. (0890-9369 (Print)).
137. Vernia, S., et al., *AMP-activated protein kinase phosphorylates R5/PTG, the glycogen targeting subunit of the R5/PTG-protein phosphatase 1 holoenzyme, and accelerates its down-regulation by the laforin-malin complex*. J Biol Chem, 2009. **284**.
138. Hawkinson, T.R. and R.C. Sun, *Matrix-Assisted Laser Desorption/Ionization Mass Spectrometry Imaging of Glycogen In Situ*. (1940-6029 (Electronic)).
139. Brewer, M.K., *BIOCHEMICAL APPROACHES FOR THE DIAGNOSIS AND TREATMENT OF LAFORA DISEASE*, in *Theses and Dissertations--Molecular and Cellular Biochemistry*. 2019, University of Kentucky
140. Brewer, M.K. and M.S. Gentry, *Brain Glycogen Structure and Its Associated Proteins: Past, Present and Future*, in *Brain Glycogen Metabolism*, M. DiNuzzo and A. Schousboe, Editors. 2019, Springer International Publishing: Cham. p. 17-81.
141. Bak, L.K., et al., *Astrocytic glycogen metabolism in the healthy and diseased brain*. (1083-351X (Electronic)).
142. Wang, Y., et al., *Laforin prevents stress-induced polyglucosan body formation and Lafora disease progression in neurons*. (1559-1182 (Electronic)).
143. Simmons, Z., *PRE-CLINICAL ADVANCEMENTS IN BIOMARKERS, TOOLS, AND THERAPEUTICS FOR A METABOLIC NEURODEGENERATIVE DISEASE*, in *Molecular and Cellular Biochemistry*. 2021, University of Kentucky.
144. Chan, E.M., et al., *Mutations in NHLRC1 cause progressive myoclonus epilepsy*. Nature Genetics, 2003. **35**(2): p. 125-7.
145. Tagliabracci, V.S., et al., *Laforin is a glycogen phosphatase, deficiency of which leads to elevated phosphorylation of glycogen in vivo*. Proc Natl Acad Sci USA, 2007. **104**(49): p. 19262-6.
146. Tagliabracci, V.S., et al., *Abnormal metabolism of glycogen phosphate as a cause for Lafora disease*. The journal of biological chemistry, 2008. **283**(49): p. 33816-25.
147. Tagliabracci, V.S., et al., *Phosphate incorporation during glycogen synthesis and Lafora disease*. Cell Metabolism, 2011. **13**(3): p. 274-82.

148. Mitra, S., E. Gumusgoz, and B.A. Minassian, *Lafora disease: Current biology and therapeutic approaches*. *LID - S0035-3787(21)00611-1 [pii] LID - 10.1016/j.neurol.2021.06.006 [doi]*. (0035-3787 (Print)).
149. Turnbull, J., et al., *Lafora disease*. (1950-6945 (Electronic)).
150. Abubakr, A., et al., *The presence of polyglucosan bodies in temporal lobe epilepsy: its role and significance*. (0967-5868 (Print)).
151. Turnbull, J., et al., *PTG depletion removes Lafora bodies and rescues the fatal epilepsy of Lafora disease*. *PLoS Genetics*, 2011. **7**(4): p. e1002037.
152. Turnbull, J., et al., *PTG protein depletion rescues malin-deficient Lafora disease in mouse*. *Annals of Neurology*, 2014. **75**(3): p. 442-6.
153. Luna, L., *AFIP manual of histologic staining methods*. New York, EUA, 1986.
154. Baba, O., *[Production of monoclonal antibody that recognizes glycogen and its application for immunohistochemistry]*. (0300-9149 (Print)).
155. Austin GI Auid- Orcid: --- Fau - Simmons, Z.R., et al., *Central Nervous System Delivery and Biodistribution Analysis of an Antibody-Enzyme Fusion for the Treatment of Lafora Disease*. (1543-8392 (Electronic)).
156. Gentry, M.A.-O., K.H. Markussen, and K.J. Donohue, *Two Diseases-One Preclinical Treatment Targeting Glycogen Synthesis*. (1878-7479 (Electronic)).
157. Migliorati, J.M., et al., *Absorption, distribution, metabolism, and excretion of FDA-approved antisense oligonucleotide drugs*. *Drug Metabolism and Disposition*, 2022: p. DMD-MR-2021-000417.
158. Damase, T.R., et al., *The Limitless Future of RNA Therapeutics*. *Frontiers in Bioengineering and Biotechnology*, 2021. **9**.
159. Crooke, S.T., *Molecular Mechanisms of Antisense Oligonucleotides*. (2159-3345 (Electronic)).
160. Mann, D.M.A., et al., *Glycogen accumulations in the cerebral cortex in Alzheimer's disease*. *Acta Neuropathologica*, 1987. **73**(2): p. 181-184.
161. Hicks, J., G. Wartchow E Fau - Mierau, and G. Mierau, *Glycogen storage diseases: a brief review and update on clinical features, genetic abnormalities, pathologic features, and treatment*. *Ultrastructural pathology*, 2011. **35**(5): p. 183-96.
162. Duran, J. and J.J. Guinovart, *Brain glycogen in health and disease*. *Molecular aspects of medicine*, 2015. **46**(1872-9452 (Electronic)): p. 70-7.
163. Tefera, T.W., et al., *CNS glucose metabolism in Amyotrophic Lateral Sclerosis: a therapeutic target?* *Cell & Bioscience*, 2021. **11**(1): p. 14.
164. Xi, Y., *Poster Presentation: #327. Pharmacology of small molecule inhibitors of GYS1 in a mouse model of Pompe disease*. *WORLD Symposium*, February 7th, 2022 in San Diego, CA.
165. Choy, R., *Poster Presentation: In-vitro characterization of MZE001, an orally active GYS1 inhibitor to treat Pompe disease*. Presented at: *WORLD Symposium*, February 7th, 2022 in San Diego, CA.
166. Pederson, B.A., et al., *Abnormal cardiac development in the absence of heart glycogen*. *Mol Cell Biol*, 2004. **24**(16): p. 7179-87.
167. Pederson, B.A., et al., *Glucose metabolism in mice lacking muscle glycogen synthase*. *Diabetes*, 2005. **54**(12): p. 3466-73.

168. Chown, E.A.-O., et al., *GYS1 or PPP1R3C deficiency rescues murine adult polyglucosan body disease*. (2328-9503 (Electronic)).
169. Savage, D.B., et al., *A prevalent variant in PPP1R3A impairs glycogen synthesis and reduces muscle glycogen content in humans and mice*. PLoS Med, 2008. **5**(1): p. e27.
170. Homburger, J., *Poster Presentation #122: Genetic reduction of muscle glycogen is well tolerated in UK Biobank participants*. Presented at: WORLD Symposium, February 7th 2022, in San Diego, CA.
171. Baumann, R.J., S.A. Kocoshis, and D. Wilson, *Lafora disease: Liver histopathology in presymptomatic children*. Annals of Neurology, 1983. **14**(1): p. 86-89.
172. Ortolano S Fau - Vieitez, I., et al., *Loss of GABAergic cortical neurons underlies the neuropathology of Lafora disease*. (1756-6606 (Electronic)).
173. Gomez-Garre, P., et al., *Hepatic disease as the first manifestation of progressive myoclonus epilepsy of Lafora*. Neurology, 2007. **68**(17): p. 1369-73.
174. Lahuerta, M., et al., *Reactive Glia-Derived Neuroinflammation: a Novel Hallmark in Lafora Progressive Myoclonus Epilepsy That Progresses with Age*. (1559-1182 (Electronic)).
175. García-Cabrero, A.M., et al., *Enhanced sensitivity of laforin- and malin-deficient mice to the convulsant agent pentylenetetrazole*. (1662-4548 (Print)).
176. Roach, P.J., *Glycogen phosphorylation and Lafora disease*. Molecular aspects of medicine, 2015. **46**: p. 78-84.
177. Sullivan, M.A., et al., *Skeletal Muscle Glycogen Chain Length Correlates with Insolubility in Mouse Models of Polyglucosan-Associated Neurodegenerative Diseases*. (2211-1247 (Electronic)).
178. Koutsifeli, P., et al., *Glycogen-autophagy: Molecular machinery and cellular mechanisms of glycophagy*. Journal of Biological Chemistry, 2022: p. 102093.
179. DiNuzzo, M., *How glycogen sustains brain function: A plausible allosteric signaling pathway mediated by glucose phosphates*. Journal of Cerebral Blood Flow & Metabolism, 2019. **39**(8): p. 1452-59.
180. Sickmann, H.M., et al., *Functional significance of brain glycogen in sustaining glutamatergic neurotransmission*. (1471-4159 (Electronic)).
181. Freeze, H.H., et al., *Neurology of inherited glycosylation disorders*. (1474-4465 (Electronic)).
182. De Vivo, D.C., et al., *Defective glucose transport across the blood-brain barrier as a cause of persistent hypoglycorrhachia, seizures, and developmental delay*. (0028-4793 (Print)).
183. Sato, M. and M. Mueckler, *A Conserved Amino Acid Motif (R-X-G-R-R) in the Glut1 Glucose Transporter Is an Important Determinant of Membrane Topology**. Journal of Biological Chemistry, 1999. **274**(35): p. 24721-24725.
184. Pragallapati, S. and R. Manyam, *Glucose transporter 1 in health and disease*. (0973-029X (Print)).
185. López-Rivera, J.A., et al., *A catalogue of new incidence estimates of monogenic neurodevelopmental disorders caused by de novo variants*. (1460-2156 (Electronic)).
186. Koch, H. and Y.G. Weber, *The glucose transporter type 1 (Glut1) syndromes*. (1525-5069 (Electronic)).

187. Klepper, J.A.-O.X., et al., *Glut1 Deficiency Syndrome (Glut1DS): State of the art in 2020 and recommendations of the international Glut1DS study group*. (2470-9239 (Print)).
188. Bekker, Y.A.C., et al., *Failure of ketogenic diet therapy in GLUT1 deficiency syndrome*. *European Journal of Paediatric Neurology*, 2019. **23**(3): p. 404-409.
189. Klepper, J. and B. Leidencker, *Glut1 deficiency syndrome and novel ketogenic diets*. (1708-8283 (Electronic)).
190. Leen, W.G., et al., *Glucose transporter-1 deficiency syndrome: the expanding clinical and genetic spectrum of a treatable disorder*. (1460-2156 (Electronic)).
191. Gras, D., et al., *A simple blood test expedites the diagnosis of glucose transporter type 1 deficiency syndrome*. (1531-8249 (Electronic)).
192. Zaman, S.M., et al., *Development of a rapid functional assay that predicts GLUT1 disease severity*. *Neurology Genetics*, 2018. **4**(6): p. e297.
193. Brockmann, K., *The expanding phenotype of GLUT1-deficiency syndrome*. *Brain and Development*, 2009. **31**(7): p. 545-552.
194. Wang, D., et al., *Glut-1 deficiency syndrome: clinical, genetic, and therapeutic aspects*. (0364-5134 (Print)).
195. Kim, H.A.-O., et al., *Diagnostic Challenges Associated with GLUT1 Deficiency: Phenotypic Variabilities and Evolving Clinical Features*. (1976-2437 (Electronic)).
196. De Giorgis, V.A.-O., et al., *Overall cognitive profiles in patients with GLUT1 Deficiency Syndrome*. (2162-3279 (Electronic)).
197. Takahashi, S., et al., *The role of molecular analysis of SLC2A1 in the diagnostic workup of glucose transporter 1 deficiency syndrome*. (1878-5883 (Electronic)).
198. Wang, D., D.C. Kranz-Eble P Fau - De Vivo, and D.C. De Vivo, *Mutational analysis of GLUT1 (SLC2A1) in Glut-1 deficiency syndrome*. (1098-1004 (Electronic)).
199. Zanaboni, M.P., et al., *Characterization of Speech and Language Phenotype in GLUT1DS*. *LID - 10.3390/children8050344 [doi] LID - 344*. (2227-9067 (Print)).
200. Bromberg, Y. and B. Rost, *SNAP: predict effect of non-synonymous polymorphisms on function*. (1362-4962 (Electronic)).
201. Tang, H. and P.D. Thomas, *PANTHER-PSEP: predicting disease-causing genetic variants using position-specific evolutionary preservation*. *Bioinformatics*, 2016. **32**(14): p. 2230-2232.
202. Olson, A.L. and J.E. Pessin, *Structure, function, and regulation of the mammalian facilitative glucose transporter gene family*. (0199-9885 (Print)).
203. Deng, D., et al., *Crystal structure of the human glucose transporter GLUT1*. *Nature*, 2014. **510**(7503): p. 121-125.
204. Almahmoud, S.W.X.V.J.L.A.U.Z.H.A.T.I.C.S.o.G.T.a.a.A.D.T. *Molecules*, 2019. **24**, DOI: 10.3390/molecules24112159.
205. Park, M.S., *Molecular Dynamics Simulations of the Human Glucose Transporter GLUT1*. (1932-6203 (Electronic)).
206. Galochkina, T., et al., *New insights into GluT1 mechanics during glucose transfer*. (2045-2322 (Electronic)).
207. Mullen, S.A., et al., *Absence epilepsies with widely variable onset are a key feature of familial GLUT1 deficiency*. *Neurology*, 2010. **75**(5): p. 432.

208. Kolic, I., et al., *GLUT1 Deficiency Syndrome-Early Treatment Maintains Cognitive Development? (Literature Review and Case Report)*. LID - 10.3390/genes12091379 [doi] LID - 1379. (2073-4425 (Electronic)).
209. Varesio, C., et al., *Quality of Life in Chronic Ketogenic Diet Treatment: The GLUT1DS Population Perspective*. LID - 10.3390/nu11071650 [doi] LID - 1650. (2072-6643 (Electronic)).
210. **Gurnett, C.**, *Multiplex analysis of variant effects for SLC2A1 gene*. 2022, The Orphan Disease Center.
211. Baranyi, R., et al. *DiaBeaThis — A gamified self-tracking portal to support people suffering from diabetes mellitus to control their blood glucose level*. in *2018 IEEE 6th International Conference on Serious Games and Applications for Health (SeGAH)*. 2018.
212. Gay, V., P. Leijdekkers, and E. Barin, *A mobile rehabilitation application for the remote monitoring of cardiac patients after a heart attack or a coronary bypass surgery*, in *Proceedings of the 2nd International Conference on Pervasive Technologies Related to Assistive Environments*. 2009, Association for Computing Machinery: Corfu, Greece. p. Article 21.
213. Alansari, Z., et al. *The Internet of Things adoption in healthcare applications*. in *2017 IEEE 3rd International Conference on Engineering Technologies and Social Sciences (ICETSS)*. 2017.
214. Jumper, J., et al., *Highly accurate protein structure prediction with AlphaFold*. *Nature*, 2021. **596**(7873): p. 583-589.
215. Zhou, Y.A.-O., et al., *Magnetic resonance imaging of glycogen using its magnetic coupling with water*. (1091-6490 (Electronic)).
216. Vinogradov, E., *MRI monitoring of energy storage in vivo using magnetization pathways*. *Proceedings of the National Academy of Sciences*, 2020. **117**(10): p. 5092-5094.

VITA

Katherine Janae Donohue

Doctoral Candidate
Department of Molecular and Cellular Biochemistry
University of Kentucky College of Medicine

Educational Institutions

University of Kentucky, Lexington KY Bachelor of Science, Chemistry	2015-2017
University of Kentucky, Lexington KY Master of Arts, Patterson School of Diplomacy and International Commerce	2011-2012
University of Kentucky, Lexington KY Bachelor of Arts, Mathematics	2011-2012
University of Kentucky, Lexington KY Bachelor of Arts, International Studies	2007-2011

Professional Positions

Adjunct Instructor of Chemistry, Transylvania University	2022-present
Science Director at Chelsea's Hope Lafora Disease Research Fund	2022-present
BGSO Outreach President	2020-2022
Biochemistry Data Club President	2019-2022
Executive Director for BUILD	2015-2016
Associate Community Organizer for BUILD	2013-2015
Global Service Corps Intern	2012
SCAPA Middle School Speech Team Coach	2008-present

Scholastic and Professional Honors

Kentucky High School Speech League: Coaching Award	2014-2022
NSF EPSCoR Graduate Student Research Fellowship	2018-2019
ASBMB Graduate Student Travel Grant Award	2017
Gaines Fellowship for the Humanities, University of Kentucky	2009 - 2011
Otis A. Singletary Scholarship, University of Kentucky	2007 - 2011

Publications

Donohue K., Bruntz, R.C., Markussen K.H., Fitzsimmons, B., Young L.E.A, Clarke, H.A., Coburn P.T., Griffith, L.E., Sanders, C., Klier, J., Minassian B.A., Sun, R.C., Kordasiewicz, H., and Gentry, M.S. (submitted)

Donohue, K., Abul-Khoudoud. M., Viana, R., Li, S., Sanz, P., Vander Kooi, C.W., and Gentry, M.S. **Rapid pathogenicity assessment defines patient cohorts for Lafora disease.** (in preparation)

Brewer, M.K., **Donohue, K.**, DePaoli-Roach, A., Simmons, Z.R., Zoe R., Wayne, J.L., Li, S., Viana, R., Segvich, D.M., Contreras, C.J., Sanz, P., Sun, R.C., Roach, P.J., and Gentry, M.S. 2021. Glycogen hyper-phosphorylation contributes to neuropathology in Lafora Disease. (in preparation)

Gentry, M.S., Markussen, K.H. & **Donohue, K.** Two Diseases—One Preclinical Treatment Targeting Glycogen Synthesis. *Neurotherapeutics* (2022).

<https://doi.org/10.1007/s13311-022-01240-9>

Donohue, K., Gentry, M.S., and Sun, R.C. 2020. The E3 ligase malin plays a pivotal role in promoting nuclear glycogenolysis and histone acetylation. *Ann Transl Med.* Mar; 8(5):254

Donohue, K., Andrea Kuchtova, Craig W. Vander Kooi, and Matthew S. Gentry. 2019. *Reversible Phosphorylation in Glycogen and Starch.* In *Enzymology of Complex Polyglucans: Glycogen and Starch.* Science Publishers.

Donohue, K. 2014. The view from seminary: Using library holdings to measure Christian seminary worldviews. In S. Brunn (Ed.), *The Changing Map of World Religion.* New York: Springer Publishing, pp1067-1090

Katherine Janae Donohue